PEOPLE'S DEMOCRATIC REPUBLIC OF ALGERIA

Ministry of Higher Education and Scientific Research

University of Amar Telidji - Laghouat

Faculty of Technology

PhD THESIS IN SCIENCE
Specialty: Energetic Mechanics

REGUE Hanane Maria

THEME

Experimental study and energetic optimization of heat exchange with variable geometry in a parabolic trough collector with a double reflection

JURY:

Pr. AOUISSI Mokhtar	*Chair*	*Professor*	*U.A.T.Laghouat*
Pr. MEDJELLED Ahmed	*Examiner*	*Professor*	*U.A.T.Laghouat*
Dr. GHARNAOUT Badia	*Examiner*	*Doctor (MCA)*	*U.A.T.Laghouat*
Pr. SAHRAOUI Kherris	*Examiner*	*Professor*	*U.Y.E. Tissemsilt*
Dr. RHMANI Kouider	*Examiner*	*Doctor (MCA)*	*U .Z.A . Djelfa*
Pr. BENCHATTI Ahmed	*Supervisor*	*Professor*	*U.A.T.Laghouat*
Dr. BOUALI Belkacem	*Co-Supervisor*	*Doctor (MCB)*	*U.A.T.Laghouat*

2019-2020

ملخص :

العمل المقدم في هذه الأطروحة مكرّس لتطوير محاكاة رقمية لتدفق السوائل ونقل الحرارة في نظام مجمع مكافئ اسطواني حراري وتجري المحاكاة علي نموذج أولي مصمم في ورشة الميكانيك من اجل تحليل أداء هذا النظام ويتمثل الهدف الرئيسي هو مقارنة أداء النظام مجمع مكافئ بعاكس ثانوي وبدونه يستخدم برنامج لتوفير قيم رقمية زمنية لتدفق الحرارة الشمسية لمدينة الاغواط الجزائر وقد أخذت قيم كثافة التدفق الشمسي لمدة أربعة أيام موسمية مختلفة ،يستخدم برنامج SOLTRACE المبني علي طريقة تتبع الأشعة التي تعتمد على طريقة مونتي كارلو لتحديد توزيع تدفق الحرارة علي الاسطوانة المستقبلة للحرارة من العاكس الأول . ويتم حل معادلات نقل الحرارة و معادلات تدفق المائع في الاسطوانة باستخدام برنامج ANSYS-CFXويجري تحليل المقارنة بين نظامين الأول التقليدي والثاني مع عاكس ثانوي مع استعمال (Therminol VP-1)زيت و ماء كمائعين وتبين النتائج التي تم الحصول عليها عند استخدام المائع الأول لنقل الحرارة (Therminol VP-1)ان أداء النظام هو نفسه تقريبا في الفصول الأربعة و علاوة على ذلك فإن أداء النظام مع عاكس ثانوي أفضل من أداء النظام بدون عاكس بنسبة 1.60تقريبا اما بالنسبة إلى المائع الثاني الماء تظهر نتائج المحاكاة أن أقصى درجة حرارة و مرد ودية النظام تصل أقصها خلال شهر جوان بينما يتم الحصول على الحد الأدنى من القيم في شهر ديسمبر أما بالنسبة لشهر سبتمبر و مارس يكاد يكون متماثلا و بالإضافة الى ذلك يمكن زيادة مرد ودية النظام بإضافة عاكس ثانوي والنسبة تزيد من .1.62إلى1.67

<u>الكلمات المفتاحية</u> :نظام مجمع مكافئ أسطواني اقتران انتقال الحرارة، الطاقة الحرارية الشمسية عاكس ثانوي، تتبع الأشعة، النمذجة البصرية

Abstract:

This thesis is devoted to the development of a numerical simulation of fluid flow and conjugate heat transfer in a solar thermal parabolic trough collector (PTC) system is presented .The simulation is being carried out on a prototype designed in the Mechanical Laboratory in order to analyze the performance of this system. The main objective is to compare the system performance with and without a secondary reflector (SR).PVSYST software is used to provide numerical temporal values of the solar heat flux in Laghouat city (ALGERIA).Solar flux density values for four days in different seasons have been taken .SolTrace code based on Monte Carlo ray tracing method, is used to determine the heat flux distribution on the absorber tube. The conjugate heat transfer and fluid flow equations in the tube absorber are solved by using ANSYS-CFX CFD software. A comparison between two cases (traditional PTC and PTC with parabolic secondary reflector) with (Therminol VP-1) oil and water as working fluid are analyzed. The obtained results for the first heat transfer fluid(Therminol VP-1) show that the system performance are practically the same for the four seasons. Moreover, the performance of the system with a second reflector is better than that without a second reflector with a ratio of about 1.65. However, for the second heat transfer fluid (water) the simulation results show that the maximum fluid temperatures, useful heat, and system efficiency are reached during the month of June while the minimum values are obtained on the month of December. However, for the months of September and March, the performance of the system is nearly identical. In addition, the performance of the system can be increased by using a secondary reflector with a ratio of about 1.62 to 1.67

.<u>Keywords</u>: Conjugate Heat Transfer, Receiver Tube, Solar Thermal Energy, Solar Parabolic Trough Collector, Secondary Reflector, Ray Tracing, Optical Modeling.

Résumé :

Cette thèse est consacrée au développement d'une simulation numérique de l'écoulement des fluides et du transfert de chaleur conjugué dans un système solaire thermique à capteurs cylindro-paraboliques (CCP). La simulation est réalisée sur un prototype conçu au laboratoire de mécanique afin d'analyser les performances de ce système. L'objectif principal est de comparer les performances du système avec et sans réflecteur secondaire (SR).le logiciel PVSYST est utilisé pour fournir des valeurs numériques temporelles du flux de chaleur solaire dans la ville de Laghouat (ALGÉRIE).des valeurs de densité de flux solaire pour quatre jours en différentes saisons ont été prises. SolTrace code basé sur la méthode de traçage de rayons Monte Carlo, est utilisé pour déterminer la distribution du flux de chaleur sur le tube absorbeur. Les équations conjuguées de transfert de chaleur et de flux de fluide dans le tube absorbeur sont résolues à l'aide du logiciel CFD ANSYS-CFX. Une comparaison entre deux cas (CCP traditionnelle et CCP avec réflecteur secondaire parabolique) avec l'huile (Therminol VP-1) et l'eau comme des fluides caloporteurs sont analysée. Les résultats obtenus pour le premier fluide de transfert de chaleur (therminol VP-1) montrent que les performances du système sont pratiquement les mêmes pour les quatre saisons. De plus, la performance du système avec second réflecteur est meilleure que celle sans second réflecteur avec un rapport d'environ 1,65. et pour le deuxième fluide de transfert de chaleur (eau) Les résultats de la simulation montrent que les températures maximales du fluide, la chaleur utile et l'efficacité du système sont atteintes au cours du mois de juin alors que les valeurs minimales sont obtenues au mois de décembre. Cependant, pour les mois de septembre et mars, les performances du système sont presque identiques. En outre, la performance du système peut être augmentée en utilisant un réflecteur secondaire avec un rapport d'environ 1,62 à 1,67

<u>Mots clés</u> : Transfert de chaleur conjugué, tube récepteur, énergie solaire thermique, collecteur solaire à cuve parabolique, réflecteur secondaire, traçage de rayons, modélisation optique.

Dedications

To my first teacher who gave me strength my father

To her who planted love in my heart my mother

To my lovely child Aziz

To the symbols of love and fait fullness my brother and sisters

H. M. Regue

Acknowledgments

This work was carried out in the Mechanical Engineering Laboratory and Development of Amar Thelidji University of Laghouat.

I would like first to express my deep gratitude and appreciation to my doctoral supervisors ***Pr. Ahmed BENCHATTI*** *and* ***Dr.Belkacem BOUALI*** *for giving me such a great scientific journey, for providing patient guidance, encouragement and support along the years of this degree. They, by their skills and talent, have inspired me to accomplish the goals of this thesis.*

I express my sincere thanks to ***Pr. Mokhtar AOUISSI****, Professor at the University Amar Télidji of Laghouat, for having accepted to chair the Jury of this dissertation.*

I would also like to say a big thank you to the members of the jury: ***Pr. Sahraoui KHERISS*** *Professor at the University of Tismsilet,* ***Dr. Kouider RHHMANI*** *Lecturer at the University of Djelfa, and* ***Pr. Ahmed MEDJELED*** *Lecturer at the University of Amar Télidji of Laghouat* ***, Dr. Badia GHARNAOUT*** *Lecturer at the University of Amar Télidji of Laghouat who have Accepted, without any reserve, to evaluate this thesis to its true value, and to share with me their remarks surely relevant, which, with a little hindsight, will undoubtedly contribute to the improvement of this work. THANKS!*

Table of Contents

List of Figures

List of Tables

Nomenclature

W	width of primary reflector	[m]
f	focal length	[m]
L	length of primary reflector	[m]
A_a	The aperture area	[m^2]
C_G	concentration ratio	[-]
r_r	mirror radius	[m]
W_1	Width of secondary reflector	[m]
Id	direct normal irradiation	[W/m^2]
L_1	length of arc of secondary reflector (m)	[m]
h_{p_1}	Vertical height of secondary reflector	[m]
f_1	Focal length of the secondary reflector	[m]
Q_a	total energy incident on aperture area of collector	[W]
Q_u	useful heat gain	[W]
W_1	width of secondary reflector	[m]
Tin	inlet temperature of heat transfer fluid	(K)
Tout	outlet temperature of heat transfer fluid	(K)
Cp	specific heat capacity	(J/kgK)
C_1	fraction of energy absorbed by absorber tube due to primary reflector	[-]
C_2	fraction of energy absorbed by absorber tube due to secondary reflector	[-]
E*	part of radiation solar energy incident on the secondary	[-]

	reflector	
E	part of radiation solar energy incident on the pimry reflector	[-]
A_{abs}	The absorber area	[m^2]
D_2	inside diameter of absorber pipe	[m]
D_3	outside diameter of absorber pipe	[m]
D_4	inside diameter of glass envelope	[m]
D_5	outside diameter of glass enveope	[m]
f	Darcy friction factor	[-]
f_2	friction factor for the inner surface of the absorber pipe	[-]
g	gravitational constant	[m/s^2]
h_1	convection heat transfer coefficient for the HTF at T1	[W/m^2K]
h_{34}	convection heat transfer coefficient of annulus gas at T34	[W/m^2K]
h_{56}	convection heat transfer coefficient of air at T56	[W/m^2-K]
K	incident angle modifier	[-]
k_1	thermal conductance of HTF at T1	[W/m-K]
k_{23}	thermal conductance of absorber wall at T23	[W/m-K]
k_{34}	thermal conductance of annulus gas at T34	[W/m-K]
k_{56}	thermal conductance of air at T56	[W/m-K]
k_{std}	thermal conductance of annulus gas at standard temperature and pressure	[W/m-K]
$\dot{m}$	mass flow rate	[kg/s]
$\dot{q}'_{12conv}$	Convection between inner absorber pipe and HTF	[W/m]
$\dot{q}'_{23cond}$	Conduction through the absorber pipe	[W/m]

$\dot{q}'_{3solabs}$	solar irradiation absorption rate into the absorber pipe per unit receiver length	[W/m]
$\dot{q}'_{5solabs}$	solar irradiation absorption rate into the absorber pipe per unit receiver length per unit receiver length	[W/m]
$\dot{q}'_{34rad}$	Radiation between outer absorber pipe and inner glass envelope	[W/m]
$\dot{q}'_{34conv}$	Convection between outer absorber pipe and inner glass envelope	[W/m]
$\dot{q}'_{45cond}$	Conduction through the glass envelope	[W/m]
$\dot{q}'_{56conv}$	Convection between the outer glass envelope and the ambient	[W/m]
$q'_{heat\,loss}$	total heat loss rate from the heat collecting element to the surroundings	[W/m]
$q''_{heat\,loss,i}$	heat loss rate per unit circumferential area to the atmosphere from receiver segment “i”	[W/m^2]
$\dot{q}'_{37rad}$	Radiation between the outer glass envelope and the sky	[W/m]
q'_{si}	solar irradiance per receiver unit length	[W/m]
$\dot{q}'_{i}$	net heat flux per unit circumferential area of receiver segment “i”	[W/m^2]
$h_{i,inlet}$	enthalpy at inlet of receiver segment “i” [J/kg]	[J/kg]
$h_{i,outlet}$	enthalpy at outlet of receiver segment “i” [J/kg]	[J/kg]
Cp	specific heat of heat transfer fluid, (J/kg.K)	[J/kg.K]
$T_{inlet,i}$	HTF temperature at inlet of receiver segment “i”	[^{o}C]
$\dot{q}'_{12conv,i}$	Convection between inner absorber pipe and HTF per unit receiver segment length for receiver segment “i”	[W/m]

$\dot{q}'_{57rad}$	radiation heat transfer rate between the outer surface of the glass envelope to the sky per unit receiver length [W/m]	[W/m]
$\dot{q}'_{57rad,i}$	radiation heat transfer rate between the outer surface of the glass envelope to the sky per unit receiver segment length for receiver segment "i"	[W/m]
$\dot{q}'_{56conv}$	convection heat transfer rate between the outer surface of the glass envelope to the atmosphere per unit receiver length	[W/m]
$\dot{q}'_{56conv,i}$	convection heat transfer rate between the outer surface of the glass envelope to the atmosphere per unit receiver segment length for receiver segment "i"	[W/m]
$\dot{q}''_{solar\,abs,i}$	incident solar irradiation absorption rate per unit circumferential area of receiver segment "i"	[W/m^2]
$\dot{q}''$	net heat flux per unit circumferential area of receiver segment "i"	[W/m^2]
t_0	The initial instant	[s]
h	Enthalpy	[J/kg]
Cp	Heat capacity	[J/kg.K]
Ai	Cross sectional area of segment i	[m^2]
T_1	Temperature of heat transfer fluid	[^{o}C]
T_2	Temperature of inner absorber tube	[^{o}C]
T_3	Temperature of outer absorber tube	[^{o}C]
T_4	Temperature of inner glass envelope	[^{o}C]
T_5	glass envelope outer surface temperature	[^{o}C]
T_6	Ambient temperature	[^{o}C]
T_7	Sky temperature	[^{o}C]
T_{23}	average absorber wall temperature, $(T_2 + T_3)/2$	[^{o}C]

T_{34}	average temperature of annulus gas, $(T_3+T_4)/2$	[^oC]
Tin	Temperature at the inlet	[^oC]
Tout	Temperature at the outlet	[^oC]
$T_{inlet,i}$	HTF temperature at inlet of receiver segment "i"	[^oC]
$T_{outlet,i}$	HTF temperature at outlet of receiver segment "i"	[^oC]
v_{56}	kinematic viscosity of air at T_{56}	[m^2/s]
$\Delta L_{aperture}$	receiver segment length	[m]
a	accommodation coefficient of annulus gas	[-]
C, m, n	constants	[-]
P	pressure	[Pa]
[A]	Coefficient matrix	[-]
Ui	Average velocity field	[m/s]
(i=1 ,2,3)		
[b]	Second Member Vector	[-]
N	Form function	[-]
nj	Exit Normal Vector	[-]
t	time	[s]
u, v, w	Velocity field components	[m/s]
ipn	Integration point	[--]

Numbers without dimensions

Nu	Nusselt number
Ra	Rayleigh number
Re	Reynolds number
Pr	Prandtl number

Greek characters

ρ_{trough}	mirror reflectance	[-]
α_{env}	absorptance of the glass envelope	[-]
τ_{env}	glass envelope transmittance	[-]
ρ_{sec}	mirror reflectance of secondary reflector	[-]
γ	intercept factor	[-]
ρ	density	[kg/m^3]
ε_3	emissivity of absorber selective coating	[-]
ε_4	emissivity of inner surface of glass envelope	[-]
ε_5	emissivity of outer surface of glass envelope	[-]
σ	Stefan-Boltzmann constant	[W/m^2-K^4]
α	thermal diffusivity of air at T_{56}	[m^2/s]
β	volumetric thermal expansion coefficient of annulus gas or air	[1/K]
δ	molecular diameter of annulus gas	[cm]
α_{abs}	absorptance of the absorber	[-]
ψ	ratio of specific heats of annulus gas	[-]

η_0	optical efficiency at the absorber	[-]
λ	mean-free-path between collisions of a molecule of annulus gas	[cm]
μ	dynamic viscosity	[kg/m·s]
θ	incidence angle of the solar radiation	[degree]
η	thermal efficiency	[-]
Φ	Solution vector (u, v, w, p)	[-]
Γ_{ij}	Interfacial mass flow rate	[-]
ζ, ξ	Local spatial coordinates	[-]
θr	Rim angle	[degree]

Abbreviation

HTF	heat transfer fluid
PTC	parabolic trough collector
SEGS	Solar Electric generating Systems
DSG	Direct Steam Generation
LFR	Linear Fresnel Reflector
CSP	Dish concentrating solar power
STS	solar tower system
CFD	Computational Fluid Dynamics
RMSE	Root Mean Square Error
NUHF	non-uniform heat flux distribution
MCM	Monte Carlo Method

FVM	Finite Volume Method
MCRT	Monte Carlo Ray-Trace
HCE	heat collection element
SRT	solar ray trace

General Introduction

General Introduction

In the recent years, energy consumption has been increased significantly with the increase of population. According to the Word Energy Outlook (2012), energy demand is estimated to be increased more than one-third for the period between 2012 and 2035 [1]. Fossil fuel is still prevailing among other carbon fuel sources for global energy supply. According to the International Energy Outlook, 84.7% of the world energy consumed is provided by fossil fuels [2]. Our country Algeria depends essentially on the two fossil sources in its own production of electrical energy (gas and oil). However, in view of the rapid development of technology in the field of renewable energy in recent years Algeria is looking for other inexhaustible and environmentally friendly sources. Among these sources, solar energy is considered the most important for the production of electricity. Algeria, which has an exceptional solar potential with more than 3000 hours of sunlight and an area of 2381745 Km^2 decided to set up a strategy to develop different applications of solar energy and in particular concentrated solar power systems for the production of electricity that would benefit the South regions. In 2011, Algeria is launching an ambitious program to develop renewable energies and energy efficiency, with a total cost of 120 billion dollars [3]. This vision of the Algerian government is based on a strategy focused on the development of inexhaustible resources such as solar, wind and biomass and their use to diversify energy sources and prepare the Algeria of tomorrow. Through a combination of initiatives and intelligence, Algeria is engaging in a new sustainable energy era. The Program consists in installing a power of renewable origin of nearly 22,000 MW between 2011 and 2030 including 12,000 MW will be dedicated to cover national electricity demand and 10,000 MW for export to Europe. The export of electricity is, however, conditional on the existence of a long-term purchase guarantee, reliable partners and external financing. Under this program, renewable energy sources are at the heart of Algeria's energy and economic policies: by 2030, around 40% of the electricity produced for national consumption will be of renewable origin.

Indeed, Algeria intends to position itself as a major player in the production of electricity from photovoltaic solar energy and concentrated thermal solar energy, which will be the engines of sustainable economic development capable of driving a new growth model.

Algeria has a surface area of 2381745 km^2 covered by an exceptional amount of sunshine estimated at nearly 3000 hours per year. This abundant and free potential has prompted the country's authorities to put in place a strategy to develop various applications of solar energy, including concentrated solar power systems for electricity generation, which would benefit the southern regions [4]. Concentrating solar thermal technology captures direct sunlight from the sun on a large reflective surface and concentrates it on a receiver to achieve higher temperatures. These high temperatures essentially allow the production of steam to power a steam turbine, and then produce electricity through an alternator. The principle of concentrated solar power can also be found in other applications, such as cooking, seawater desalination or the treatment of pollutants. There are four main types of solar concentrators for the production of energy from the sun's rays, namely: parabolic trough concentrators, parabolic concentrators, Fresnel mirrors, and solar towers [5]. In the field of solar energy conversion, the parabolic trough concentrator technology appears to be the most economical, mature and robust technology [6]. The sun's rays are concentrated on a solar receiver using mirrors, which are converted into heat or electricity. The conversion of solar radiation into thermal energy can either be used directly (e.g. to heat a building), or indirectly (to produce water vapor used in thermal power plants to drive alternators and thus obtain electrical energy). Parabolic trough collector sensors consist of parabolic mirrors arranged at the rear of a tube-shaped sensor. The parabolic shape of the mirrors allows the sun's rays to be concentrated throughout the tube. By circulating the heat-transfer fluid in the center of this tube, the fluid is heated and conducts the heat to the container with a determined flow rate [7].

In the realization of a solar thermal concentrator, we try to minimize heat loss in order to increase performance. The work done focused on an experimental study to convert solar energy into thermal energy using a cylindrical parabolic solar concentrator. The experiment was conducted on a sample prototype for concentration with an opening of $4m^2$. This prototype was set up in the mechanical laboratory using local means. The development of a simple theoretical model can estimate the global solar irradiance at the reflector (Sun meters). To measure the wind speed we used an anemometer, as well as other parameters at the receiver, including the temperatures (thermocouple). The overall system is the subject of a digital computer simulation. The software (myPCLab), designed for this purpose, controls the device system and ensures the acquisition of certain parameters by means of a recorder communicating through a computer. In the second experiment, we focus on the temperature difference (input - output) of the water and oil , the temperature obtained is of the order of 75C° with an average flow difference. [7bis]

This thesis is devoted to the experimental study and energy optimization of the conjugate heat exchange, with variable geometry, in a double reflection of parabolic trough collector. The main objective is to improve the performance of the conventional parabolic trough concentrator by incorporating a second reflector. Several geometries of the latter are tested in order to homogenize the solar flux distribution on the lateral surface of the absorber tube. The key parameter is the temperature of the heat transfer fluid at the tube outlet. The optimum geometry chosen is the one that allows the highest outlet temperature. This temperature is directly proportional to the amount of energy absorbed by the tube. Therefore, the efficiency of the system will be better as the exit temperature of the tube is higher. So, the procedure will be based, in the first instance, on obtaining the solar flux data present in the LAGHOUAT region. To do this, PVSYST software is used to provide numerical temporal values of the solar heat flux for four days of the year (analyzed only by numerical simulation). The next step concerns the numerical study of the optical and geometrical performances of the system using SolTrace software. This analysis is used to obtain the flux distribution of the solar radiation concentrated by the two reflectors on the absorber tube, followed by CFD analysis of the fluid flow in the tube and the associated conjugate heat transfer. To do so, ANSYS-CFX solver is used to model and solve the coupling of the different equations that govern the transport phenomena (heat transfer and flow) that occur at the absorber. Note that the flow distribution data, obtained in the previous step, are introduced into the solver as variable boundary conditions on the lateral surface of the absorber tube. This simulation will thus describe the performance of this system over a period of one day from 9:00 a.m. to 6:00 p.m. for four days of different seasons. Note that all experimental tests and numerical simulations are performed for two cases: Concentrator with and without a second reflector. The objective is to show the interest of using a secondary reflector. In order to analyze the system performance, several absorber tube base materials are also tested. In order to reach the objectives mentioned above, we believe that it is useful to organize the manuscript in six rather uneven development chapters:

- **The first chapter** provides an overview of the different types of solar energy, the historical development of parabolic trough technology, and its applications. The focus is particularly on the absorber tubes, the composition and the materials used. Articles, text Books and even software dealing with this subject will be quoted in broad outline in order to describe the state of the art in this field of research.
- **The second chapter** presents, the optical analysis of the parabolic cylindrical concentrator. The aim is to determine the distribution of the concentrated solar flux on the lateral area of the absorber tube. To do this, the open source code SolTrace is used for the ray tracing using the generalized Monte Carlo method. The application of this method to the concentration system is discussed in detail in this chapter.
- **The third chapter** is devoted to the theories and definitions relating to the different modes of heat transfer in a parabolic cylindrical concentrator with its geometrical parameters. The system of equations governing this conjugate heat transfer (solid-fluid) and the flow of fluid within the absorber tube will be presented in its adapted form (relative to the system in question and under the appropriate assumptions).
- **The fourth chapter** presents the numerical modeling of the conjugated heat transfer and the fluid flow inside the absorber tube. This modeling is carried out in two steps: optical modeling established with SolTrace software, which calculates the concentrated solar flux received at the absorber. CFD modeling of the absorber with ANSYS- CFX software, which allows to determine the temperature distribution and consequently the energy absorbed by the tube.
- **The Fifth chapter** is about the presentation and interpretation of the various results obtained by experimental and numerical methods. The objectives of the tests are the validation of the numerical model and the comparison of systems with and without secondary reflector. In order to optimize the energy system, possible improvements to the system will be presented and discussed.

Finally, we will end with a general conclusion and we will quote in perspective the future work to be initiated in continuity to this thesis work.

Chapter I

Review on Thermal Solar Concentrators

Review on Thermal Solar Concentrators

I.1. Introduction

The electricity production process in a CSP is similar to that of conventional thermal power plants with the only difference that the heat does not come from coal, gas or fuel, but rather from the sun. Reflectors or mirrors are used to reflect and concentrate the sun's rays onto a heat exchanger called a solar receiver. Concentrating the sun's energy on the receiver generates high-temperature heat. A heat transfer fluid (HTF) circulates in this receiver to absorb the thermal energy, thus increasing its temperature. The heat transfer fluid is then used to power a thermodynamic cycle directly or indirectly by circulating in storage tanks. Electricity is then generated through an alternator coupled to the turbine of the thermodynamic cycle [8].

Four types of CSP are currently in use around the world [9-11]. Throughout the literature, these four types are called CSP with parababolic trough collector, CSP with parabolic collector, CSP with Fresnel linear collector and tower CSP.

The geometry of the different reflectors implies a significant difference in the way they reflect and concentrate the sun's rays. The different types of CSP are thus classified into two categories, namely linear concentration systems [12,13] and point concentration systems [14]. Linearly focused systems refer to CSP that focus the sun's rays on the focal line of the reflector; while point focused, systems refer to CSP that focus on the focal point.

I.2. Different CSP technologies

I.2.1. Parabolic Trough Concentrators

Parabolic-trough solar concentrating systems are parabolic-shaped collectors made of reflecting materials. The collectors reflect the incident solar radiation onto its focal line toward a receiver that absorbs the concentrated solar energy to raise the temperature of the fluid inside it as shown in Figure **(I.1)**.

The receiver is an absorber tube, which is usually a black metal pipe, coated with a glass pipe in order to reduce heat losses by convection. Selective coating is applied to the internal pipe, to enhance tube absorbance and reduce its emittance. The glass pipe is instead covered by anti-reflective coating, in order to increase trasmissivity. Since the collector is linear, with the parabolic shape only in one dimension, the receiver has a tubular shape, with a single axis tracking required. Furthermore, these concentrators have a modular feature, since each row of reflectors is an independent system, with its own receiver tube, and tracking the sun autonomously [16].

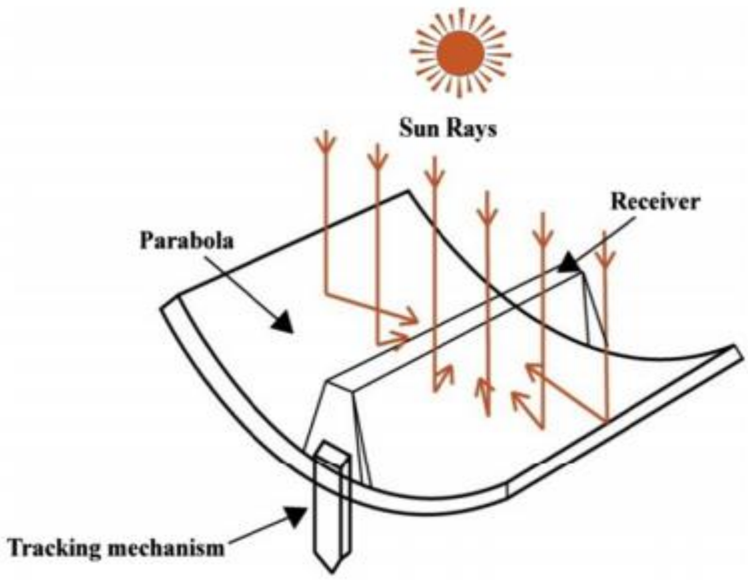

Figure I.1. *Schematic of a parabolic-trough solar concentrator [15].*

Thermal oil, in particular diphenyl-oxide/byphenyl eutectic mixture, is usually used as Heat transfer fluid (HTF), but the operating temperature has to stay below 400°C to avoid decomposition. Thermal energy storage can be easily implemented in this type of plant, usually with a dual tank of molten salt, for hot and cold wells. Molten salts might be directly used also as HTF, offering the advantage of being less corrosive and having a higher boiling/decomposition point rather than synthetic oils; however they usually have a high solidification temperature (around 150°C), thus a trace heating system has to be included along the tubes to avoid freezing of the salt [16]. In addition, water has been used in existing plants, and usually the preferred configuration is Direct Steam Generation (DSG), where the water/steam HTF is directly sent to the turbine [17].

PTC offers the most mature technology among the CSP applications, and 75% of the existing facilities are based on this technology [16]; a large number has been installed around the world, for instance, the SEGS (Solar Electric generating Systems) has been installed in the California desert, with a total capacity of 354 MW [17]. This system see Figure (I.2) consists of a long parabolic-shaped collector with curved mirrors that focuses the sun's rays on a receiver pipe (absorber tube) located at the focal point of parabolic troughs. These troughs can be more than 600 m in length and the metal absorber tube is usually embedded into an evacuated glass tube to reduce heat losses. The troughs are rotated throughout the day as the sun moves from east to west to maximize the received solar energy. The metal absorber tube is filled with fluid, typically synthetic oil, which can be heated up to 400°C. Because of the parabolic shape, the troughs can focus the sun at 30–100 times its normal intensity. The fluid is then pumped through a heat exchanger that transfers heat to water which produces steam on boiling the water. The steam is used to run a turbine , which generates electricity.

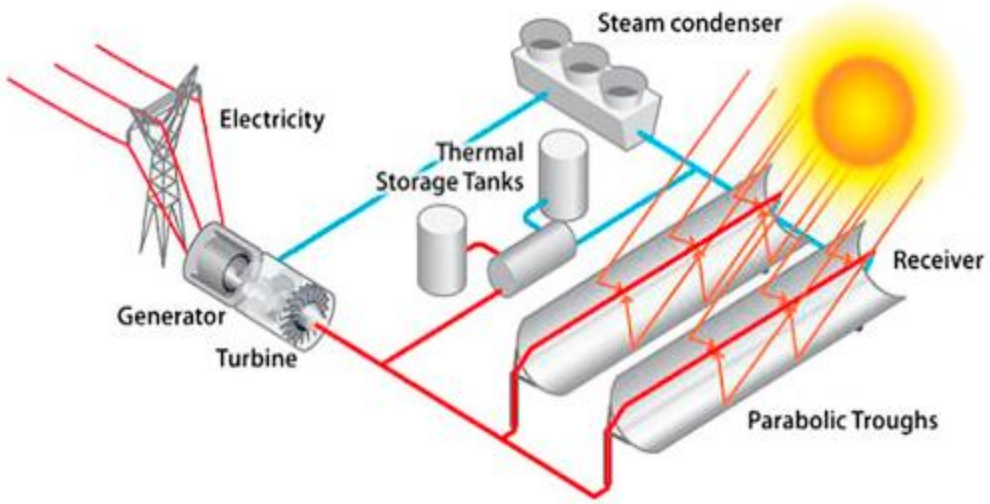

Figure I. 2. *Parabolic trough system.*

The use of other heat transfer fluids like molten salts or direct steam allows the operation up to 550°C, hence improving the plant efficiency. These systems can also be designed as hybrids by using fossil fuel to back the solar thermal output during nighttime or during periods of cloudy days [15]. This technology (sometimes designated as PT for Parabolic Trough) is considered to be the most mature today, mainly through from SEGS plants in California, connected to the grid for more than 20 years. The consequence of this maturity is that the vast majority commercial power plants in operation or planned today operate with this technology. The most recent significant example is the inauguration in March 2013 of the Shams 1 power plant in Abu Dhabi, in the United Arab Emirates. This plant, with a unit capacity of 100 MW, uses synthetic oil as a heat transfer fluid and has an auxiliary power unit (fuel burners) by way of as a supplement for periods of low sunlight [15].

I.2.1.1. **The oil heat transfer fluid**

Synthetic oil is the most commonly used heat transfer fluid in power plant absorbers today. There are more than 25 years of experience with this HTF in parabolic trough power plants. It has been proven that the technology is reliable, which is also an important argument for investors and operators to go on using it. Synthetic thermo oil satisfies quite well the mentioned requirements. It is liquid until 12°C, which means that freeze protection is quite easy or even unnecessary. It has quite a high specific heat capacity and it can be acquired in large quantities. However, it has also some disadvantages and limitations:

- The maximum operation temperature is about 400°C. Beyond this temperature, thermal cracking happens, which destroys the thermo oil. It resists higher temperatures than mineral oil. However, live steam temperature is limited to about 370 °C, which limits the power block efficiency.
- Thermo oil has to be replaced periodically because of aging processes (i.e. the chemical structure changes over longer time spans).
- Thermo oil is quite expensive. About 5% of the investment costs for the Andasol power plants must be afforded for the HTF.
- The high costs and also high vapour pressures at the operation temperatures impede that thermo oil is used as storage medium.
- Thermo oil is environmentally less friendly than some other possible media. Leakages are not only a problem for the plant operation but also for the environment.

I.2.1.2. **Mineral oil heat transfer fluid**

Mineral oil was used in the first SEGS plant, which started operation in 1985. It had the advantage that a direct storage system could be implemented, i.e. a storage system that uses the HTF directly as storage medium, because mineral oil can be used as thermal storage medium as well. However, the main disadvantage of mineral oil, which motivated its substitution by thermo oil, is its operation temperature limit. At temperatures above 300°C, it gets unstable. [22].

I.2.1.3. **The Water heat transfer fluid: direct steam generation**

While having a significant potential to reduce construction and operating costs compared to PT (oil) power plants, Direct Steam Generation (DSG) in parabolic trough collectors is currently used in only one commercial power plant, the TSE-1 plant in Thailand. This 5 MW plant was inaugurated in 2012 and was developed by the German company Solarlite. Other projects for the construction of similar power plants in Thailand are currently underway. The DSG consists in using the working fluid of the thermodynamic cycle also as a fluid heat transfer medium: water vapor is generated directly in the solar field of the power plant, which eliminates the oil circuit and expensive water/oil exchangers. The difficulty with this technology is under the high-pressure and high-temperature conditions required for turbining the fluid, as well as to the presence of two-phase flow in the absorber tubes [22].

I.2.1.4. **Molten salts heat transfer fluid**

Research teams from the Italian Agency for Energy Research (ENEA) are studying currently the use of molten salts as a heat transfer fluid in parabolic trough collectors [22]. As part of the Archimede project, a power plant using molten salt as both a heat transfer and storage fluid is in the demonstration phase at the ENEL site in Priolo Gargallo, Sicily.

I.2.2. **Linear Fresnel Reflector**

This technology, known by the acronym LFR (for Linear Fresnel Reflector) is the second most advanced in the world [17]. Linear Fresnel reflector systems produce a linear focus on a downward facing fixed receiver mounted on a series of small towers as shown in Figure (I.3). With very long, narrow and with a light curvature (tending to be flat) collectors, which reflect light onto the surface of a linear absorber; this absorber is a fixed structure, which is placed above the mirrors and it is the same for all the rows [16]. The name of this technology refers to the principle of the Fresnel lens, which makes it possible to obtain a short focal length without the high weight and volume of a conventional lens. The flat mirror set acts as a kind of Fresnel lens. [17]

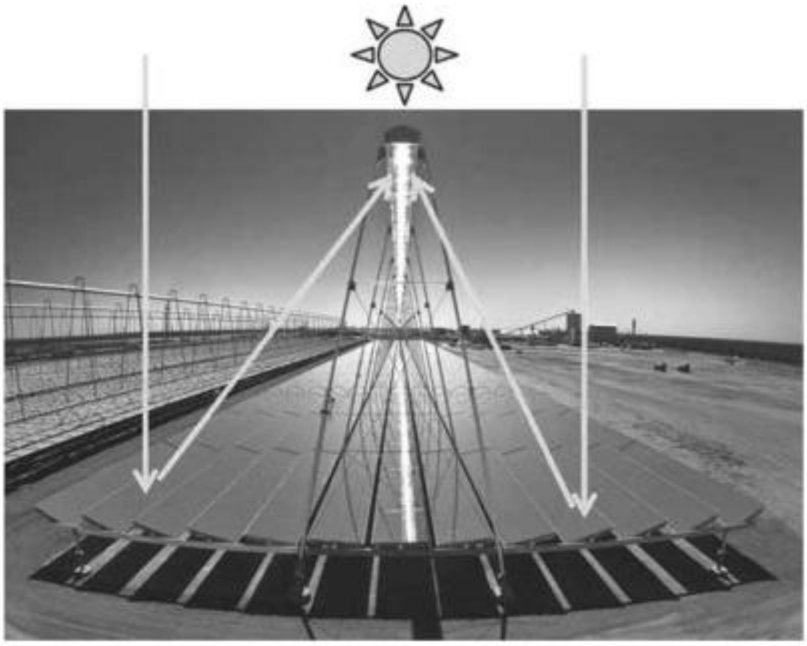

Figure I. 3. *Linear Fresnel Reflector [18].*

The receiver configuration used in LFRs can vary, but often includes a secondary reflector to further concentrate the radiation, and one or more absorber tubes. The technology has several advantages over parabolic-cylinder technology:

- A set of flat mirrors replaces the parabolic concentrator: the manufacturing process is therefore more simple and less expensive;
- The fixed position of the receiver lends itself better to the use of direct steam generation. The use of floor space is optimized [17].

Linear Fresnel reflector solar power generation Figure (I.4) is a system that concentrates solar beam radiation into a receiver tube mounted at the focal point of the Fresnel mirror through the FLR mirror tracking of the movement of the sun and generates high-temperature working media for thermal cycle power generation. Major components of LFR power generation include the liner reflective mirror, receiver tube, and transmission system. The LFR power generation system is a simplified parabolic trough power generation system. The parabolic trough concentrator is replaced by a surface mirror; the mirror features a small distance to ground, low wind load, a simple structure, an intensive layout, and higher land-use efficiency. Furthermore, vacuum treatment for the receiver tube is not necessary, thus reducing technical difficulties and costs. The total cost of the system is comparatively low. However, due to the system's low concentration ratio, the operational temperature stays low, resulting in low system efficiency as well. [19].

Figure I. 4. *Linear Fresnel reflector solar power generation [19].*

Fresnel's linear reflector technology is very young, having only recently entered the commercialization phase. The Puerto Errado 1 power plant located in the Murcia region of Spain was, in 2009, the first LFR plant in the world to be connected to the electricity grid. With a capacity of 1.4 MW electric, it was followed in 2012 by Puerto Errado 2 with a capacity of 30 MW.

I.2.3. **Parabolic Dish Systems**

A dish system consists of a parabolic shaped concentrator, tracking system, solar heat exchanger (receiver), an (optional) engine with generator, and a system control unit Figure (I.5). The concentrator tracks the sun bi-axially in such a way that the optical axis of the concentrator always points to the sun. The solar radiation is focused by the parabolic concentrator onto the solar receiver, which is situated close to the focal point of the parabola. The receiver absorbs the solar radiation; the absorbers usually used are direct illumination receivers, heat pipes or volumetric receivers [9]. The receiver captures the high temperature thermal energy into a fluid that is either the working fluid for a receiver-mounted engine cycle, or is used to transport the energy to ground-based processes. In the case of a receiver-mounted engine, a directly coupled generator finally converts mechanical energy into electricity

A reflective surface on the paraboloidal concentrator, either metallized glass or plastic, reflects incident sunlight to a small region called the focus. The ideal shape of the reflecting surface of a solar concentrator is a paraboloid. The size of the focus depends on the precision of the shape of the concentrator, surface reflectivity and condition as well as focal distance. Common dish concentrators achieve geometric concentration ratios between 1,500 and 4,000. Dish concentrator diameters range from 1–2 m up to 25 m. [21]

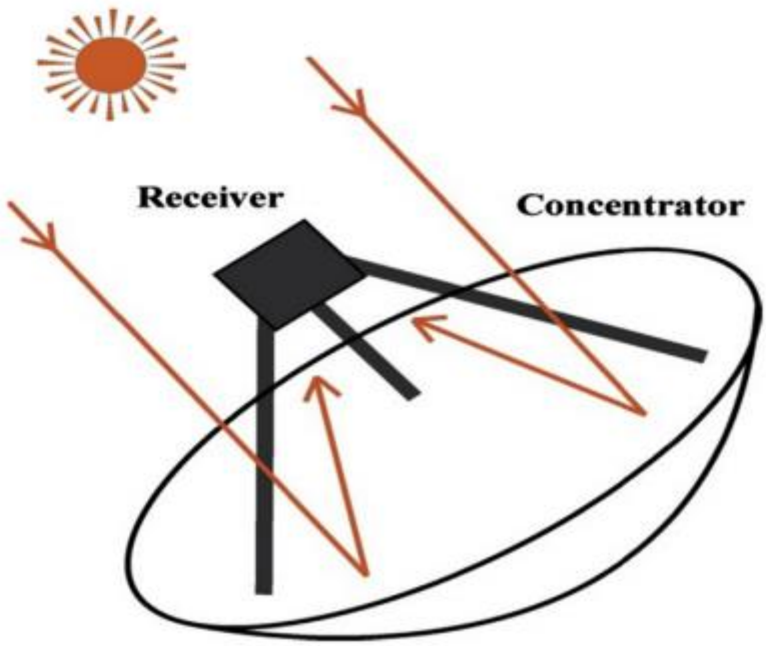

Figure I. 5. *Schematic of a parabolic-dish solar concentrator [15].*

Dish concentrating solar power (CSP) systems Figure (I.6) use paraboloidal mirrors, which track the sun and focus solar energy into a receiver where it is absorbed and transferred to a heat engine/generator or else into a heat transfer fluid that is transported to a ground-based plant. Dish concentrators have the highest optical efficiencies, the highest concentration ratios and the highest overall conversion efficiencies of all the CSP technologies. The bulk of commercial CSP activity with dish concentrators involves the use of receiver integrated Stirling engines for direct production of electricity. However, dish concentrators can be used to drive the whole range of energy conversion processes that are open to CSP technologies in general. The field of possible applications covers, on the one hand, the support of smaller or large grid connected systems, and on the other hand, stand-alone systems that can power, for example, water pumps or desalination plants. If dish Stirling systems are installed in clusters, applications up to 10 MW can be realized. Above this range, other solar thermal systems may be economical or more efficient. [21]

Figure I. 6. *Parabolic dish concentrating solar power (CSP) systems [21]*

Today there is no such commercial plant in operation. The Maricopa Solar Plant, located in Arizona, was dismantled in 2011. With a capacity of 1.5 MW, the plant had 60 dish units and operated between 2010 and 2011 [22].

I.2.4. **Solar Power Towers**

The solar tower takes a slightly different approach to solar thermal power generation. While the parabolic trough array uses a heat collection system spread throughout the solar array, the solar tower concentrates heat collection at a single central facility. The central facility includes a large solar energy receiver and heat collector, which is fitted to the top of a tower. The tower is positioned in the center of a field of special mirrors called heliostats, each of which is controlled to focus the sunlight that reaches it onto the tower-mounted solar receiver. This type of solar thermal plant is referred to as a point-focusing solar thermal plant. The arrangement is shown schematically in Figure (I.7) [23].

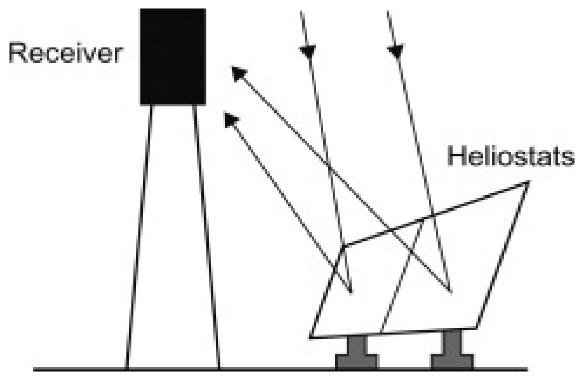

Figure I. 7. A solar tower system. [23]

The power tower systems Figure (I.8) consist of a field of thousands of sun-tracking mirrors, which direct insolation to a receiver atop a tall tower [24].

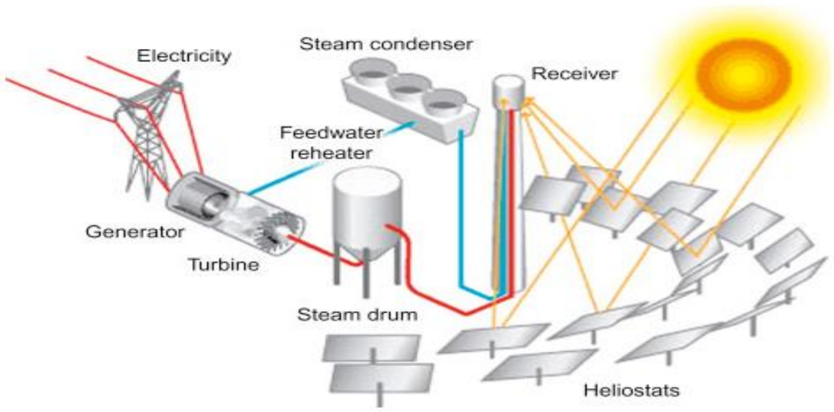

Figure I. 8. *A solar tower power plant [24]*

This field also includes several different technologies, depending on the type of heat transfer fluid used.

I.2.5. **Molten salt heat transfer plants**

With this technology see Figure (I.9), the liquid salt serves as both a heat transfer and storage fluid. The multiplication of heliostats makes it possible to produce punctually heat in excess of the electrical demand and store it in the hot tank of the power plant. As the molten salt is heated than in linear sensors, the temperature difference between the hot and cold tanks is higher than in linear sensors. Cold is higher and the amount of fluid to store the same amount of energy is therefore lower.

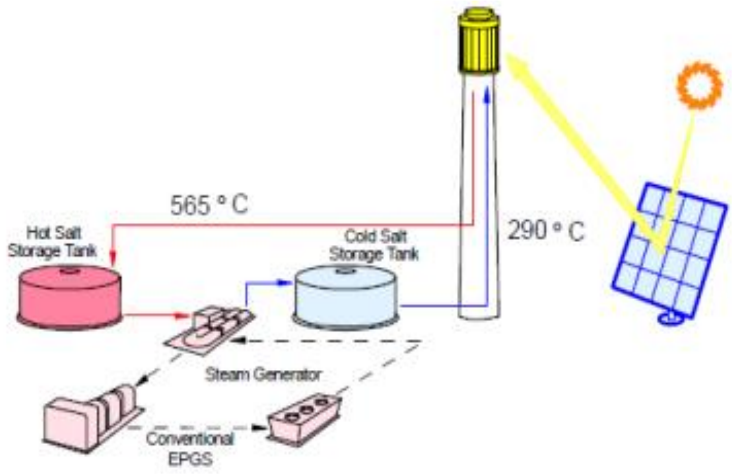

Figure I. 9. *Schematic diagram of direct storage salt heat transfer power plants [25]*

The state of the art of this technology is represented by the Gemasolar commercial power plant (also named Solar Tres) built by Torresol Energy and inaugurated in Andalusia in 2011 Figure (I.10). This plant provides 19.9 MW of electricity and has inherited the experience gained from the THEMIS projects in France, and Solar One and Solar Two in the United States. Gemasolar has a field of 2650 heliostats. Spread at 360°C around the tower over an area of 185 hectares. It has storage tanks to ensure 15 hours of production without sunshine [26].

Figure I. 10. *Vue de la centrale Andalouse Gemasolar (source : Torre sol Energy) [22]*

I.2.6. **Water/steam heat transfer plants**

As with the linear-sensor die, direct steam generation in tower power plants eliminates the need for a heat transfer fluid/working fluid heat exchanger. The water is vaporized in the tower receiver and used directly in the thermodynamic cycle, possibly with a small amount of temporary storage. The generation of superheated steam allows, on the one hand, the use of turbines that are more compact and less costly than saturated steam. [26], and on the other hand working close to maximum efficiency. Overheating, generates, however the same problems of high thermal gradients in receivers than in linear sensor technologies.

The Spanish commercial power stations PS10 and PS20 Figure (I.11), which were the first to be connected to the grid (in 2007 and 2009 respectively) use saturated steam generation.

Figure I. 11.*View of the PS20 power plant (source: Abengoa Solar) [22].*

The American IvanPah project currently under way in the United States is planning to bring the desert into service. Mojave of three production units using superheated steam, for 377 MW electrical products see Figure (I.12).

Figure I. 12. *View of Ivanpah power plant (source: Ivanpah Solar) power plants [22].*

I.2.7. **Air heat transfer plants**

The configuration is similar to that of salt heat transfer towers, but the fluid used is air at atmospheric pressure heated in a porous volumetric receiver. The air receiver makes the thermal inertia of the plant quite low. It does not exist at our knowledge of tower trading centers using this technology. Only the experimental facilities have been exploited, in particular at PSA by DLR and CIEMAT [26].

I.3. **Parabolic trough technology development**

In 1870, a successful engineer, John Ericsson, a Swedish, designed and built a 3.25 m^2 aperture collector, which drove a small 373W engine. Steam was produced directly inside the solar collector (today called Direct Steam Generation or DSG). During the next years, he built seven systems similar to the first one. However, he used air instead of water as a working fluid [27]. In 1883, Ericsson constructed a large “sun motor” (3.35 m long and 4.88 m wide), exhibited in New York, which focuses the sunrays on a 15.88 cm diameter boiler tube. The trough comprised of wooden staves, and iron rips that were attached to the sides of the trough. The reflector surface was made of window glass, and they were installed on staves. The whole system tracked the sun manually [28].

The next reference is dated 1907, Wilhelm Meier and Adolf Remshardt from Germany obtained a patent on parabolic trough collector technology. The goal of the system was to generate steam [29]. From 1906 to 1911, Frank Shuman, an American engineer, constructed and tested a number of solar engines including different sorts of non-concentrating and low-concentrating solar collectors (an absorber with flat reflector wings). Some of them were used for pumping irrigation water in Tacony, Pennsylvania (United States). After gaining experience with these systems, in 1912, he constructed a large irrigation pumping plant as shown in Figure I.13 in Meadi, small village near Cairo, near the Nile River Egypt, with the help of an English consultant, Charles Vernon Boys. An alternative change was suggested by C.V. Boys, which is that glass-cover boiler tubes were positioned along the parabolic trough collector. The system consisted of 5 rows of PTSC facing north-south. Each row has a length of 62.17 m and width of 4.1 m with absorber diameter of 8.9 cm and concentration ratio of 4.6. The total collecting surface was 1250 m^2, and the total land area occupied was 4047 m^2 [27-29]. The system was capable of producing 27,000 liters of water per minute [28].

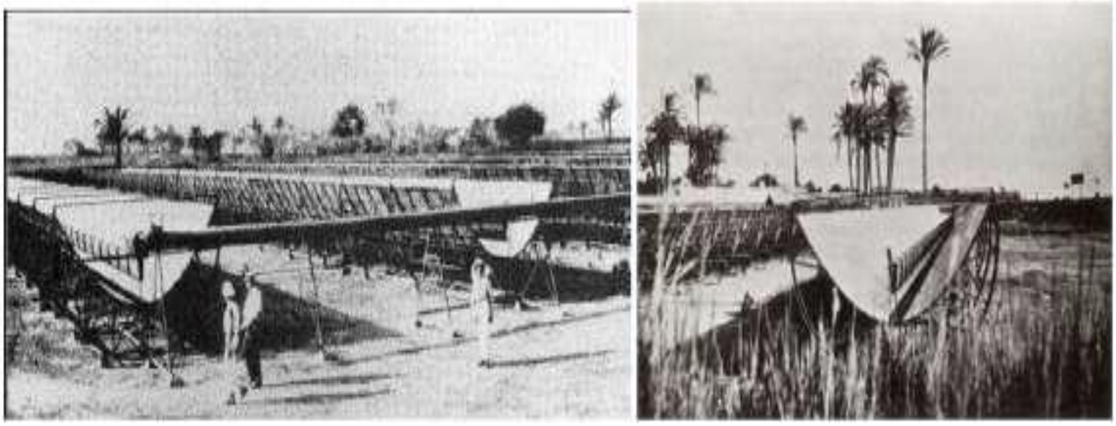

Figure I. 13. *Irrigation pump plant in meadi, Egypt. Adopted from [28].*

In 1936, C.G. Abbot converted solar energy into mechanical power by using a PTC and steam engine with an overall efficiency of 15.5%. To reduce heat loss, He used a single tube covered double-walled evacuated glass placed along the focal axis. The system was designed so that saturated steam was produced at 374 °C after exposure the PTSC to the sun for five minutes [27, 29]. In 1938, he used a similar boiler in Florida to power a 0.15 kW steam engine. As quoted by Spencer, Abbot suggested that a system using this boiler to produce steam at 225 C should obtain a theoretical overall efficiency of 15.5% and a real efficiency of 11.7% [30].

The interest in solar concentrating technology was negligible for almost 60 years. However, PTSC activities started again in the mid-1970s in response to the oil crisis. The Honeywell International Inc and U.S. Government's Sandia National Laboratories designed the first two collectors in the United States in the mid-1970s, and they were designed to function with temperatures below 250°C. Later, in 1976, three PTSCs were constructed and tested at Sandia to 3.66 m long, 2.13 m wide, and black chrome coated absorber covered by 4 cm glass envelope [31]. In 1979, a company, LUZ international Inc., was constituted in The United States and Israel, and the goal was to develop and construct cost-effective parabolic trough collectors for solar thermal heat applications. Luz built three new generations of parabolic trough collectors which known as; LS-1, LS-2, and LS-3 Figure (I.14) which were installed in Solar Electric Generation Systems (SEGS) plants. The first two generations, LS-1 and LS-2, had similar assemblies. They had same length, but the aperture width of LS-2 is twice of LS-1. The structure was based on a rigid structural support tube known as the torque tube. In LS-3, the length was twice of LS-2, and the width was 14% wider than LS-2. An alternative mode of tracking was adopted which is a hydraulic control system instead of mechanical gear [27,32].

Figure I. 14. *Front (left) and rear (right) views of LS-3 collector.*

In the1980s, parabolic trough technology was introduced into the marketplace. Many American companies manufactured and sold parabolic trough collectors such as:

- Acurex Solar Corp manufactured Acurex 3001 and 3011 models Figure (I.15).

Figure I. 15. *Front (left) and rear (right) views of the Acurex 3001 collector.*

- Suntec Systems Corp. –Excel Corp manufactured IV and 360 models
- Solar Kinetics Corp built T-700 and T800 models
- Solel solar energy constructed IND-300 model
- The Suntec Systems Inc. built IV parabolic trough collector model

In 1998, a group of European companies and research laboratories was founded to develop and build a new generation of PTSC. After studying many different collector structures, the first reading of a new figure was constructed which is known as ET-100. The model consisted of 8 modules with an aperture area of 545 m^2. After that, the second version was developed and named as ET-150. It had a number of modules of 12 with an aperture area of 820 m^2 [32]. In 2003, a third version of European collector was constructed, and it was named as SKAL-ET. It had a modules number of 12 with effective aperture area of 4360 m^2. It had been erected at SEGS-V plant in California, USA since that time [27]. In 2005, a new PTSC called SENERTROUGH-I was developed by the Spanish company, SENER. It had the same size as the LS-3 collector, but the support structure was same as LS-2 collector. A loop of 600 m of SENERTROUGH-I collector was installed in the Andasol -1 concentrating solar power plant in Spain [27] [33].

The first parabolic trough power plant in Europe is Andasol 1 in Spain. The construction of the plant started in 2006 and the power production began in November 2008. Andasol 1 is the first parabolic trough power plant with storage system where 7.5 hours storage system is integrated in the plant. There are many other plants in Spain of similar characteristics either operational such as Anadasol 2 (50 MW with 7.5h storage) and Majadas 1 (50 MW with storage), or under construction like Vallesol 50 (50 MW with 7.5h storage) [28].

In the Middle East and North Africa (MENA) region, recent implementation of parabolic trough plants has taken place. Two Integrated Solar Combined Cycle utilizing parabolic trough are now in operation since mid-2011, the first one is ISCC Algeria in Hassi R'mel (Algeria) with a capacity of 25MW. The second one is ISCC Morocco in Ain Beni Mathar (Morocco) with a capacity of 470MW. Another ISCC plant is under construction now in Egypt. The plant, ISCC Al Kuraymat, has a capacity of 140MW with a solar share of 20MW. There are many other plants under development now in the MENA region as part of the renewable energy targets of the MENA countries and as an output of the collaboration with the European countries. [28]

I.4. **Applications of PTC**

There are various applications of parabolic trough solar collectors. The following presents the most common applications

I.4.1.**Solar PTC for electricity generation:**

Parabolic trough sensor technology is currently the most tried and tested of the solar concentration and Because of the increased level of CO_2 emissions and energy consumption, solar thermal power has been widely applied. PTSCs can be integrated with solar thermal power plants in two ways:

- First, running a steam turbine by steam generated directly from PTSCs which is known as DSG technology,
- Second, heating up a heat transfer fluid (HTF) in the solar field, and then use it in a heat exchanger to generate steam that drive the steam turbine.

The typical installation consists of three main elements Figure (I.16):

- The solar field, which uses a series of long parabolic trough concentrators.
- The heat transfer system.
- The power generation system, which uses turbines steam and an electric generator. In order to limit losses in the heat exchangers, it is possible to vaporize water directly in the solar concentrator (Direct Steam Generation - DSG) [34].

The advantage is double. On the one hand, to save investment costs, due to the elimination of thermal oil, which is very expensive. On the other hand, in order to reach higher temperatures, which increases the efficiency. From an economic point of view, this reduces the cost by about 30%. The feasibility of such a system has been demonstrated on a prototype of the solar platform in Almeria, south of of Spain [35]. The possibility of hybridization of these installations with Conventional heat generation systems guarantee stable electricity production regardless of fluctuations in solar radiation.

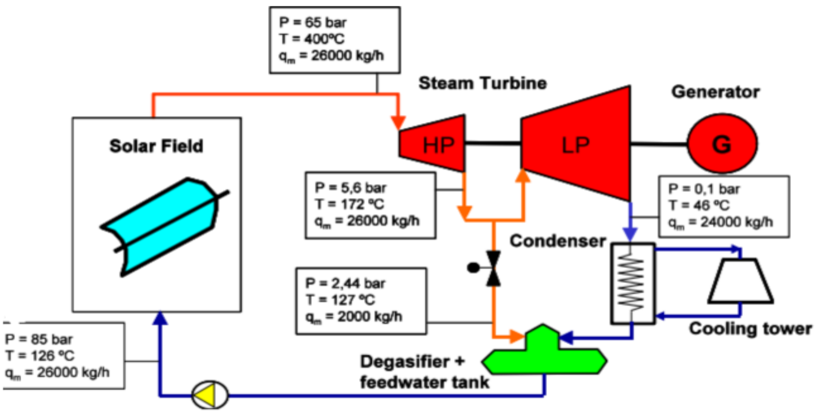

Figure I. 16. *Principle of functioning of a solar power plant with parabolic trough collectors and water/steam (heat transfer fluid): Direct Steam Generation (DSG) [36]*

I.4.2. **Solar PTC for industrial purposes**

The utilization of solar energy decreases the consumption of available electricity as a result of industrial processes such as cooking, drying, cleaning or degreasing, and Pasteurization purification. Most industrial processes require temperature of less than 300 °C [37]. Solar PTC can provide the heat required for industrial processes due to its ability to produce temperature higher than 300 °C [38, 39, 40].

I.4.3. **Solar PTC for desalination process**

Water is one of the most abundant resources on earth, covering three-fourths of the planet's surface. About 97% of the earth's water is salt water in the oceans; 3% of all fresh water is in ground water, lakes and rivers, which supply most of human and animal needs. Water is essential to life .The demand of fresh water has become an urgent need as a consequence of rapid industrial growth, contamination of rivers and lakes, and population explosion [41]. Desalination processes require significant quantities of energy to achieve separation. This is highly significant as it is a recurrent cost, which few of the water-short areas of the world can afford. Water desalination requires large amounts of energy. 230 million tons of oil per day has been estimated to be used to desalinate 25 million m^3/day of salty water [42]. Groundwater is the main source of drinking water in the Algerian Sahara; most of the water is brackish and unfit for human consumption. PTC can be used to desalinate brackish water, by connecting the solar system to a solar power plant. Thermal desalination by the different processes (single effect, multiple effects, multiple stages) [41]. In the single-effect distillation process by example, the circulation of the heat transfer fluid allows to heat the salt water in an evaporator, or indirectly through the production of electricity for processes where the main source of energy is electricity such as: Reverse Osmosis [RO] and Electro dialysis [ED].

Parabolic trough technology can be utilized to desalinate seawater since it is abundant in many parts of the word. There are two categories used to desalinate water. [43].

- Direct collection system
- Indirect collection system

Seawater desalination via MSF (multi-stage flash) and MED (multiple effects distillation) using solar heat as the energy input are promising desalination processes based on renewable energy. The desalination plant consists of two parts, i.e. solar heat collector and distiller. The process is referred to as indirect process if the heat comes from a separate solar collector or solar ponds whereas it is referred to as direct if all components are integrated in the desalination plant [41]. Particularly attractive is desalination associated with concentrating solar power (CSP) plants. CSP plants (Figure I.17) collect solar radiation and provide high-temperature heat for electricity generation. Therefore, they can be associated to either membrane desalination units (reverse osmosis, RO) or thermal desalination units. CSP plants are often equipped with thermal storage systems to extend operation when solar radiation is not available, and/or combined with conventional power plants for hybrid operation. This paves the way to a number of design solutions which combine electricity and heat generation with water desalination via either thermal or membrane separation processes. CSP plants are also large enough to provide core energy for medium- to large-scale seawater desalination. In desert regions (e.g. MENA) with high direct solar irradiance, CSP is considered a promising multi-purpose technology for electricity, heat and district cooling production, and water desalination. An analysis by German Aerospace Centre (DLR, 2007) for the MENA region shows that the choice between the CSP-MED process and the CSPRO may depend on feed water quality. The CSP-MED process is more energy efficient than the CSP-RO process in the Arabian Gulf where seawater has high salinity level. An example scheme of CSP-MED is shown in Figure(I.17) [44].

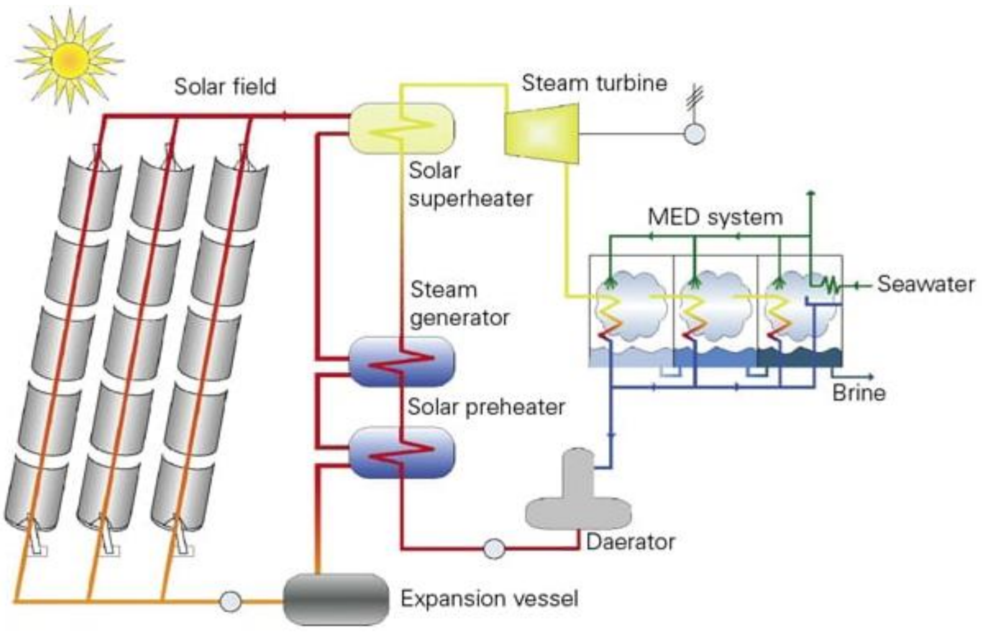

Figure I. 17. *Solar parabolic trough power plant with oil steam generator and MED desalination**.** [45]*

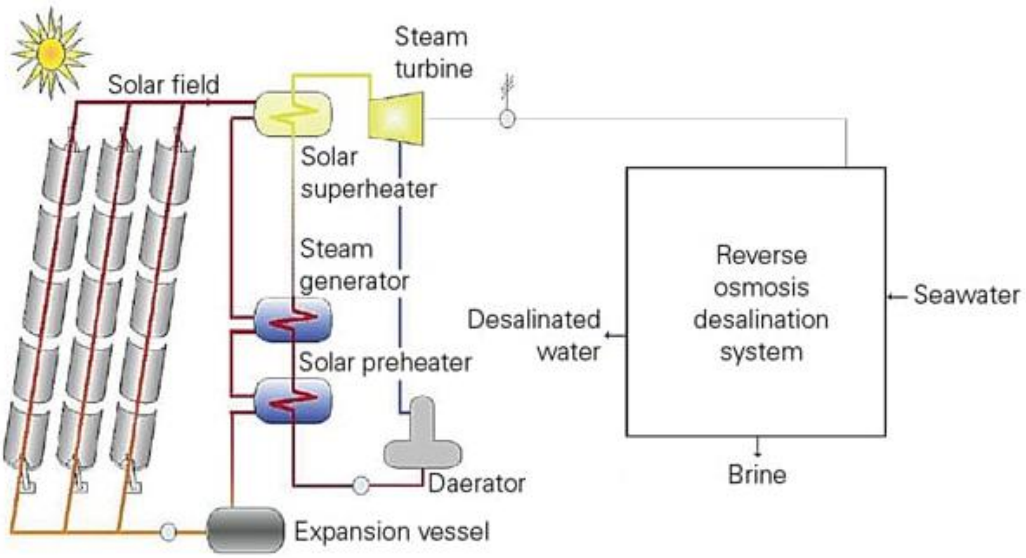

Figure I. 18. *Solar parabolic trough power plant with oil steam generator and SWRO desalination.* ***[45].***

I.4.4. **Solar PTC for Air conditioning and refrigeration**

Solar cooling can be considered for two related processes: to provide refrigeration for food and medicine preservation and to provide comfort cooling, and in hot and humid regions, humidity is removed using conventional air conditioners (A/C), which involves a considerable load on the air conditioning device. Solar energy is used in refrigeration and air conditioning systems, whereas in air conditioning, the air temperature is reduced below dew point through dehumidification and then by reheating the air for the remainder of the required comfort level. Solar refrigeration systems usually operate at intermitted cycles and produce much lower temperatures (ice) than in air conditioning. When the same cycles are used in space cooling, they operate on continuous cycles, the absorption and adsorption. During the cooling portion of the cycles, the refrigerant is evaporated and reabsorbed [42]. The Direct Boiling PTC (DSG) can be combined with an adsorption refrigeration system via the steel pipes that convert the heat to the adsorbent bed [46].

The system does not require external pumping, the Compression of fluids (water, ammonia) is ensured by the tension that the fluid takes on under the action of heating energetic. A typical diagram of a solar refrigerator with adsorption is presented in Figure (I.19).

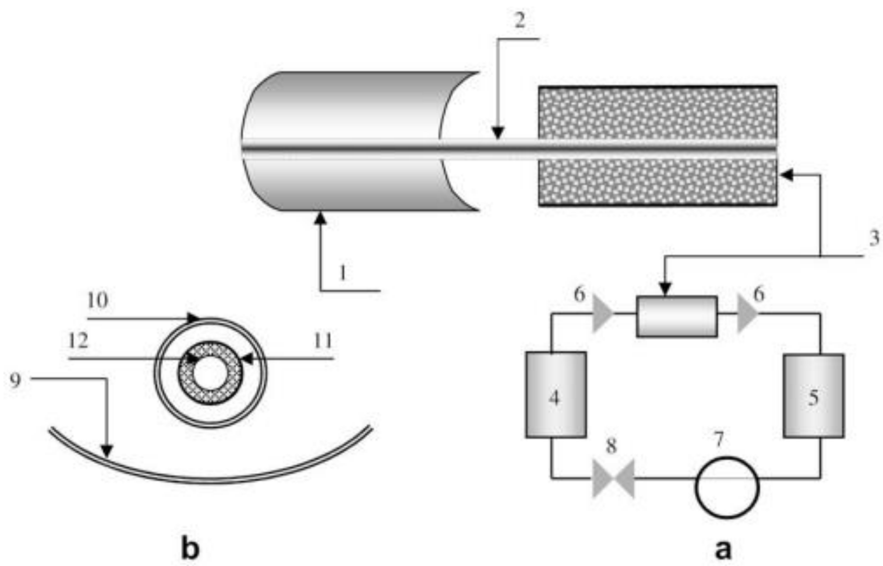

Figure I. 19. *Diagram of a solar refrigerator with adsorption [46]. (a) Simplified scheme of the hybrid system: 1. PTC; 2. Heat pipe; 3. Adsorber; 4. Evaporator; 5. Condenser; 6. Valves; 7. Ammonia liquid tank; 8. Expansion valve. (b) Cross section of the receiver assembly: 9. Reflective surface; 10. Glazing; 11. Absorber; 12. Wick.*

I.4.5. **Domestic water heating**

This is the way solar energy is used. The most common one, we can replace the collectors solar planes used in the equipment of water heating by a PTC because it provides a high operating temperature with a smaller catchment area. As a result, higher demands can be covered by mixing the hot water to another cold one. Examples of applications with high rates of hot water consumption are numerous: factories, hospitals, sports equipment. Engineer

I.5. Literature Review

More than 90% of the energy used on earth today comes from fossil fuels, but fossil fuels are causing more and more problems on earth. The question of their replacement arises and is inevitable. However, how to replace them? Today, mankind is seeking to replace energy sources because of the multiple forms of pollution caused and their impact on the environment, but also (and especially) because of the increasing cost of purchasing, extracting and using these energy sources. The future energy supply will certainly come from renewable energies.

A great deal of effort has been made, especially in the last decade, to improve systems for converting solar energy into heat and especially for the production of electricity. The most widely used thermal conversion systems for electricity generation are parabolic trough concentrators and improving the efficiency of these concentrators is the concern of several researchers. In the following, we cite some of the works done in this field:

Bin Zou and al. [47] developed a small-sized experimental parabolic trough solar collector see Figure (I.20), which has been introduced specially for water heating in cold areas. Several conclusions could be drawn as follows: under the condition of fluid temperature below 100°C, the thermal efficiency of the proposed PTC is increased with the increase of fluid temperature, due to the increase of Reynolds number caused by the increasing fluid temperature, and finally reached a relatively stable level of 67%. The final thermal efficiencies in the conditions of wind velocity of 1.7 m/s and 5.0 m/s were 67% and 56%, respectively, which indicated that the heat loss of the proposed PTC was sensitive to the heat convection. In the normal operation condition, the thermal efficiencies of the coated group and the uncoated group were almost the same, and both could finally reach about 67%. The time interval during which the outlet and inlet fluid temperature difference was kept positive for both the two groups were more than 20 min.

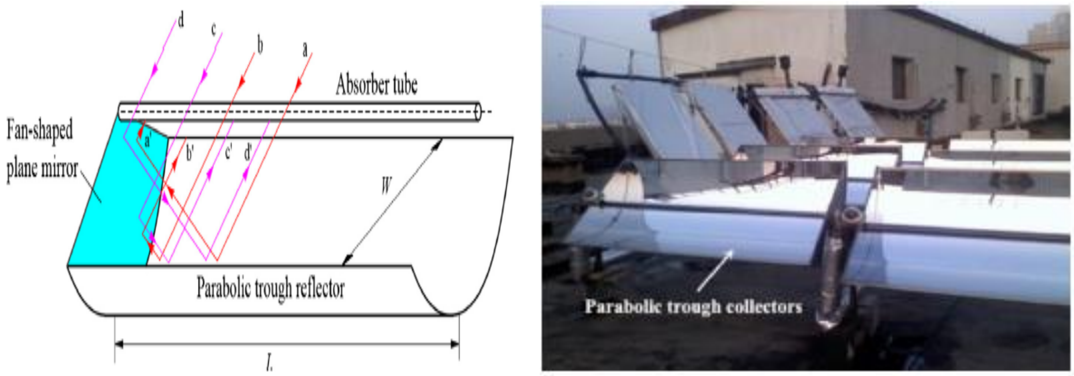

Figure I. 20. *(a) Schematic of compensation for end loss by setting fan-shaped plane mirror (b) the experimental platform [47]*

Mohamed Chafie et al. [48] conducted and realized an experimental study in Tunisia on a PTC system Figure (I.21). The mean objective is to evaluate the thermal performance of a PTC. Many experimental tests were carried out. The thermal efficiency, the heating and cooling time constants and the incidence angle modifier of the collector were measured. The intercept and the slope given by the efficiency curve of the collector were found to be 0.551 and 0.316, respectively. The time constants for heating and cooling are 137 and 205s, an experimental performance investigation of typical days (sunny and cloudy 25 days) is presented. The final cost for the experimental device has been calculated.

Figure I. 21.*The photograph of the experimental device PTC [48].*

Ma et al. [49] designed a compact PTC with lenses as primary reflectors, which is illustrated in Figure (I.22). This design is similar to a great cylinder with lenses in the upper part and the receiver tube in the center. They found that this design reaches up to 84% optical efficiency and it is able to operate at 250°C with thermal oil (YD320). Moreover, they stated that the receiver has to be located 150 mm over the focal point in order to improve the optical performance in a greater range of incident angles. Another interesting idea is the rotation of the solar field in order to follow the sun azimuth angle.

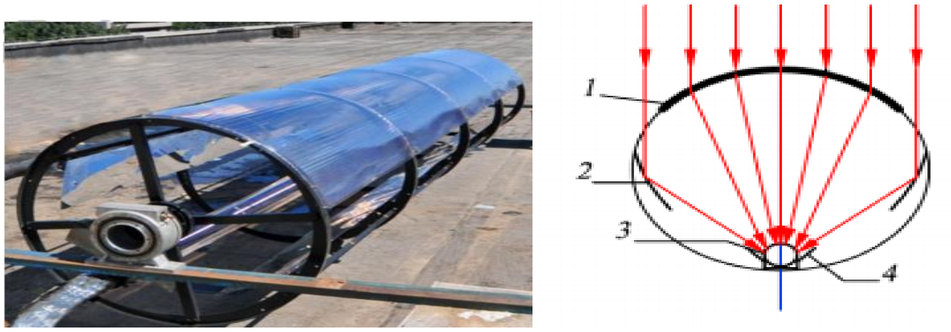

Figure I. 22.*The examined compact PTC with lenses. There is a cylindrical absorber and the lenses in the top part rotate in order to track the sun 1-Spherical Fresnel lens, 2-Parabiloc reflector, 3-Receiver, 4-Secondary reflector [49].*

Wang et al. [50] conducted a study for enhancing the methanol reforming process. The new suggested configuration is depicted in Figure (I.23). This idea aims to achieve the optimum heat flux distribution along the receiver and consequently to create the ideal temperature levels in the different parts of the receiver. Finally, it is found that this idea is able to increase the process efficiency up to 16% compared to the conventional PTC case. This idea is a promising choice for applications of methanol reforming but is not clear if it is beneficial for conventional solar thermal systems.

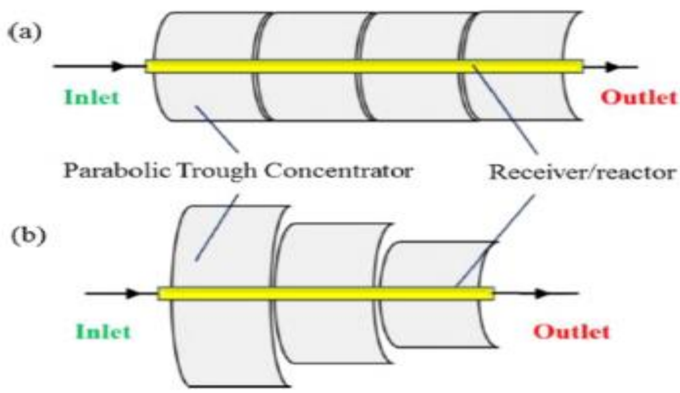

Figure I. 23. *Comparison of a traditional solar concentrator with a new solar concentrator structural. (a) Traditional solar concentrator structure. (b) New solar concentrator structure [50]*

Qu et al. [51] studied a PTC solar field in a rotating platform, as it is depicted in Figure (I.24). The examined configuration was a prototype with a nominal power of 300 kW operating with Dowtherm A. Their results showed that the daily performance of this system could be increased by up to 5% compared to the conventional system with single-axis tracking. Moreover, they found that the daily performance with this system is about 63% in the summer and 40% in the winter, while the mean annual efficiency is about 50%. Finally, the authors stated that the rotating platform is a promising idea for reducing the collecting area and creating more cost-effective designs with higher thermal efficiency. However, it is important to test this idea with a detailed financial analysis for commercial systems of greater nominal power.

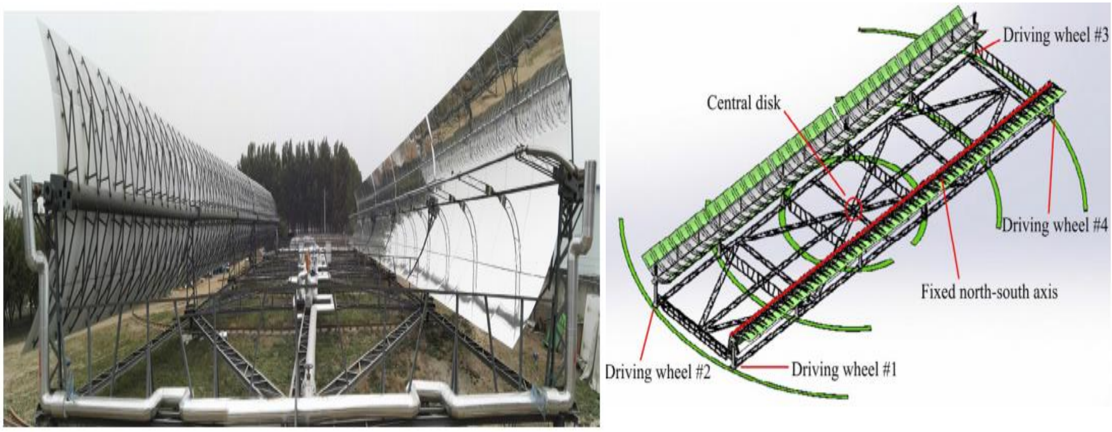

Figure I. 24. *Photo of the 300-kWth solar parabolic trough collector with rotatable axis tracking Schematic of the rotatable axis tracking apparatus [51]*

Bader et al. [52] introduced an innovative concept for fabricating solar trough concentrators based on pneumatic polymer mirrors supported on precast concrete frames see Figure (I.25). Optical aberration is corrected by means of a secondary specular reflector in tandem with a primary cylindrical concentrator. The optimal design is formulated for maximum solar flux concentration. The Monte Carlo ray-tracing technique is applied to determine the effect of reflective surface errors and structural beam deformations on the performance of the combined primary and secondary concentrating system. It is found that this collector has thermal efficiency up to 65% for temperature levels at 125 °C and up to 42% for temperature levels at 500 °C with air as working fluid.

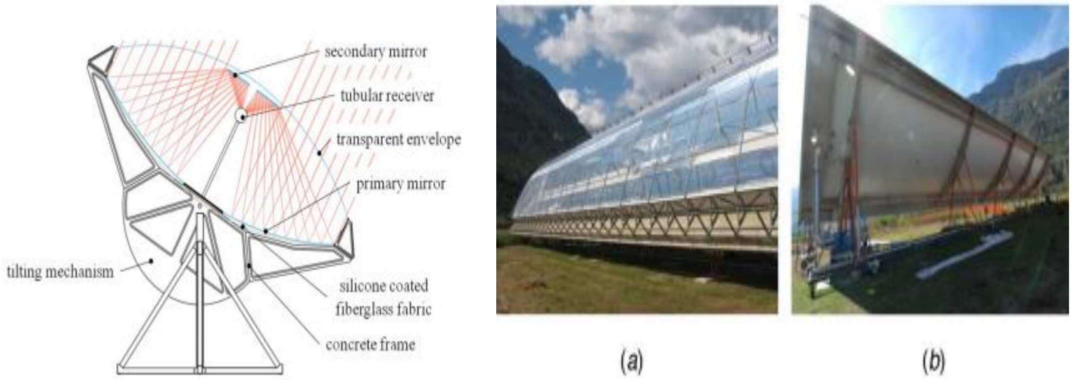

Figure I. 25. *Scheme of conceptual design of solar trough concentrator based on pneumatic polymer mirrors supported on precast concrete frames and Photograph of the 49.4 m length and 7.9 m width sun tracking solar trough-concentrating prototype: (a) front view and (b) rear view [52]*

Good et al. [53] examined a PTC with air as working fluid with an alternative design. This PTC has a dome and inside it, there is the receiver. The use of a flat absorber with an asymmetrical reflector for steam generation was examined. They stated that this system is able to operate up to 500 °C.

Bortolato et al. [54] studied an innovative flat aluminum absorber for process heat and direct steam generation in small linear solar concentrating collectors see (Figure I.26). After defining its optimal width through a Monte Carlo ray-tracing analysis, this absorber has been manufactured with the bar-and-plate technology, including an internal offset strip turbulator in the channel. This configuration presents 82% optical efficiency and 64% thermal efficiency for temperature levels close to 100-120°C. The authors stated that the examined design is a flexible configuration, which gives the possibilities for an overall cost effective design.

Figure I. 26. *(a) Prototype of the asymmetrical parabolic trough linear solar concentrator (b) Bar-and-plate flat receiver arranged on the support bar and illuminated with concentrated solar radiation during a test run [54]*

Halimi et al. [55] studied a PTC with a U-tube absorber, as it is given in Figure (I.27) They examined different locations of the internal U-tubes and they found the parallel configuration of Figure(I.27) to be the best design with a thermal efficiency of 40%.

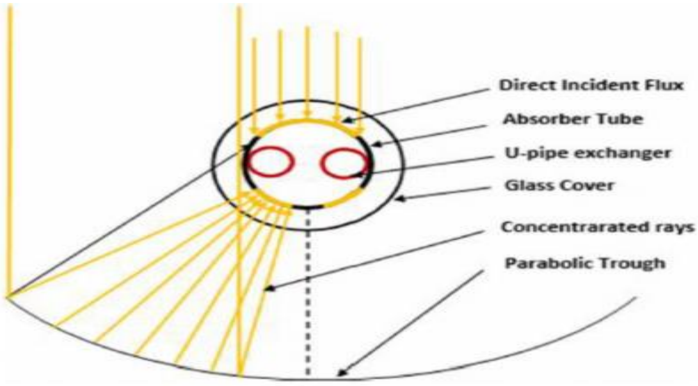

Figure I. 27. *PTC with a U-tube absorber [55]*

Various researchers in the literature have examined the use of a secondary reflector and different types of secondary reflectors have been studied:

Bharti et al. [56] developed an experimental analysis of a small-sized solar PTC Figure (I.28) with and without secondary reflectors. Theoretical examination of receiver tube misalignment and design of secondary reflector are presented. Experimental analysis of PTC has been done using a parabolic secondary reflector (PSR) and triangular secondary reflector (TSR) and compared with PTC without secondary reflector (WSR). The maximum outlet temperature of heat transfer fluid is observed as

49.2°C, 47.3°C and 44.2°C in the case of PSR, TSR and WSR conditions, respectively. The maximum thermal efficiency of 24.3%, 22.5% and 17.8%. The results show that the use of a secondary reflector can improve the performance of a solar PTC system.

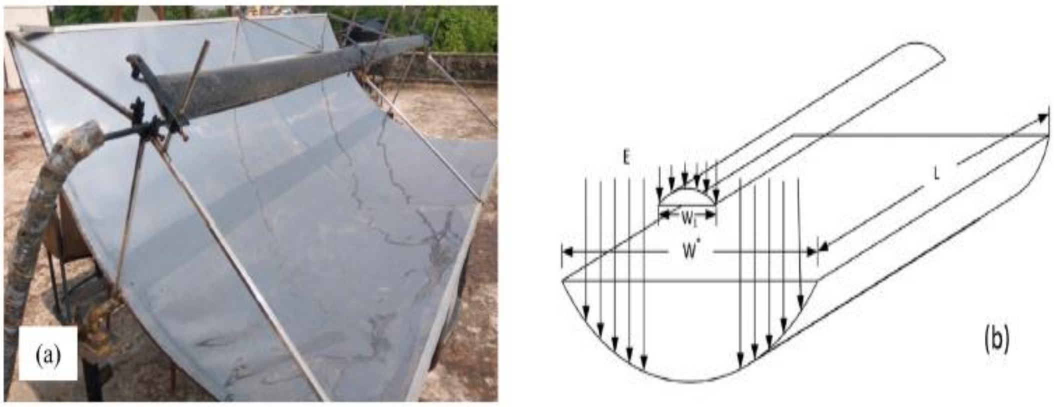

Figure I. 28. *Experimental set-up with (a) parabolic secondary reflector and (b) primary reflector with secondary parabolic reflector [56]*

Rodriguez-Sanchez et al. [57] suggested the use of a flat secondary concentrator over the absorber Figure (I.29) in order to increase the concentration ratio. Their idea is to reduce the absorber diameter and to concentrate the solar energy in a smaller absorber area. They managed to increase the concentration ratio up to 80% for collectors with great focal distance and rim angles close to 80°. The calculations and the simulations showed an increase of the concentration ratio for a PTC when a secondary flat reflector is used compared to a classical single mirrored PTC. The increase of concentration ratio reaches a maximum for rim angles around 80 with shadowing factors of approximately 10%. An interesting possibility for the use of a secondary flat reflector is to install it in already built plants since no ground redistribution of the primary mirrors is required. For this purpose, it would be recommended to develop an economic analysis that includes the cost of changing the receivers, possible structure modifications to place the new absorber, and new pumping power requirements in the plant.

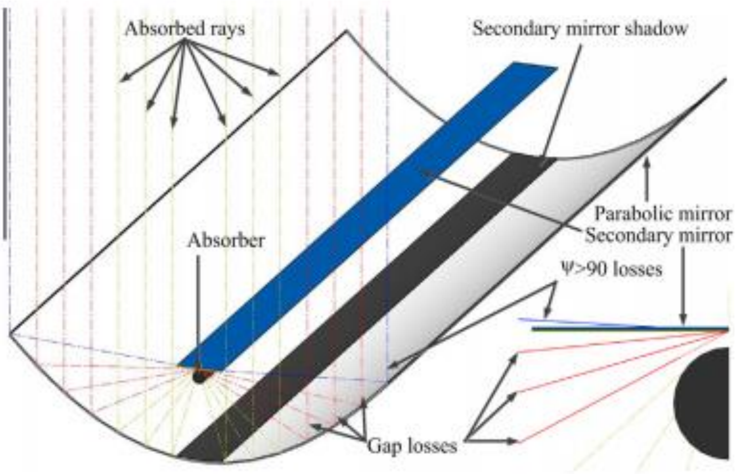

Figure I. 29. *PTC with a secondary flat reflector and gap losses [57]*

Krissadang et al. [58] presented a construction of a 2-stage parabolic trough solar concentrator see Figure (I.30). A Secondary reflector constructed of multi-piece mirrors forming a hyperbolic-shaped reflector by using water as a heat transfer fluid its capability to heat transfer and load high temperature (100°C). The performance of a 2-stage PTC was evaluated using outdoor experimental measurements including the useful heat gain. The experimental results shown that the maximum thermal efficiency was 23.43% and the optical efficiency was 76%.

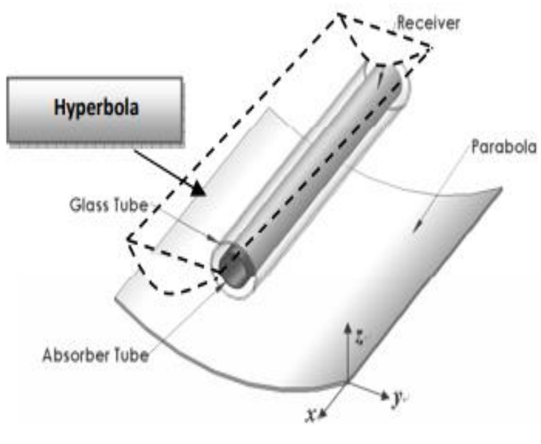

Figure I. 30. *A photograph of the experimental setup Size of a 2-stage PTC for construction and fabrication* ***[58].***

Zhu et al. [59] designed a PTC with non-continuous primary absorber which is similar to an LFR design idea Figures (I.31 and I.32), as it is depicted for enhancing the optical efficiency. They used a secondary reflector and they used a movable receiver in order to eliminate the end losses. According to their results, this system is able to reach up to 66% thermal performance with transcal oil, while the thermal loss coefficient is about 1.32W/m^{2}K. They stated that this system presents higher performance than the conventional linear Fresnel reflector (LFR) and it has a comparative efficiency (a bit lower) than the conventional PTC. They stated that the examined idea has a potential for reduced investment cost compared to the conventional PTC.

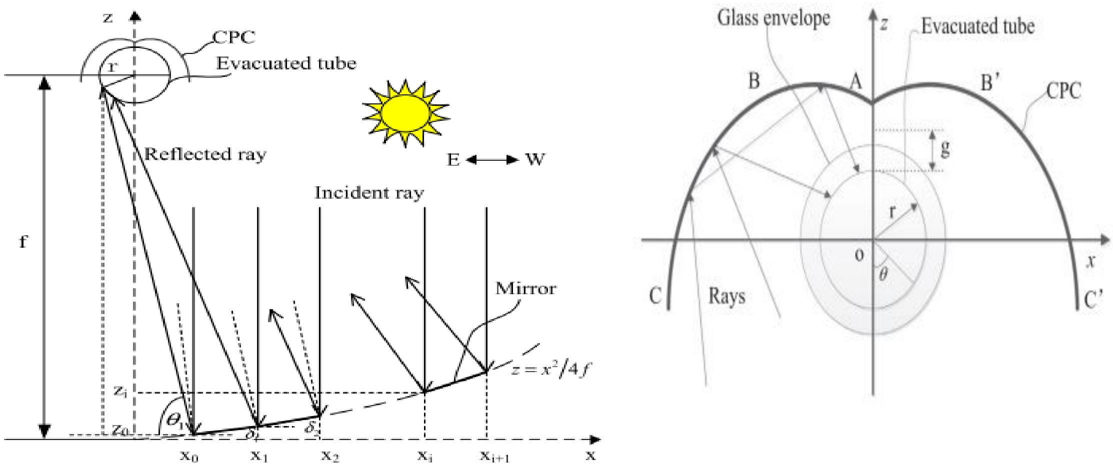

Figure I. 31. *Schematic design of primary mirror field layout of SPLFR collecting system Sketch of CPC and evacuated tube [59]*

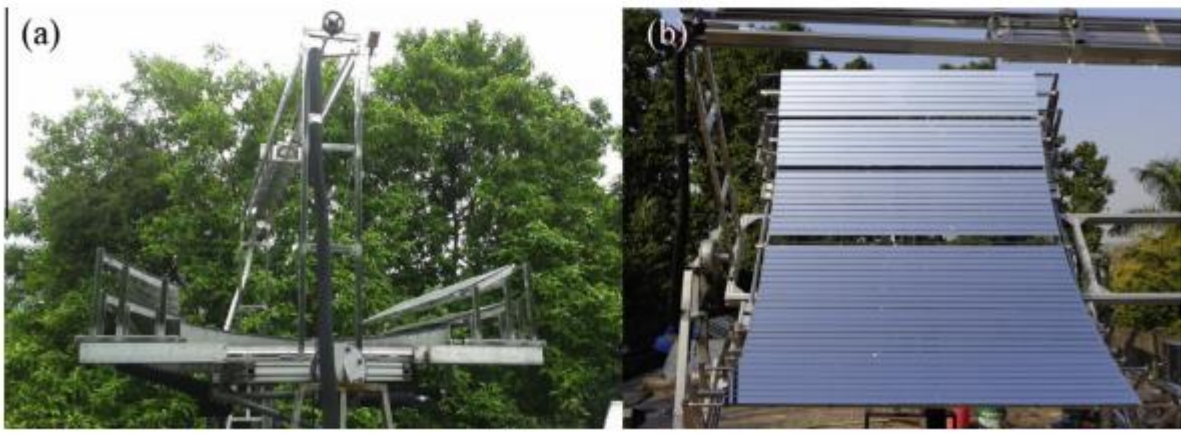

Figure I. 32. *Photographs of experiment device (a) in retracted state and (b) in working condition [59].*

Abdelhamid et al. [60], in order to increase the concentration ratio, carried out a two-stage PTC with a secondary compound parabolic shape concentrator Figure (I.33). The examined configuration presents a concentration ratio around 60 and it can operate at an outlet temperature of 365 °C with thermal oil (Duratherm 600), while the thermal efficiency was about 37%. It is important to state that the use of two-stage concentration with high concentration ratio increases the need for a precise design, something that increases the installation cost.

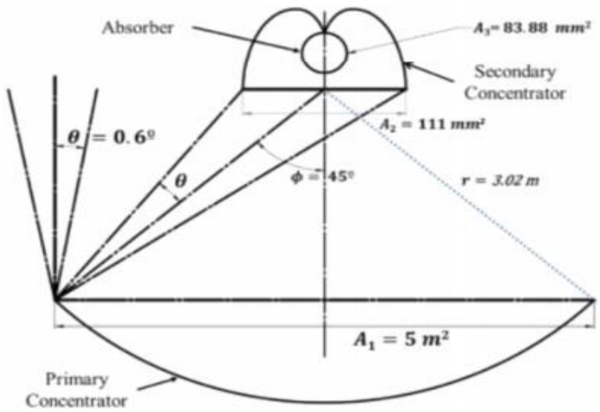

Figure I. 33. *The use of a compound parabolic concentrator for increasing the total concentration ratio [60].*

Ullah et al. [61] studied the use of a multi-stage PTC for lighting purposes Figure (I.34) as exhibits for a location of 37.5° latitude. They used optical fibers for transferring the reflected solar rays inside a building. They found that this technique could lead to adequate indoor lighting. More specifically, they found that this technique creates higher interior illuminance uniformity than the traditional lighting systems. Lastly, they stated that the examined idea presents a high cost and there is a need for the proper optimization for reducing the investment cost.

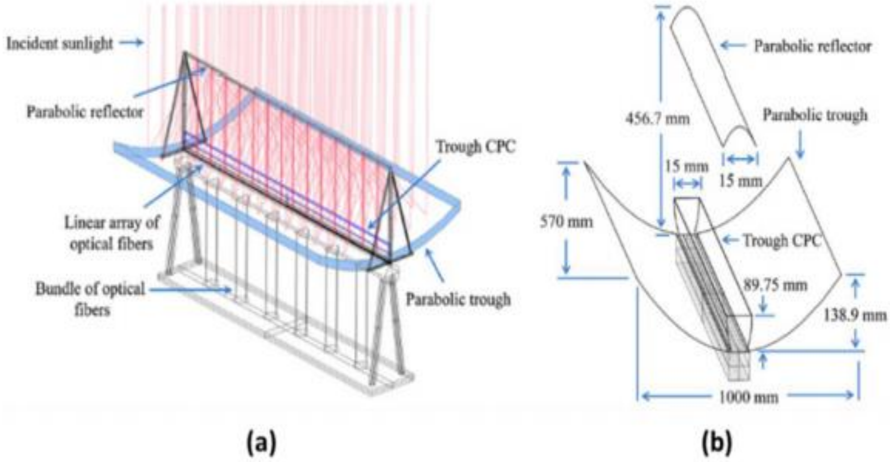

Figure I. 34. *The use of a PTC for lighting purposes (a) The total configuration (b) The PTC design [61]*

Liang et al. [62] examined optically a trapezoidal cavity receiver Figure (I.35) and they found the optical efficiency of the total configuration to be around 85% while the optical efficiency of the absorber tube to be about 45%. Moreover, they stated that this system has satisfying performance in the cases with increases tracking errors of the primary reflector

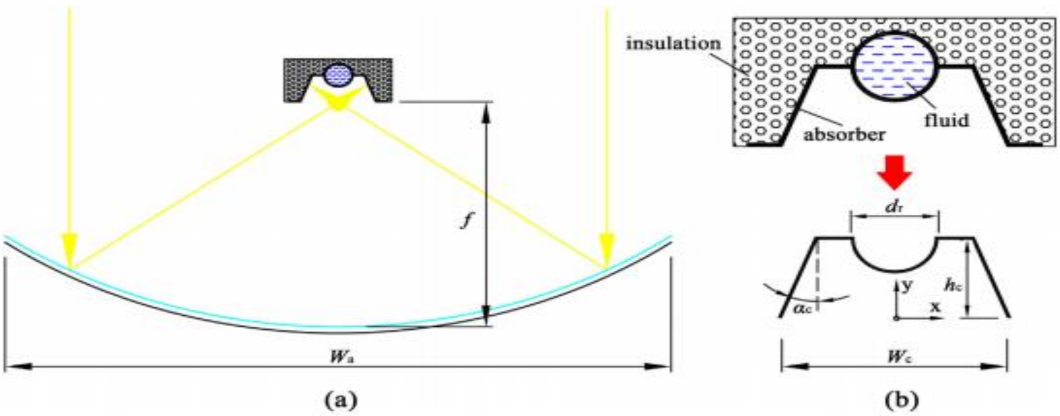

Figure I. 35. *Schematic of the cavity receiver [62]*

Bennett et al. [63, 64], tested a hybrid solar collector using a two-stage parabolic trough compound parabolic optical system and double-junction InGaP/GaAs solar. The cross section of the hybrid heat-collecting element (HCE) is shown in Figure (I.36).

Concentrator (CPC) with secondary reflector has reached a 63% optical efficiency and a 40% thermal efficiency at 650 °C.

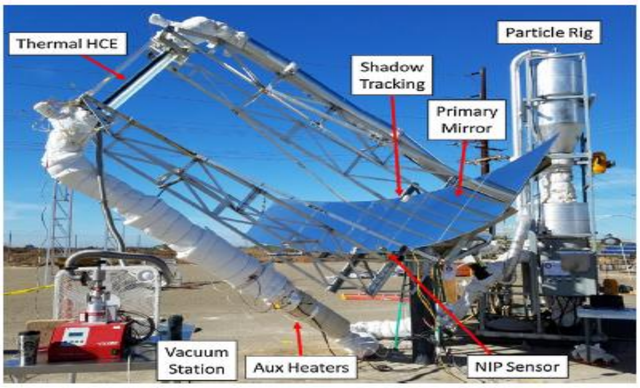

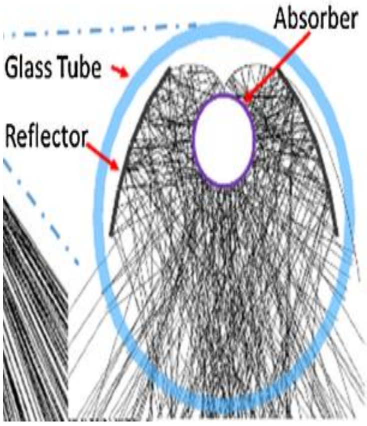

Figure I. 36. *Experimental test platform (front end) and the Ray tracing diagram with exploded view of the HCE in the top right corner [63]*

Wirz et al. 2014 [65], in order to enhance the optical and thermal efficiencies, examined ideas which are a reflective glass, a reflecting insulation layer, aplanatic mirrors and tailored seagull secondary reflector Figure (I.37). They found that the initial design has 65% optical efficiency and only the aplanatic mirrors are able to increase the optical efficiency at 65.1%. The thermal analysis was performed with synthetic oil as working fluids and for temperature level at 390 °C. In terms of thermal performance, they found that all the configurations enhance the collector performance.

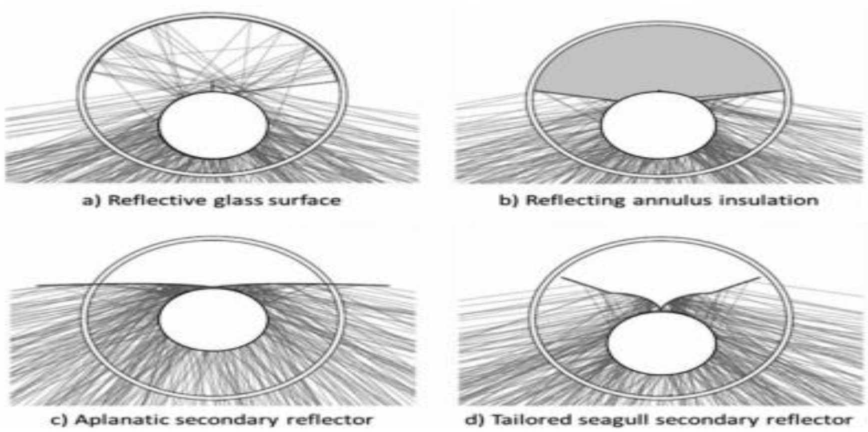

Figure I. 37.*Various secondary reflectors inside the evacuated tube a) reflective glass surface b) reflecting annulus insulation c) aplanatic secondary reflector d) tailored seagull secondary reflector [65]*

In the concentration process of sunrays, non-uniform heat flux distribution (NUHF) forms outside the absorber tube. Temperature gradients and temperature peaks in the absorber tube emerge, which bring challenges to the efficiency and reliability of parabolic trough receivers (PTRs). In the following, many researches papers have been developed on NUHF of PTCs, including the calculation methods of NUHF and simulation studies of PTRs:

Eck et al. [66] presented and compared a three different receiver models: A three-dimensional FEM model, an empirical one-dimensional model of Sandia, and a two-dimensional analytical model. The results show that the Sandia model is a good tool for the determination of the thermal parameters of the receiver tubes but is not suited for a more detailed analysis of the receiver temperature. The developed FEM-model is a helpful tool for the investigation of the heat losses as well as for the detailed analysis of the temperature field, and the heat loss of a receiver tube calculated with the FEM model and the Sandia model are in good agreement with measured data.

Cheng et al. [67] performed a three-dimensional numerical simulation of coupled heat transfer characteristics in the receiver tube. They combined in this simulation the MCRT method and FLUENT software, with Syltherm 800 liquid oil as a heat transfer fluid. The validation, of the mathematical model and modelling, was done by comparison with data from previous experimental studies (Dudley et al. [68]). Numerical results show that the predicted results agree well with the experimental data, the average relative error is within 2%.

He et al. [69] established a method of MCRT and FVM to simulate the photo-thermal process of parabolic trough solar thermal power generation. The MCRT code is used to gain the heterogeneous heat flux distribution on absorber tube, and FVM software FLUENT is used to solve the fluid and heat transfer problem. The same mesh systems have been used in MCRT and FLUENT. The results show that the curve of heat flux distribution is divided into 4 parts: shadow effect area, heat flux increasing area, heat flux reducing area, and direct radiation area. The heat flux distribution on the outer surface of absorber tube was heterogeneous in circle direction but uniform in axial direction (x).

Cheng et al. [70] Studied three-dimensional model of the parabolic trough solar collector and numerical simulations of the flow and heat transfer fluid of some HTF under two methods: the Finite Volume Method and the Monte Carlo Ray-Trace. They concluded that properties of HTF affect the temperature distributions on the receiver, thus the thermal loss and the collector efficiency. Numerical results show that the MCRT code calculating the non-uniform solar energy flux distribution of the whole PTC system, the only FVM model simulating the entire receiver with no-sun operation conditions, and the integrated FVM and MCRT combined model are feasible and reliable. The average Nusselt number of the two synthetic oil HTFs (Therminol VP1 and Syltherm 800) increase with increasing HTF inlet temperature.

To establish a more realistic 3-D model, the accurate calculation of realistic NUHF of PTRs is necessary. Realistic NUHF can be derived with analytical methods **Jeter 1986** [71], Khanna et al. [72].

Wang et al. [73] combined a solar ray trace (SRT) method and the finite element method (FEM) to solve the complex problem coupled with fluid flow, heat transfer and thermal stress in a PTC system. The effects of the key operating parameters on the performances of the receiver are numerically investigated. The distributions of the stress intensity and the thermal deformations of the receiver are numerically studied. Numerical simulation results indicate that the circumferential temperature difference (CTD) of the absorber decreases with the increases of inlet temperature and velocity of the heat transfer fluid (HTF) and increases with the increment of the direct normal irradiance (DNI).

Qiu et al. [74] studied the temperature distribution of the receiver using molten salt as HTF. They found that the circumferential temperature difference (CTD) of the absorber increases with decreasing HTF inlet velocity or temperature and increasing direct normal irradiance (DNI).

Wu et al. [75] combined a MCRT code and FLUENT software for numerical simulation of temperature distribution of a parabolic trough receiver. The results indicate that CTD of the absorber tube increases with decreasing inlet temperature of HTF. Their different conclusions may be due to the different HTFs they adopted.

The more detailed characteristic of the flow and heat transfer of HTF under NUHF is also researched. One of the most distinguishing feature of NUHF is that it can induce natural convection in the absorber tube.

Ghomrassi et al. [76] carried out an analysis and an optimization of the thermal performance of the tube receiver with coupling the concentrated solar heat flux densities, in the solar concentrator focal zone (calculated by SOLTRACE software), used as wall heat flux boundary conditions for the receiver tube. The effect of the receiver tube diameter variation on the PTC thermal performance is studied. It has been found that increasing tube metallic thickness enhances the performance of PTC system comparing to the tubes of the same diameter and crossed by the same flow rates.

Huang et al. [77] presented a numerical investigation of the mixed turbulent flow in receiver tube heated with NUHF and found that the magnitude of secondary flow velocity increases with the increase of Grashof number (Gr) and decreases with the increase of Re. The Nu number of mixed convection is increased under NUHF due to secondary flow but the friction factor is also increased. Besides, the intensity of secondary flow is also related to the variation of properties with temperature.

Bin Zou et al. [78] studied the optical performance of a parabolic trough solar collector (PTC) depend on theoretical analysis and Monte Carlo Ray Tracing method (MCRT). Firstly, The MCRT models are established with theoretical equations of several critical parameters are derived after that the results of different geometrical parameters on the optical performance are discussed. The distribution of local concentration ratio around the absorber tube changes greatly. Consequently, the optical properties for different critical parameters are discussed. The size relationship between the reflected light cone and the absorber diameter affects the optical efficiency significantly because of the rays escaping effect. The results revealed that the absorber diameter should be larger than the size of the reflected light cone to avoid great optical loss caused by rays escaping.

Li et al. [79] performed a numerical investigation with the flow and heat transfer performances are analyzed for forced and mixed laminar convection in receiver tube heated by uniform and non-uniform heat fluxes with different Gr numbers, Re numbers and solar elevation angles. The study is focused on the effect of the buoyancy force induced by the non-uniform heat flux on the laminar flow and heat transfer characteristics in the solar receiver tube of parabolic trough collector. The results show that the natural convection can increase heat transfer rate of laminar forced convection by more than 10% when the Grashof number is greater than a threshold value.

Okafor et al. [80] studied the effect of NUHF intensity and profile, namely circumferential angle span, on convection heat transfer and friction factors in the laminar flow regime considering buoyancy-driven secondary flow. They concluded that the wall temperature increases with increasing heat flux span. However, it seems that the overall heat flux increases with the circumferential angle span in this study. Without secondary flow, average internal heat transfer coefficient is independent of flux intensity and profile. The friction factor decreases with increasing Re or increasing HTF inlet temperature. With buoyancy effect, the friction factor is higher.

Wang et al. [81] calculated and compared the thermal efficiency under UHF and NUHF when HTF is Dowtherm A and solar salt respectively. They concluded that NUHF has a little influence on the thermal efficiency of PTCs transfer in the absorber tube under NUHF.

Hongbo Liang et al. [82], carried out three different optical models based on ray tracing for a PTC. Model 1 was based on MCM (Monte Carlo Method). Model 2 initialized photon distribution with FVM (Finite Volume Method). Model 3 utilized FVM to determine ray positions. The running time and computation effort of Model 3 was shorter and less than Model 1, approximately 40% and 60% of Model 1 from his work. Above all, the simulation result of Model 3 was not affected by the algorithm of generating random numbers; however, it needed to consider suitable grid configurations for different sections of the system. Additionally effects of varying the geometric parameters for a PTC on optical efficiency were estimated. Effect of offsetting the absorber in width direction of aperture was greater than that in its normal direction at the same offset distance, which was more obvious with offset distance increasing.

Zhi wang et al. [83] reviewed many calculation methods of non-uniform heat flux distribution, simulations of fluid flow and heat transfer in PTRs and optimization methods. Outcome of the study is summarized below: 1- The ray-tracing methods including MCRT method and commercial software are efficient to simulate the concentration process of sunrays of PTCs. 2- NUHF can increase overall convective heat transfer in the absorber tube. The challenge of NUHF is that relative uniform convection heat transfer within the tube cannot match NUHF outside the absorber tube. As for simulation works, the future researches should be directed towards the raise of non-dimension parameters for scaling models of PTCs. Given that, the development direction of PTC is higher operation temperature to increase efficiency; more studies on the flow of molten salt or gas as HTF in PTR are needed. 3. As for heat transfer enhancement methods, there are no set standards available for comparison and selection of these methods. More efforts are needed for theoretical studies to avoid repeated works and for economic studies to justify these optimization methods.

Agagna et al. [84] firstly, developed a 3D optical model depend on the Monte Carlo Ray Tracing method written in MATLAB software. After that, they calculated the local concentration ratio to validate the MCRT method. In the second part, they analyze the heat flux distribution on the absorber tube under some tracking error values. The results of the MCRT code has been coupled with FVM method using ANSYS software. The results show higher tracking error imply losses of the heat flux distribution received by absorber tube and make this distribution not symmetrical. The optical efficiency of the trough collector decreases with the increase of tracking error angle. It was clearly seen from CFD model that the effects of tracking error increasing both the outlet temperature and the thermal efficiency of PTC system.

Spirkl et al. 1997 [85] presented a secondary reflector above the receiver, which reflects the irradiance to the upper half part of receiver to homogenize the distributed radiation onto the absorber and finally reduced the thermal expansion strains.

Serrano-Aguilera et al. [86] proposed a new method called Inverse Monte Carlo Ray Tracing (IMCRT) to calculate the numerical description of line-focus concentrator geometries, and the IMCRT method provides the chance to redefine the reflector geometry in order to get homogeneously distributed radiation onto the absorber without secondary reflectors.

Liu et al. [87] applied the minimum circumferential temperature difference on the absorber (CTD) of the absorber tube as the optimization objective to establish optimization flow equation of HTF and solved it with FLUENT software. They found that the optimal flow field of HTF is featured by longitudinal vortexes in the cross section and the flow with much more vortexes would further reduce the CTD. Their findings provide a theoretical guidance for the structural optimization of PTRs.

Sundaram and Senthil [88] conducted experiments including PTC without SR, triangular SR, and a secondary curved reflector. They have concluded that the thermal efficiency is increased by 10% and heat loss is decreased by 0.5 kW with the use of a SR.

Loni et al. [89] presented a study of thermal performance of the dish collector, which is compact system for converting solar radiation energy into thermal energy. All of the incoming solar irradiation to the dish aperture area is concentrated at the dish focal point where the solar receiver is located. The heat flux rate over each coil of the absorber is estimated by using SolTrace.

An elliptical cavity geometry, as a SR, with flat plate reflector was proposed and analyzed by **Cao et al**. [90]. The study shows that increasing the tracking error angle and increasing the PTC focal distance would both decrease the cavity blackness.

Introducing a flat plate reflector at the elliptical cavity open inlet can largely increase the cavity darkness.

A concept of reflecting surface at an inner portion of the glass envelop has been provided by **Price et al.** [32]. This idea avoids the use of additional attachment for a SR.

Islam et al. [91] investigated the optical performance of solar parabolic trough collector by considering some optical parameters. They concluded that increase in rim angle leads to an increase in non-uniform distribution of heat flux. Glass cover would increase the collection efficiency but increase the non-uniformity in flux distribution, and dislocation would lead to more uniform distribution at the lower half of receiver tube where dislocation had taken in terms of radius of receiver tube. In order to ensure that the absorber tube of the concentrator captures a maximum amount of light, a secondary reflector (SR) is essential in large aperture PTCs forming then a so-called 2-stage concentrator. Adding a SR could also, increase the concentration ratio and rim angle [92-93].

I.6. **Optical and CFD software**

In the following, we present many software that can be used to analyze different concentrating solar power (CSP) technologies, which include linear concentrator systems parabolic trough.

I.6.1.**SolTarce**

SolTrace is a software tool developed at the National Renewable Energy Laboratory (NREL) to model concentrating solar power optical systems and analyze their performance. Although originally intended for solar applications, the code can also be used to model and characterize many general optical systems. The creation of the code evolved out of a need to model more complex optical systems than could be modeled with existing tools SolTrace can model parabolic trough concentrators as well as dishes, towers or other unique geometries (linear power towers, etc.). It models optical geometries as a series of stages composed of optical elements that possess an extensive variety of available attributes including shape, contour, and optical quality. The optical modeling in Soltrace is based on the Monte Carlo Ray Tracing method (MCRT) [94]. MCRT is a statistical method that simulates the concentration process with stochastic movement of sunrays. Rays are generated randomly and traced as they undergo several optical interactions, including reflection by the reflector, refraction by the glass cover and absorption by the absorber tube. As a result, distributions of rays that reach the target surface are obtained. The accuracy of simulation results increases with the number of rays traced, but larger ray numbers mean more processing time. This method is flexible and rigorous to simulate the concentration process of CSP systems and codes can be developed by researchers themselves. Its advantages include simple theoretical model, convenient operating process and easy programming [95, 96].

I.6.2. **ASAP**

ASAP is commercial software that can be used to model the optics of the parabolic trough or linear reflector systems. Currently, the flux distribution on the receiver can only be projected onto planar surfaces, but the next version should allow the flux distribution to be mapped onto non-planar surfaces. [94].

I.6.3. **CIRCE**

Although CIRCE was originally developed for the analysis of point-focus dish collector systems, CIRCE can also be used to analyze the optics of parabolic trough and linear reflecting systems as well using USERDISH input, which requires a point-by-point tubular receiver. A need still exists for the ability to specify an analytic mirror shape, error profile, and horizontal analytic tubular receiver with integration capabilities. [94].

I.6.4. **ANSYS CFX**

Ansys CFX is a high-performance computational fluid dynamics (CFD) software tool that delivers reliable and accurate solutions quickly and robustly across a wide range of CFD and multiphysics applications such as conjugate heat transfer. CFX is recognized for its outstanding accuracy, robustness and speed when simulating turbo machinery, such as pumps, fans, compressors and gas and hydraulic turbines.

I.6.5. **ANSYS FLUENT**

FLUENT is a computational fluid dynamics code that could be used to rigorously model the heat transferred to the linear receiver. Radiative flux distributions obtained from one of the optics codes described above can be used as boundary conditions in FLUENT to simulate the heat transfer and losses to and from the working fluid in the receiver. The annulus between the outer sleeve and the inner pipe can also be rigorously modeled [94].

I.7. Chapter summary

The solar parabolic trough collector system is used for generation of power as the system is capable of producing high temperature. In this chapter, a detailed description of four types of CSP technologies has been presented: Parabolic trough collector, CSP with parabolic collector, CSP with Fresnel linear collector, and Tower CSP. Then, a historical overview development of parabolic trough collector and its various applications have been reviewed. The second part presents a general overview including the experimental innovation reviews and various works carried out in this domain. From this overall review, we can draw the following conclusions:

- PTC is the most commonly used system in solar thermal energy today.
- Recent studies are much more focused on the absorber tube.
- The main focus of current research studies is to improve the performance of the traditional PTC system. Among other things, the addition of a secondary reflector is an important solution and is under investigation. This solution makes it possible to have a uniform distribution of the solar flux around the absorber tube. Therefore, a high temperature of the heat transfer fluid can be obtained at the outlet of the tube.
- The research studies concerning this system are directed towards the numerical simulation of the conjugate heat transfer and fluid flow in the absorber tube. For this purpose, several optical analysis software and CFDs are used. Among others, we cite: SolTrace, ANSYS-FLUENT and ANSYS-CFX.

Chapter II

Optical Analysis of the Parabolic Trough Concentrator

Optical Analysis of the Parabolic Trough Concentrator

II.1. Introduction

Parabolic trough concentrators are the most widely used technology in large thermodynamic solar power plants for the production of electricity. The concentrator mirror is a cylinder with a parabolic cross-section and has only one direction of curvature. Concentration takes place on the line where the tubular receiver is placed in which the heat transfer fluid (water or oil) circulates, which can be heated up to 450°C. Optical and thermal analysis of these collectors is very important for the calculation of optical and thermal losses, and allows the effects of collector degradation to be evaluated. In this chapter, a theoretical model of PTC has been presented in detail. The model is mainly consists of two parts. The first part is estimating the solar radiation that reaches the collector by using PVSYST software to provide numerical temporal values of the solar heat flux in Laghouat city (ALGERIA). The second part is optical analysis. The aim is to determine the distribution of the concentrated solar flux on the periphery of the absorber tube. To do this, the open source code SolTrace is used for ray tracing using the generalized Monte Carlo method, so in this chapter we will describe the methodology for using this software.

II.2. Solar radiation in Algeria

Algeria is a country situated in the North of Africa on the Mediterranean coast with a total area of 2,381,741 square kilometers. Algeria is the tenth-largest country in the world and the largest in Africa and the Mediterranean. The country is bordered in the northeast by Tunisia, in the east by Libya, in the west by Morocco, in the southwest by Western Sahara, Mauritania, and Mali, in the southeast by Niger, and in the north by the Mediterranean Sea as shown in Figure II.1. Algeria is divided topographically into three main regions that generally run east west. The first is the Tell, which is the Mediterranean coastal region. The second is the High Plateaus, which are more inland and are fairly consistent, until the third region, the Sahara, which covers almost 80% of Algeria's land [97].

Figure II. 1. *Map of Algeria [97]*

Algeria has an important solar deposit, apart from its climate, the maximum solar power in any point of our country is about 1Kw/m². The average maximum daily energy (clear sky, month of July) exceeds 6Kw/m² and the maximum annual energy in Algeria is about 2500 Kw/m². The sunlight received annually in Algeria by climatic region is given in the Table II. 1: (Ministry of Energy and Mines)

Table II. 1. *The sunlight received annually in Algeria*

Regions	littoral	High plateaus	Sahara
Surface area (%)	4	10	86
Sunlight (h/year)	2650	3000	3500
Energ, Average received (KWh/m²/year)	1700	1900	1900

II.2.1. Solar radiation with PVSYST software

II.2.1.1. PVsyst Software:

PVsyst was selected as the simulation software, because it is a powerful tool for studying, sizing and analyzing data of a PV system. It contains databases of both meteorological data and PV system components from several manufacturers. For this study, version 6.77 is used. Figure (II.2) shows an outline of the different steps of the meteorological data file and simulation in PVsyst [98].

The meteorological data file can be chosen from one of the databases included in PVsyst, which are NASA-SSE and Meteonorm 7.1, imported from another database that PVsyst supports or created based on measured data from e.g. Weather stations. The required parameters in the meteorological file are horizontal global irradiance and

ambient temperature. Horizontal diffuse irradiance and wind velocity are optional parameters, but the result will be more accurate if they are included. Since the simulation in PVsyst is operated at hourly intervals, hourly meteorological data are required to perform a simulation. For the meteorological data sources only containing monthly data,

Synthetic hourly data are constructed from the monthly values. Table (I.1) shows the acquired meteorological data from the specified site based on Meteonorm 7.1 database. Hourly meteorological data was synthetically generated for the databases that only had monthly values [98], and provide numerical temporal values of the solar heat flux in Laghouat city (ALGERIA).

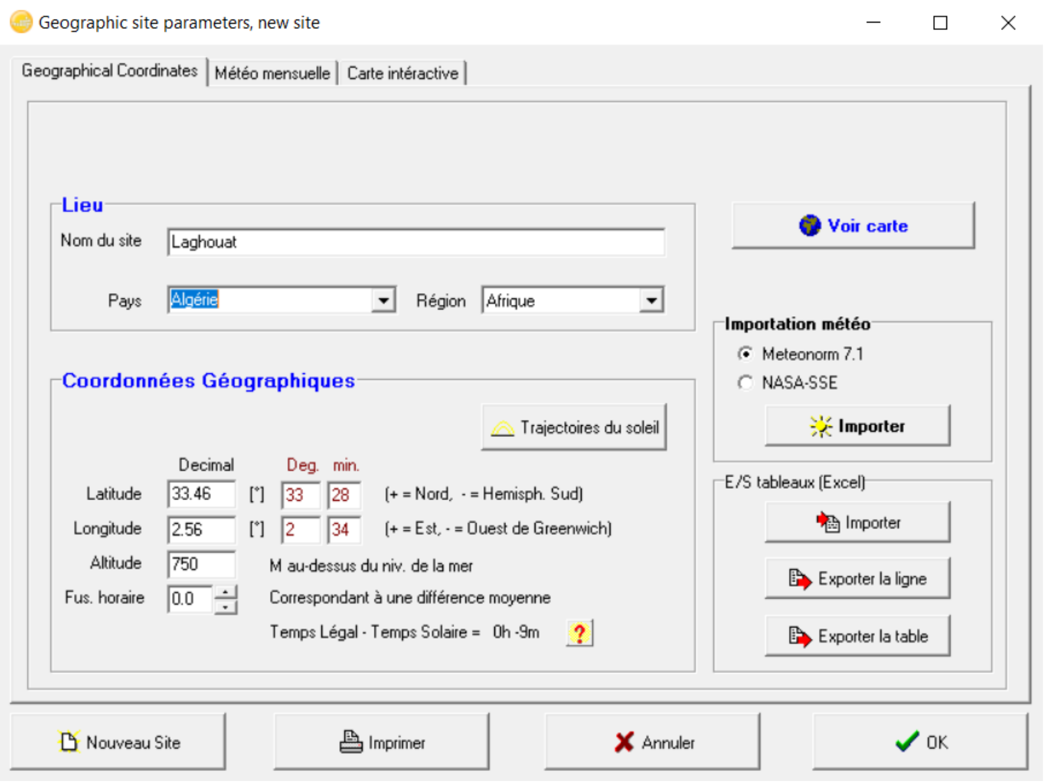

Figure II. 2. *Steps of the meteorological data file in PVsyst*

The geographical location is listed in Table (II.2**)**. These coordinates were used for all weather data and site specific data throughout the study.

Table II. 2. *Geographical location of Laghouat (ALGERIA)*

Latitude	Longitude	Altitude
33°46	**2°56**	**750 m**

II.2.1.2. Meteorological data

Solar flux density values for four days in different seasons are listed in Table (II.3).

Table II. 3. *Hourly meteo data of solar flux density values for four days in different seasons 2019*

Horizontal global radiation W/m²				
Hourly of day(h)	**21 March**	**21June**	**21September**	**21December**
04	0	0	0	0
05	0	0	0	0
06	4	232	45	0
07	214	447	272	6
08	441	646	490	182
09	636	815	674	357
10	785	942	808	489
11	877	1018	885	566
12	906	1037	898	583
13	869	999	846	539
14	770	906	734	437
15	614	764	569	285
16	414	584	363	97
17	181	378	133	0
18	0	161	0	0
19	0	0	0	0

II.3. Collector geometry

The collector, the parabolic trough, is a trough the cross-section of which has the shape of a part of a parabola. More exactly, it is a symmetrical section of a parabola around its vertex see Figure (II.3).

Radiation concentration at a parabolic trough, parabolic troughs have a focal line, which consists of the focal points of the parabolic cross-sections. Radiation that enters in a plane parallel to the optical plane is reflected in such a way that it passes through the focal line [28].

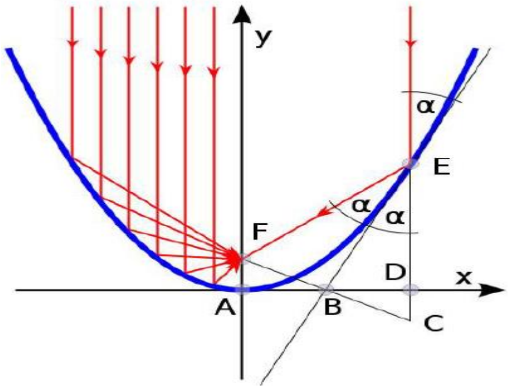

Figure II. 3. Path of parallel rays at a parabolic mirror [28]

An appropriate analytic representation of a parabola is:

$$Y = \frac{1}{4f}x^2 \qquad \textbf{(II.1)}$$

Where f is the focal length, the distance between the vertex of the parabola and the focal point.

II.3.1. Parameters for the geometrical description of a parabolic trough

To describe a parabolic trough geometrically, the parabola has to be determined, the section of the parabola that is covered by the mirrors, and the length of the trough.

The following four parameters are commonly used to characterize the form and the size of a parabolic trough See Figures (II.4) and (II.5): trough length, focal length, aperture width, distance between one rim and the other, rim angle, and angle between the optical axis and the line between the focal point and the mirror rim.

The rim angle **(**angle between the optical axis and the line between the focal point and the mirror rim) has the interesting characteristics that it alone determines the shape of the cross-section of a parabolic trough. That means that the cross-sections of parabolic troughs with the same rim angle are geometrically similar. The cross-sections of one parabolic trough with a given rim angle can be made congruent to the cross-section of another parabolic trough with the same rim angle by a uniform scaling (enlarging or shrinking). If only the shape of a collector cross-section is of interest, but not the absolute size, then it is sufficient to indicate the rim angle [28].

Two of the three parameters **rim angle**, **aperture width** and **focal length** are sufficient to determine the cross-section of a parabolic trough completely. Shape and size. This also means that two of them are sufficient to calculate the third one can be expressed as a function of the ratio of the aperture width to the focal length:

$$\tan\theta_r = \frac{W/f}{2-\frac{1}{8}\cdot\left(\frac{W}{f}\right)^2} \qquad \textbf{(II.2)}$$

Or, alternatively, the ratio of the aperture width to the focal length can be expressed as a function of the rim angle:

$$\frac{W}{f} = -\frac{4}{\tan\theta_r} + \sqrt{\frac{16}{\tan^2\theta_r}+16} \qquad \textbf{(II.3)}$$

The diagram in Figure (II.6) represents the w-f ratio in dependence on the rim angle.

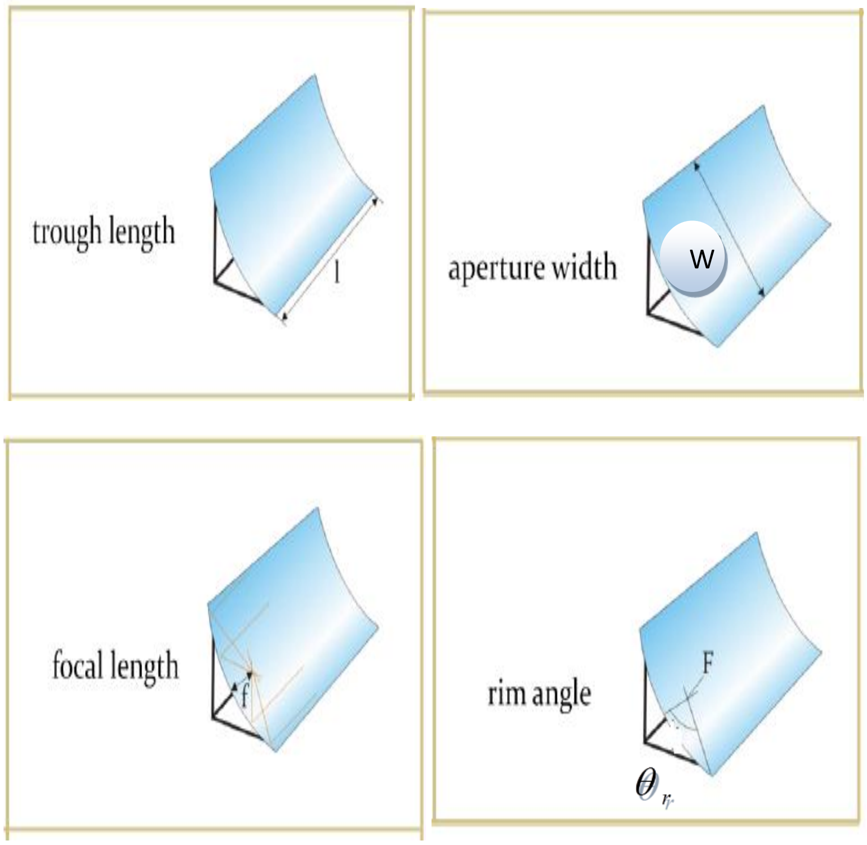

Figure II. 4._Geometrical parabolic trough parameters [28]_

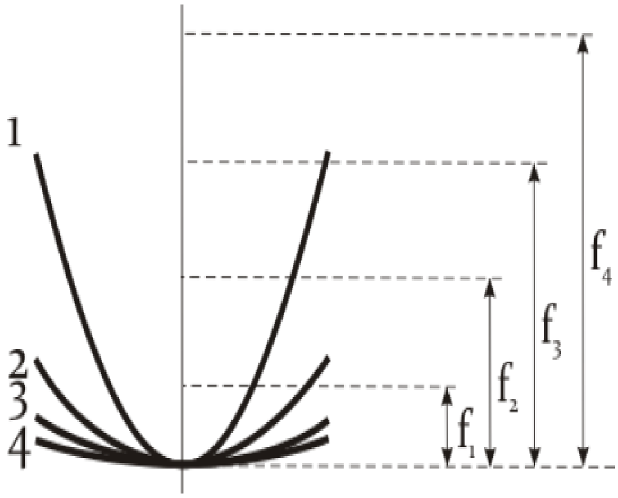

Figure II. 5. *Focal length as shape parameter [28]*

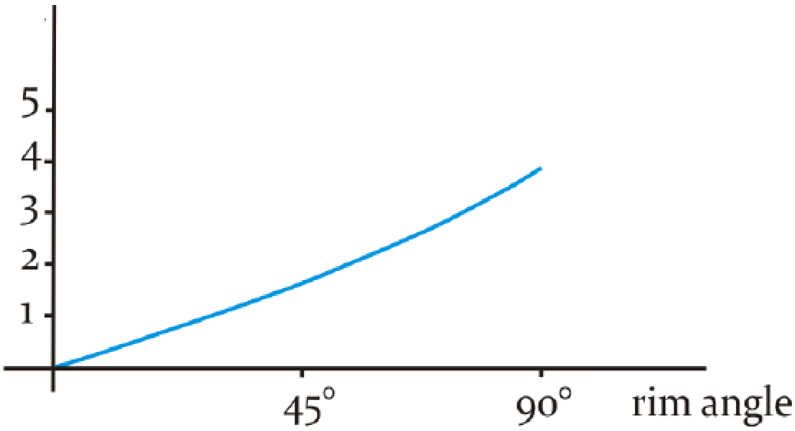

Figure II. 6. *Relation between the rim angle and the w/f-value*

II.3.2. Geometrical parameters of real parabolic troughs

We will have a look now at the values that take these parameters at real parabolic troughs. First, we see that the rim angle should neither be too small nor too large. The rim angle is related to the distance between the different parts of the mirrors and the focal line. Taking a fixed aperture width, Figure (II.7) represents this relation [28].

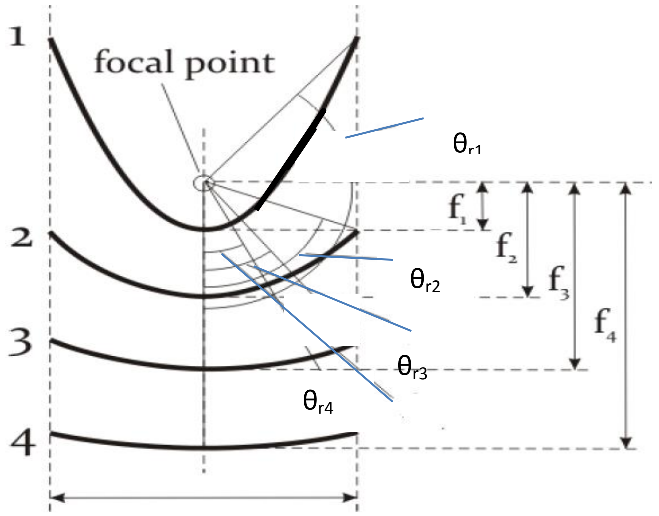

Figure II. 7. *Relation between the focal length and the rim angle for a constant trough aperture width [28]*

The rim angle is a very important constructive trait of collectors. For instance, it has an effect on the concentration ratio and on the total irradiance per meter absorber tube [W/m]. Qualitatively, we can understand in the following way that there must be some ideal rim angle range and that is should neither be too small nor too large:

- We consider, first, perfect mirrors, disregarding possible slope errors.
- If the rim angle is very small, then the mirror is very narrow and it is obvious that a broader mirror (with a larger rim angle) would enhance the power projected onto the absorber tube.
- If the rim angle is very big, then the way of the reflected radiation from the outer parts of the mirror is very long and the beam spread is very big, reducing, hence, the concentration ratio. A mirror with a smaller rim angle and the same aperture width would permit a higher concentration ratio. [28]

II.3.3. Mirror area and aperture area

Besides the mentioned linear measures, also surface area measures are important. There is, first, the aperture area, which is an important constructive measure. At a given DNI and a given Sun position it determines the radiation capture. The aperture area A_{ap} is calculated as the product of the aperture width and the collector length L:

$$A_{ap} = W.L \quad \textbf{(II.4)}$$

The surface area of a parabolic trough may be important to determine the material need for the trough. The area is calculated as follows [28]:

$$A=\left(\frac{W}{2}\sqrt{1+\frac{W^2}{16f^2}}+2f.\ln\left(\frac{W}{4f}+\sqrt{1+\frac{W^2}{16f^2}}\right)\right).L \qquad \textbf{(II.5)}$$

II.3.4. Concentration ratio

The concentration ratio is one of the central parameters of the collector. It is decisive for the possible operating temperatures of the parabolic trough power plant. The concentration ratio C is defined as the ratio of the radiant flux density at the focal line, or, what is the same, G_{im} at the Sun image, to the direct irradiance at the aperture of the collector, $G_{b,ap}$ [28]:

$$C=\frac{G_{im}}{G_{b,ap}} \qquad \textbf{(II.6)}$$

Now, the irradiance is different in different points of the Sun image. That is why we can consider, first, a punctual concentration ratio. In this case, G_{im}, has to be determined at a point within the focal line in order to determine the concentration ratio in relation to that specific point. Alternatively, we can consider, second, a mean concentration ratio taking C as the ratio of the mean irradiance at the focal line to the direct normal irradiance.

Concerning the mean concentration ratio (contrary to the punctual one) there is an easy way to specify it without any measurement: The geometrical concentration ratio C_G is a useful approximation. It is defined as the ratio of the collector aperture area to the receiver aperture area (see Figure II.8).

$$C_G=\frac{A_{ap,c}}{A_{ap,r}}=\frac{A_a}{A_{abs}} \qquad \textbf{(II.7)}$$

While it is clear what the collector aperture area is (see above), it is much less clear what has to count as the receiver aperture. In many cases, the projected area of the absorber tube is chosen. In this case, the receiver aperture area is a rectangle with the area D.L, where D is the absorber tube diameter [28].

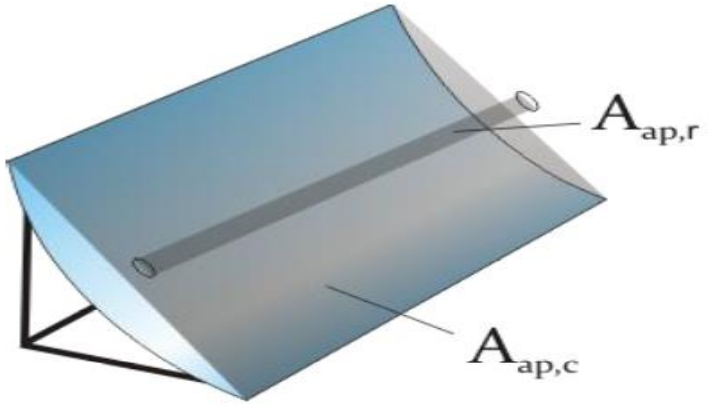

Figure II. 8.*Collector aperture area and receiver aperture area [28]*

Possibility is to take the irradiated absorber surface area as the receiver aperture area. In real parabolic troughs, this would mean that the whole absorber tube surface area $\pi.D.L$ is the receiver aperture area [28]:

$$C_G = \frac{W.L}{\pi.D\ .L} = \frac{W}{\pi.D} \qquad \textbf{(II.8)}$$

II.4. Optical Model

In ideal conditions, 100% of the incident solar energy is reflected by the concentrator and absorbed by the absorber. However, in reality, the reflector does not reflect all solar radiation due to imperfections of the reflector causing some optical losses. The optical efficiency relies on many factors such as tracking error, geometrical error, and surface imperfections.

A cross section of a receiver and a reflector is shown in Figure (II.9). It shows several important factors. When incident radiation hits the reflector at the rim collector, it makes an angle, which is known as rim angle θ_r. For ideal alignment, the diameter of the receiver has to intercept the entire solar image, and it is given as follows [99]:

$$D = 2r_r \sin\theta_m \qquad \textbf{(II.9)}$$

Where θm equal to half of acceptance, r_r is mirror radius.

The radius, *r*, which is shown in Figure II.9, can be determined by the following equation:

$$r = \frac{2f}{1+\cos\theta} \qquad \textbf{(II.10)}$$

θ is the angle between the reflected beam at the focus and the collector axis, f is the parabola focal length. θ varies between 0 and rim angle θr. Thus, the radius r, also varies from the focal length f , and r_r , and the theoretical image size varies from $2f\sin\theta_m\,to\,2r_r\sin\theta_m/\cos(\theta r+\theta_m)$ [99].

Equation (**II.10**) at the rim angle, θr, become:

$$r_r = \frac{2f}{1+\cos\theta_r} \tag{II.11}$$

The aperture of the parabola is another important factor, which is related to the rim angle and parabola focal length, and it is given by [100]:

$$W = 4f\tan\left(\frac{\theta_r}{2}\right) \tag{II.12}$$

The geometric concentration ratio of tubular absorber can be defined as follows [100]:

$$C = \frac{\sin\theta_r}{\pi\sin\theta_m} \tag{II.13}$$

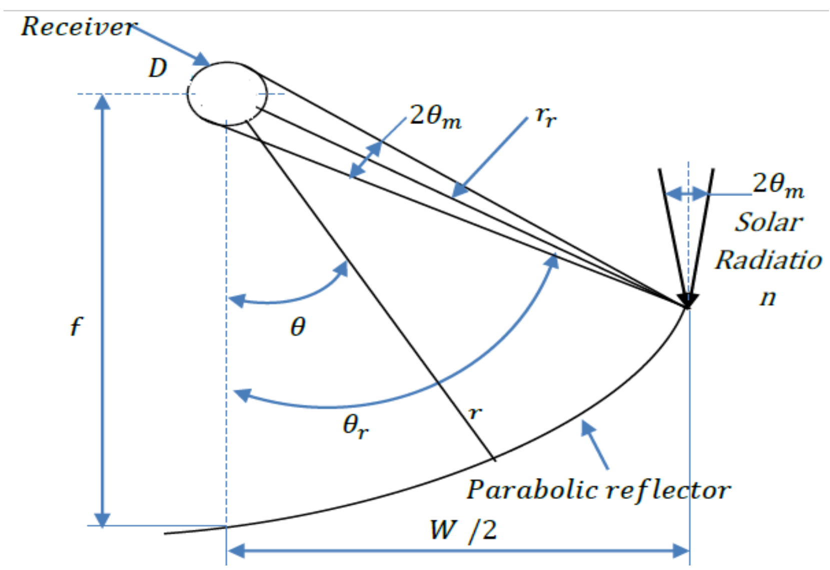

Figure II. 9. *A cross section of the receiver and the reflector showing different angles [100]*

II.4.1. Optical efficiency

As mentioned before, the optical efficiency of PTC is defined as the ratio of energy reaching the absorber tube to that received by the collector [101]. It can be presented as it follows:

$$\eta_0 = \left[\rho_{Trough}\tau_{env}\alpha_{abs}\gamma\right]K\left(\theta\right)X_{end} \quad \textbf{(II.14)}$$

Where ρ_{trough} is the mirror reflectance, τ_{env} is the glass envelope transmittance, α_{abs} is the absorber surface absorptance, γ is the intercept factor, K (θ) is incident angle modifier, and X_{end} is end effect loss.

II.4.2. Incident angle modifier

The incident angle modifier accounts the effect of increasing or decreasing the angle of incidence. The incident angle modifier is defined as the ratio of thermal efficiency at a given angle of incidence to the peak efficiency at normal incidence [102].

$$K(\theta) = \frac{(\eta_{th})_\theta}{(\eta_{th})_p} \quad \textbf{(II.15)}$$

The incident angle modifier relies on the geometrical and optical properties of the collector. It can be generated by empirical fit to experimental data, and it is described as a polynomial function of the absolute value of θ [103]:

$$K(\theta) = b_o + b_1\theta + b_2\theta^2 \quad \textbf{(II.16)}$$

II.4.3. Intercept factor

Another factor affecting the optical efficiency is called intercept factor. It is defined as the fraction of incident solar flux that is intercepted by the concentrator. Ideally, if the mirror and receiver are aligned perfectly and the tracking drive system is perfect and the mirror surface is clean without surface imperfections, the intercept factor will be unity. However, in reality, there are some errors related to the collector; imperfections of mirror surfaces and misalignment of the mirror exist because of manufacturing and assembly [104]. In addition, there are errors with the accuracy of the tracking system. Forristall [105] presents the terms that affect the intercept factor:

Heat collection element (HCE) shadowing (bellows, shielding, and support)

- Tracking error
- Geometry error (mirror alignment)
- Dirt on mirrors
- Dirt of heat collection element (HCE)
- Unaccounted

II.4.4. End loss

At zero angle of incidence, the solar radiation that reflected from the concentrator hit the entire heat collection element (HCE). However, when the angle of incidence starts to increase, some areas near the end of the receiver are not illuminated by the solar radiation as illustrated in Figure (II.10). These losses are addressed with the term of end losses.

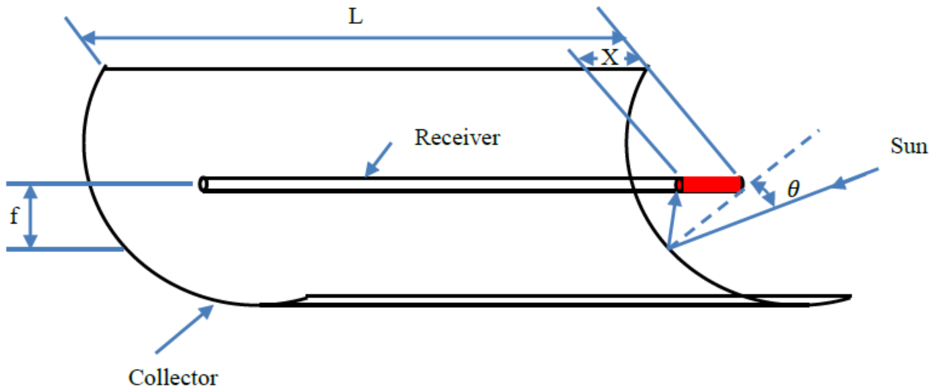

Figure II. 10. *End losses. Adopted from [106]*

The distance X, which is the part of HCE that is not illuminated can be calculated as it follows [106]:

$$X = f \operatorname{Tan}\theta \tag{II.17}$$

The end loss which is a function of the focal length of the collector, length of the collector, and angle of incidence is defined by [107].

$$X_{end} = 1 - \frac{f}{L} \operatorname{Tan}\theta \tag{II.18}$$

Other factors taken in account when predicting the optical efficiency of the collectors are the selective coating absorptance, emittance and the glass envelope absorptance, emittance, and transmittance. The coating emittance depends on the temperature of the outer absorber surface, and Table (II.3) lists coating emittance equations for all coating types [105].

Table II. 4. *Emittance for different coating types*

Coating type	Coating emitance
Luz black chrome	0.0005333(T+273.15)-0.0856
Luz cermet	0.000327(T+273.15)-0.065971

However, the glass envelope absorptance and emissivity are assumed independent of temperature. The glass absorptance and emissivity have values of 0.02 and 0.86 respectively [105].

II.5. Heat Flux Estimation - Ray Tracing

In the present study, the concentrated solar irradiation heat flux distribution as reflected by the PTC was obtained by using a general purpose ray trace code SolTrace. It follows a sequential coupled method to obtain the concentrated heat flux distributions on the absorber tube surface. A brief introduction to the ray-tracing code

II.5.1. Introduction to SolTrace

SolTrace (version 2012.) developed by the National Renewable Energy Laboratory (NREL) is a general-purpose ray trace code based on the Monte-Carlo method. The code is capable of modeling the concentrating solar power optical systems and analyzes their performance. Although originally intended for solar applications, the code can also be used to model and characterize many general optical systems. SolTrace can model parabolic trough concentrators as well as dishes, towers or other unique geometries (linear power towers, solar furnaces, etc.). It models optical geometries as a series of stages composed of optical elements that possess an extensive variety of available attributes including shape, contour, and optical quality. Figure (II.11) shows the screenshot of the SolTrace software. The code utilizes a ray tracing methodology developed by Spencer and Murty 1962. The system under study for the solar thermal / optical analysis need to be modeled within the software. The sun, sun position, shape of sun intensity, optical elements to be tested and the absorber are modeled within the SolTrace. Figure **(**II.12) shows the components of the SolTrace software such as Sun, Optical Properties, System Stages and Trace Options [106].

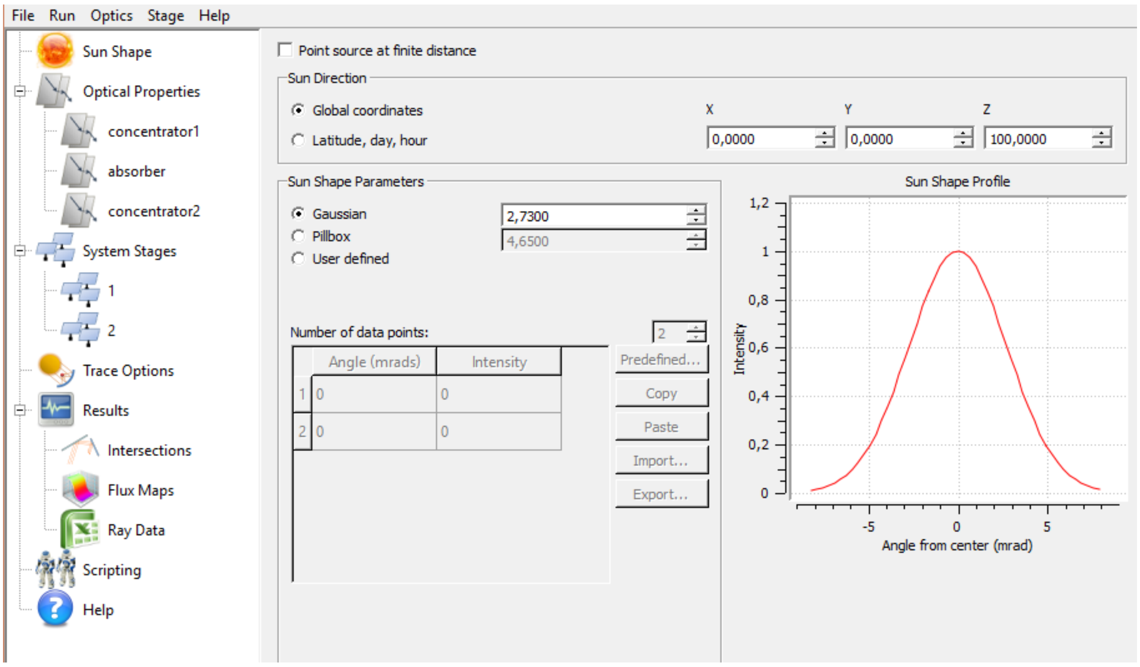

Figure II. 11. Main menu of SolTrace software

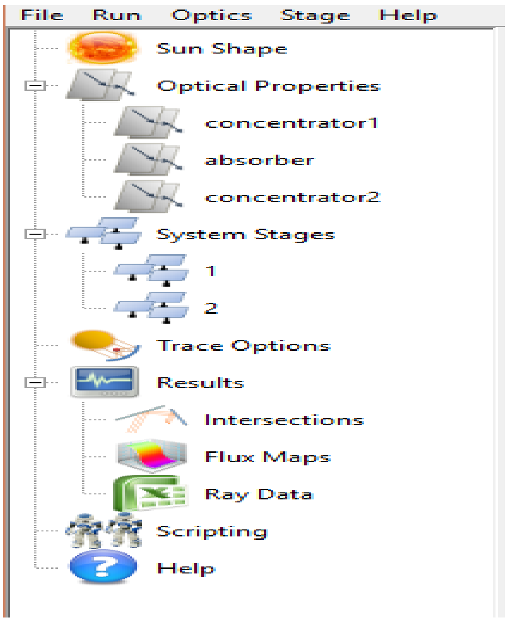

Figure II. 12. Components settings window in SolTrace software

Rays falling from the sun are traced through the system while encountering various optical interactions was modeled. Some of these interactions are probabilistic in nature (e.g. selection of sun angle from sun angular intensity distribution) while others are deterministic (e.g. calculation of ray intersection with an analytically described surface and resultant redirection). SolTrace has the advantage over other codes such as Comsol, Star ccm+ Trnsys since SolTrace has been more user friendly.

Therefore, SolTrace can provide accurate results for complex systems that cannot be modeled otherwise. Accuracy of ray prediction increases with the number of rays traced and larger ray numbers means more processing time. In addition, complex geometries translate into longer run times. Fewer rays (and therefore less time) are needed to determine relative changes in optical efficiency for different sun angles on a given solar concentrator than that are needed to accurately assess the flux distribution on the receiver of that same concentrator.

The PTC system of investigation was modeled in SolTrace code with the solar trough collector and the single tube absorber, as independent elements, positioned relative to each other in the same coordinate system similar to the experiments. The sun position was specified with respect to the PTC system to model the impinging solar rays using global coordinate system approach. The stage properties modeled in the 1 with the parabolic trough collector and the absorber tube with secondary reflector is shown in Figure (II.13) (a). The element surface and aperture modeling details for the parabolic trough surface and the absorber tube surface with secondary reflector is shown in Figures (II.13) (b) and (c) respectively [106].

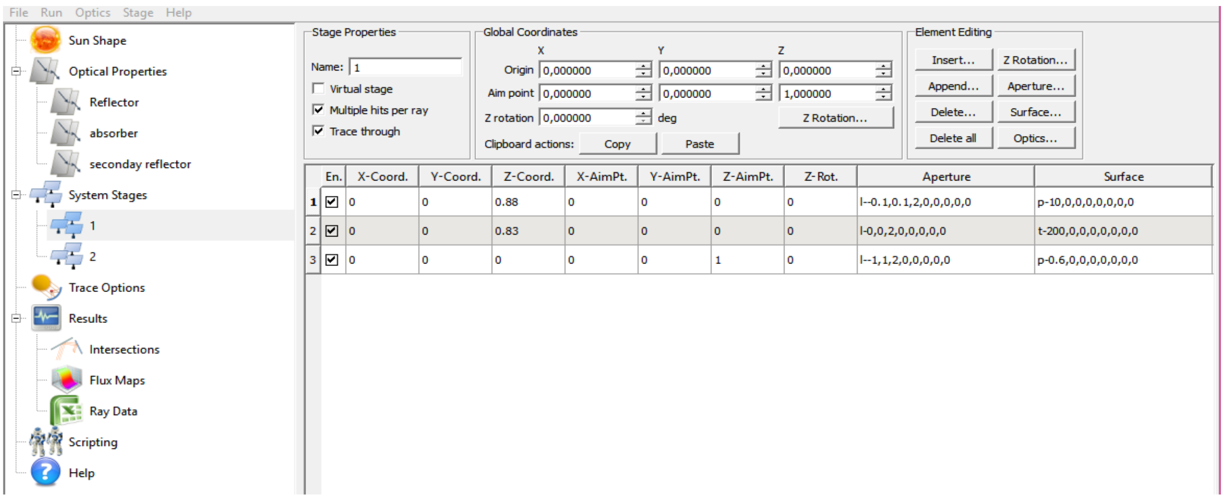

(a) Stage properties as defined in SolTrace

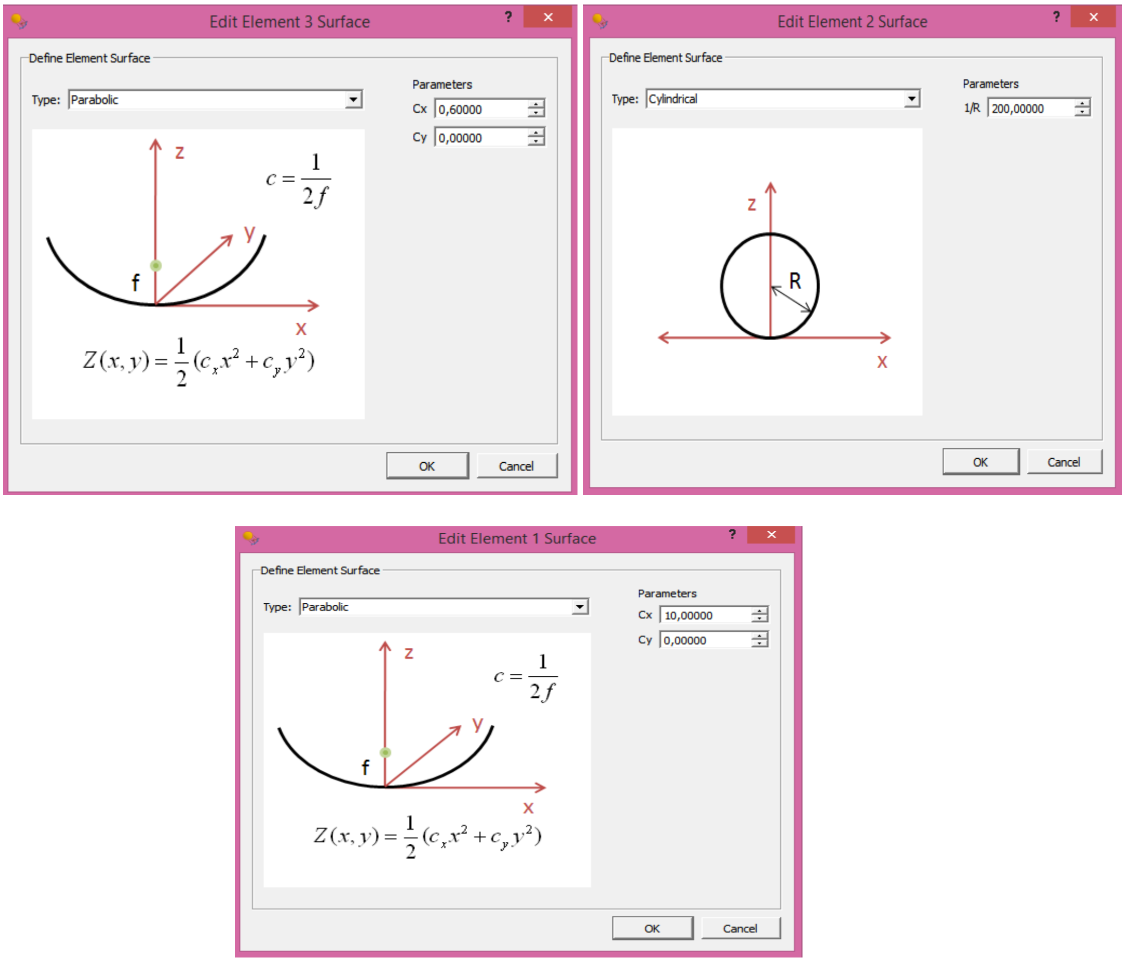

(b) Surface definition for the PTC, the absorber and secondary reflector

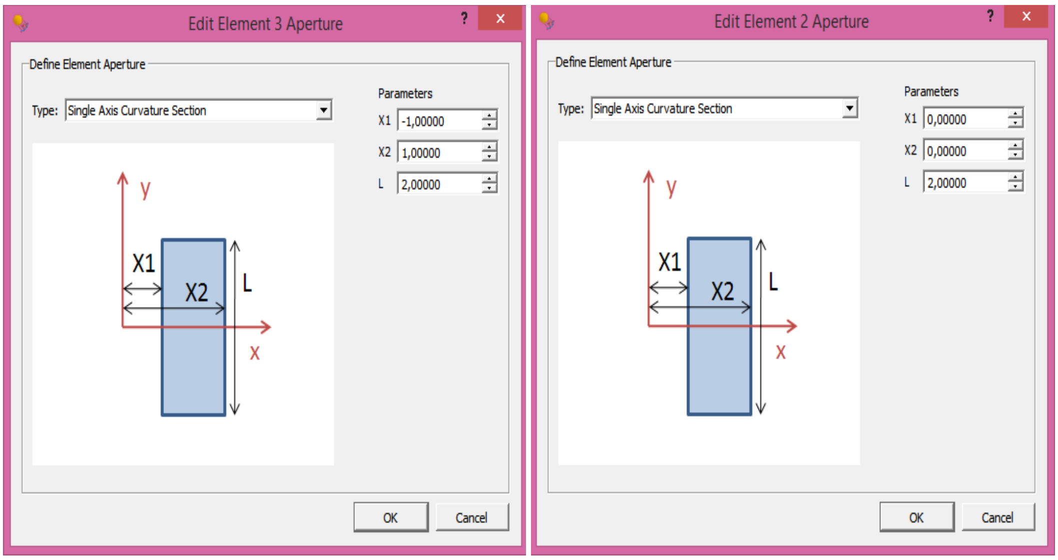

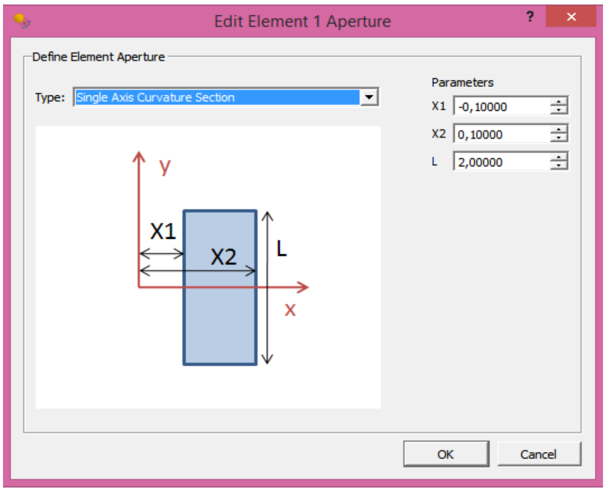

(c) Aperture definition for the PTC, the absorber and secondary reflector

Figure II. 13. *Modeling of elements in SolTrace*

Two characteristics completely define the "sun" as the light source in SolTrace code: (1) the angular intensity distribution of light across the sun's disk (referred to as the sun shape) and (2) the sun's position. A predefined sun profile was chosen with a peak beam radiation flux of 1000 W/m^2, as observed in the test. Total number of solar rays traced for the present study was 100 rays in SolTrace. Figure **(**II.14) shows only a sample set of 100 rays (1-100 no's) traced in the PTC system to avoid clutter. Figure II.14 (a) shows the front view of the rays traced from the sun hitting the reflector and the reflected rays hitting the absorber tube. It is to be noted that the picture aspect ratio is not to scale and reproduced here as obtained from the SolTrace code. The solar rays were made to hit the reflector from the top towards the bottom. The corresponding location of the sun is specific to a particular instant of the experimental day. [106]Figure. (II.14) (b) shows the isometric view of the PTC system with the solar rays. Figure (II.14) (c) shows the isometric view of the PTC system with secondary reflector

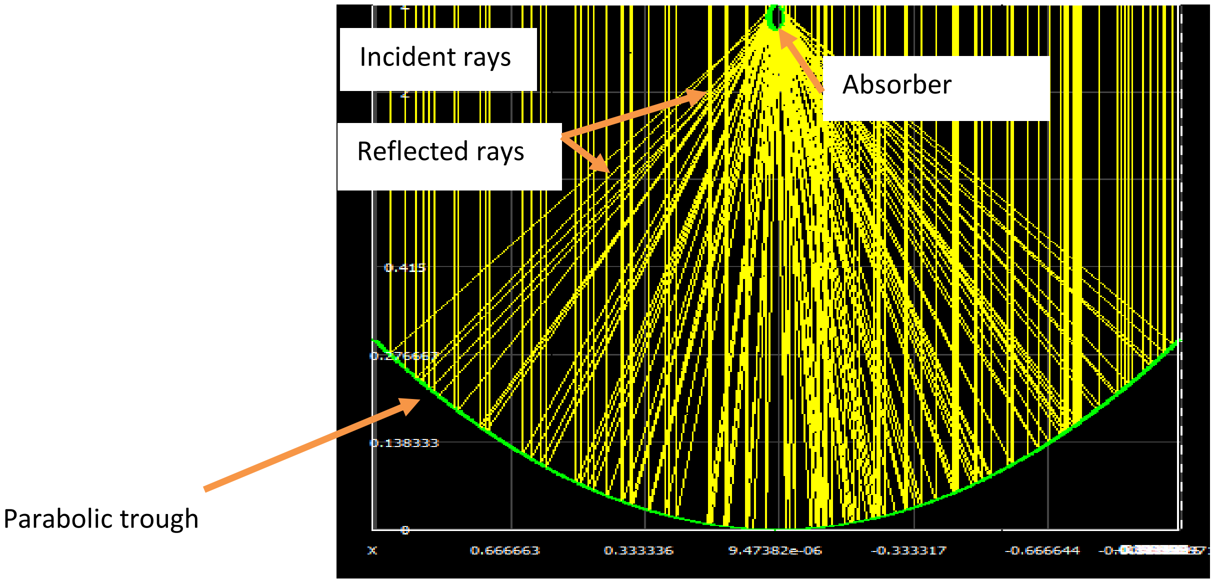

(a) Front view PTC

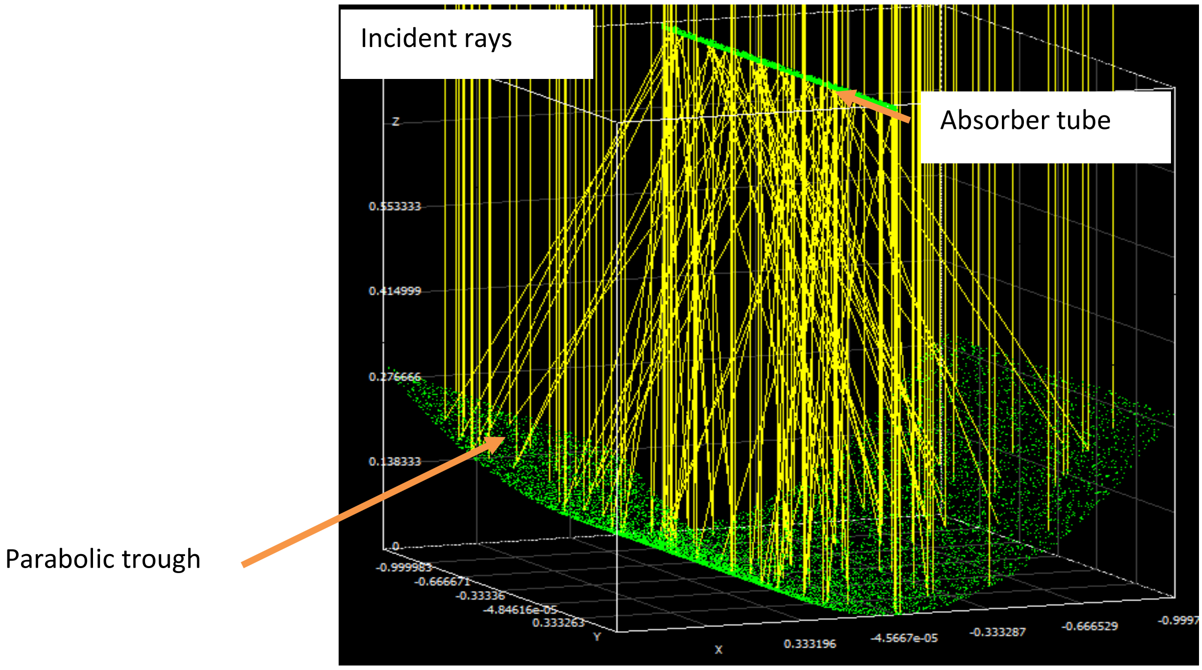

(b) Isometric view PTC

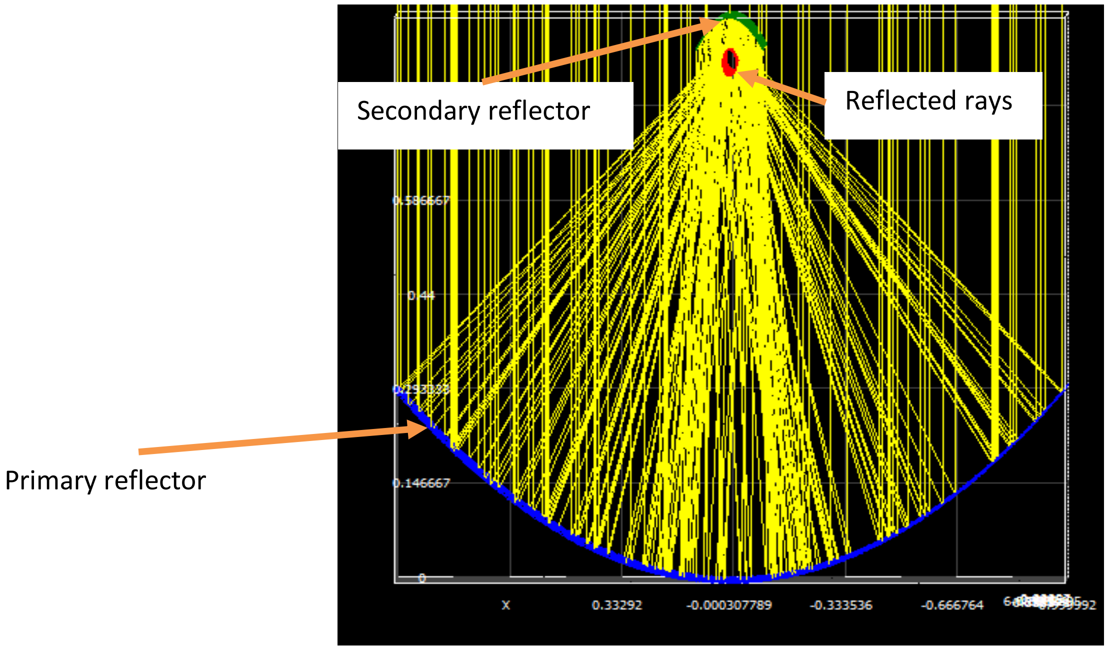

(c) Front view of PTC with secondary reflector

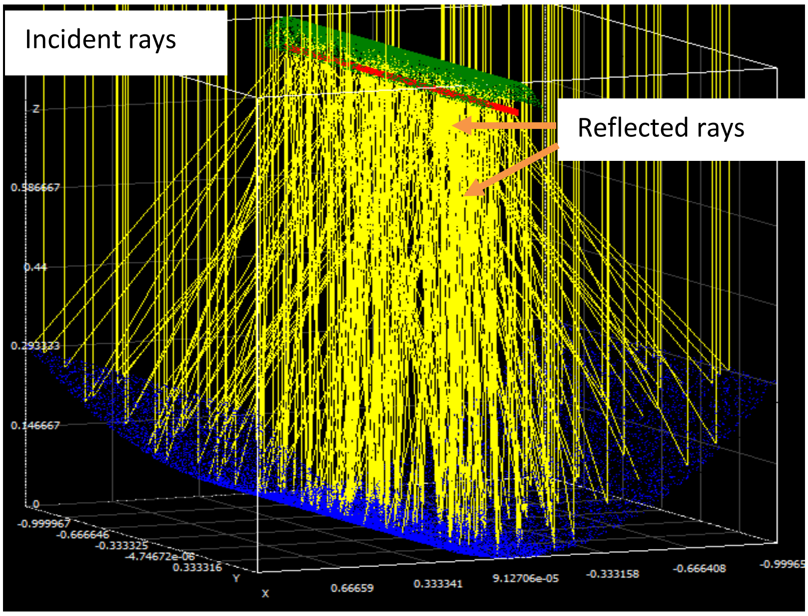

(d) Isometric view of PTC with secondary reflector

Figure II. 14. *Sample set of solar rays traced in SolTrace for F = 0.83 m*

Working Procedure in SolTrace, an optical system is organized into “stages” within a global coordinate system. A stage is loosely defined as a section of the optical geometry which, once a ray exits the stage, will not be re-entered by the ray on the remainder of its path through the system. Complete system geometry may consist of one or more stages. It is incumbent on the user to define the stage geometry accordingly. The motivation behind the stage concept is to employ efficient tracing and therefore save processing time and allow for a modular representation of a system. The other significant benefit of stages is that they can also be saved and employed in other system geometries without the need for recalculating element positions and orientations. Segmentation of the geometry via stages may also be useful in assignment of different coordinate systems for specific geometries and can make adjustment of locations far more straightforward. [107]

A stage is comprised of "**elements**". Each element consists of a surface, an optical interaction type, an aperture shape and, if appropriate, a set of optical properties. The location and orientation of stages are defined within the global coordinate system whereas the location and orientation of elements are specified within the coordinate system of the particular stage in which they are defined. Stages can be one of two types: optical or virtual. An optical stage is defined as one that physically interacts with the rays and can potentially altering their trajectories. Conversely, a virtual stage is defined as one that does not physically interact with the rays. The virtual stage is useful for determining ray locations and directions and incident power or flux at various positions along the optical path without physically affecting ray trajectory and has no optical properties. Beyond this, optical and virtual stages are identical in how they are defined and used. Stages can be duplicated and moved around as groups of elements and saved for use in other system geometries. It is not possible to mix virtual and optical elements within single stage at present SolTrace uses three right-handed coordinate systems: the global coordinate system, the stage coordinate system and the element coordinate system. These are illustrated in Figure (II.15). Each element in a stage has a local coordinate system (i.e. location and orientation) defined relative to the stage coordinate system. Each stage has a coordinate system defined relative to the global coordinate system. The direction of the sun is defined relative to the global coordinate system [107].

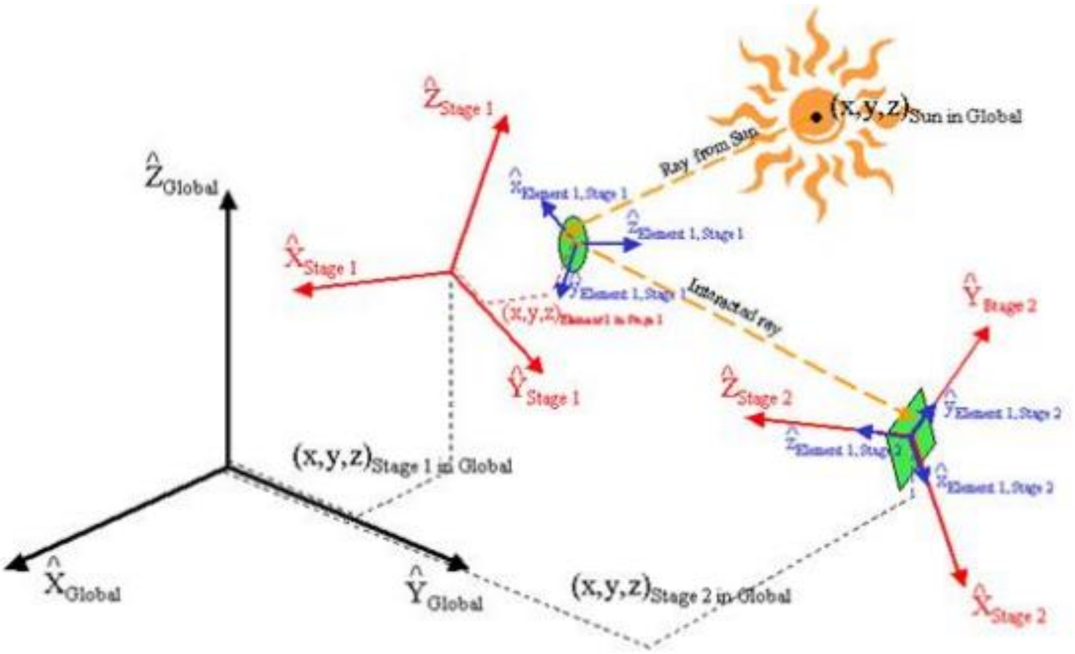

Figure II. 15. *SolTrace coordinate systems - Generalized version [107]*

The sun direction can be input in either vector form, or in time-of-day, day-of year format with latitude specified. For the present numerical analysis, the vector form of specification for the sun was used. Light rays are generated from the sun and then traced sequentially through each stage in the geometry. The position and direction of each ray in each stage is stored in memory for later processing and output [107].

II.6. Mathematical modelling

II.6.1. Assumptions

- Reflection is considered two times (including primary reflector reflection and secondary reflector reflection).
- Scattering of the solar rays is considered as negligible.
- Part of the radiation that is striking the receiver tube is completely absorbed by tube material.
- Part of the radiation that is striking the receiver tube, is absorbed by the fluid through conduction through the tube material and internal convection in the receiver tube.
- Part of the radiation heat loss, which is recovered by the primary reflector and secondary reflector, is not considered in the calculation.
- The Absorptivity of the receiver tube material is considered as maximum.

- Radiation striking on two reflectors are considered in two parts, primary part in which ray is completely reflected and secondary part that is not reflected. Effect of absorption, transmission, and scattering are considered in the second case.
- Effect of wind is considered as negligible when rays are transmitted in a secondary or non-imaging reflector to avoid the condition of scattering.
- Exact focal length = 0.83 m

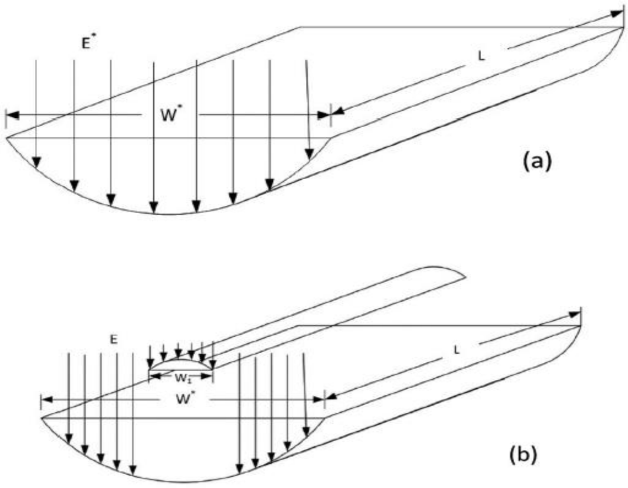

Figure II. 16. *(a) Primary reflector and (b) primary reflector with secondary parabolic reflector [56]*

II.6.2. Mathematical modelling procedure of secondary reflector

No. of rays striking the primary reflector (in SolTrace) = 100

No. of rays, focused on the receiver tube = 80 (so, C1 = 0.8)

No. of rays, not focused on receiver tube = 20 (so, 1 – C1 = 0.2)

The number of rays considered to be 100 in ordered to simplify the mathematical formulation [108] Accordingly, we have considered that 80% of the total number of rays is focused on the center line of the receiver tube and 20% is not focused on the receiver tube [56]

$$C_1 = 0.8, C_2 \approx C_1 = 0.8$$

$$E^* = I_b\left(W.L\right) \quad \textbf{(II.19)}$$

$$E = I_b\left[\left(W - W_1\right)L\right] \quad \textbf{(II.20)}$$

$$W_1 \le \frac{WC_2\rho_{\sec}\left(1-C_1\right)}{C_1+C_2-C_1C_2\rho_{\sec}} \quad \textbf{(II.21)}$$

For the sake of simplicity, C_1 and C_2 can be considered as equal because the material used and procedure followed is same for both primary and secondary reflectors.

Procedure to find out the dimensions of the secondary reflector- (W_1) max is calculated from Equation (**II.21)** [56].

$$\left(W_1\right)_{\max} \le \frac{WC_2\rho_{\sec}\left(1-C_1\right)}{C_1+C_2-C_1C_2\rho_{\sec}} \quad \textbf{(II.22)}$$

$(W_1)_{\min}$ is calculated from the maximum value of acrylic cover outer diameter [56].

$$\left(W_1\right)_{\min} \le W_1 \le \left(W_1\right)_{\max} \quad \textbf{(II.23)}$$

Length of secondary reflector is decided by the length of primary parabolic collector. Rim angle is decided by manufacturing simplicity. Now, value of W_1, L, of the secondary reflector is decided and based on these values other parameters can be calculated.

Focal length of the secondary reflector [56]:

$$f_1 = \frac{W_1}{4\tan\left(0.5\theta_r\right)} \quad \textbf{(II.24)}$$

Vertical height of secondary reflector [56]:

$$h_{p_1} = \frac{W^2{}_1}{16 f_1} \quad \textbf{(II.25)}$$

Radius of the secondary reflector [56]:

$$r_{r_1} = \frac{W_1}{2\sin\theta_r} \quad \textbf{(II.26)}$$

Length of arc of secondary reflector [56]:

$$L_1 = \int_{-0.5W_1}^{0.5W_1} \sqrt{1+\left(\frac{dy}{dx}\right)^2}\, dx \quad \textbf{(II.27)}$$

Surface area of the secondary reflector [56]

$$A_1 = L_1 \times L \quad \textbf{(II.28)}$$

II.7 Chapter Summary

The optical analysis plays an essential role in the study of a PTC system. Indeed, the concentration of solar radiation around the absorber tube is the key parameter in any study of the thermal balance of this system. It represents an important thermal boundary condition for CFD analysis.

To begin this analysis, it is first necessary to acquire the climatological data of the site where the system is installed. In the present study, the data that we considered concern the city of Laghouat located in southern ALGERIA (400 km from Algiers). The geographic coordinates of the city are: 2°56 Longitude, 33°46 Latitude, and 736m Elevation above sea level. To obtain the evolution of the solar flux in this city, we can proceed in two ways: Use a solarimeter or a specialized software. The first solution is complicated because it takes a long time to acquire the data for different seasons. The second solution seems to be the best especially if it is validated by the first solution. In this study, PVSYST software is used to determine the solar irradiance for this location during four days from different seasons of the year 2019: March 21, June 21, September 21, and December 21.

The purpose of the optical modeling is to determine the concentration of heat flux on the portion of the receiver tube surface exposed to the reflected rays from the primary reflector. To do this, we used the SolTrace code, which uses Monte Carlo Ray-Tracing method. This program allows to introduce the geometry optical characteristics of the system, the geographic data, and the solar flux density. The key output is the flux distribution around the tube absorber, which serves as a thermal boundary condition for CFD analysis. In order to compare traditional PTC and improved PTC, two cases are considered: PTC without secondary reflector and PTC with secondary reflector.

Chapter III

Thermal Analysis

Thermal Analysis

III.1. Introduction

The last part is thermal analysis, and the aim of this part is to predict the thermal efficiency of PTC: the ratio of energy absorbed by the heat transfer fluid (HTF) to that hits the reflector. The HCE (heat collection element absorber) performance model is based on an energy balance about the collector and the HCE. The energy balance includes the direct normal solar irradiation incident on the collector, optical losses from both the collector and HCE, thermal losses from the HCE, and the heat gain into the HTF. For short receivers a one-dimensional energy balance gives reasonable results; for longer receivers a two- dimensional energy balance becomes necessary. All the equations and relationships used in both the one- and two-dimensional HCE performance models are described in the following sections.

III.2. The parabolic reflector

The mirrors are made of low-iron glass with a transmissivity of up to 98%. This glass is covered with a silver film on the underside, and a special protective coating. A good quality reflector can reflect 97% of the incident radiation. The concentration factor for a parabolic cylinder sensor is approximately 80%.

III.3. The absorber tube

The absorber tube is often made of selectively coated copper and is surrounded by a transparent glass envelope, as shown in Figure (III.1).It is placed along the focal line of the parabolic trough concentrator. It shall have the following characteristics:

- **Good absorption of radiation:** its absorption coefficient must be as high as possible in order to avoid any reflection of incident radiation.
- **Limited heat loss**: The temperature of the tube generally exceeds 400C°, the losses by convective and radiative exchanges are very important. In order to limit them, the tube is surrounded by a glass envelope under vacuum.

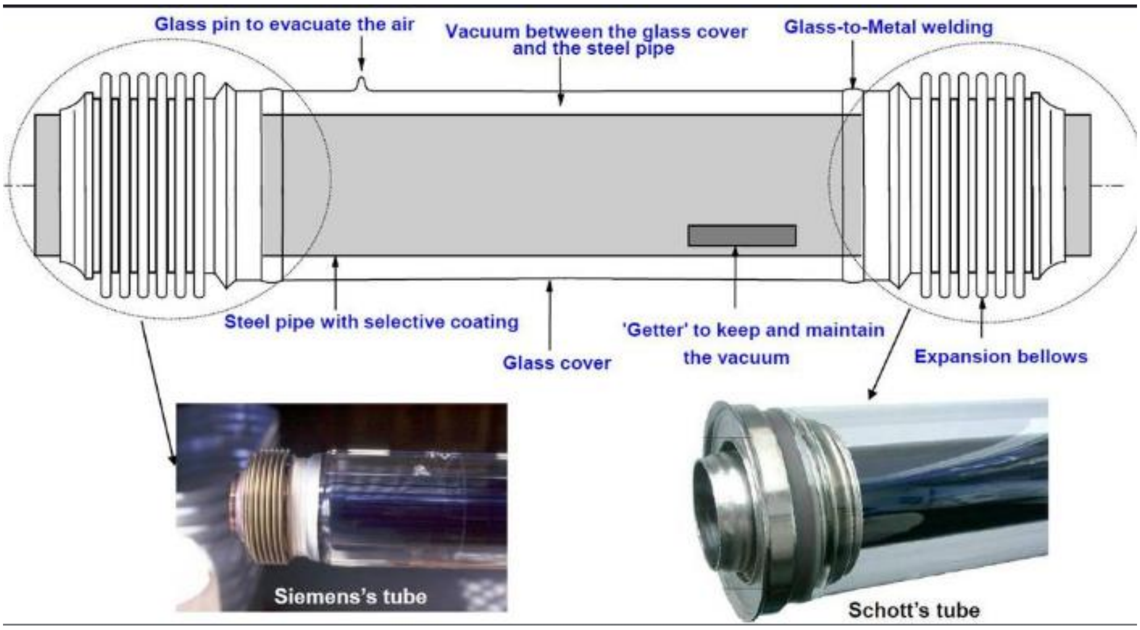

Figure III. 1. *Absorber tube structure*

III.4. Thermal model

The HCE performance model uses an energy balance between the HTF and the atmosphere, and includes all equations and correlations necessary to predict the terms in the energy balance, which depend on the collector type, HCE condition, optical properties, and ambient conditions. Figure (III.2) shows the one-dimensional steady-state energy balance for a cross-section of an HCE, with and without the glass envelope intact, and Figure (III.3) shows the thermal resistance model and subscript definitions. For clarity, the incoming solar energy and optical losses have been omitted from the resistance model. The optical losses are due to imperfections in the collector mirrors, tracking errors, shading, and mirror and HCE cleanliness. The effective incoming solar energy (solar energy minus optical losses) is absorbed by the glass envelope ($\dot{q}'_{5solabs}$) and absorber selective coating ($\dot{q}'_{3solabs}$). Some energy that is absorbed into the selective coating is conducted through the absorber ($\dot{q}'_{23cond}$) and transferred to the HTF by convection ($\dot{q}'_{12conv}$), remaining energy is transmitted back to the glass envelope by convection ($\dot{q}'_{34conv}$) and radiation ($\dot{q}'_{34rad}$). The energy from the radiation and convection then passes through the glass envelope by conduction ($\dot{q}'_{45cond}$) and along with the energy absorbed by the glass envelope ($\dot{q}'_{5solabs}$) is lost to the environment by convection ($\dot{q}'_{56conv}$) and radiation ($\dot{q}'_{57rad}$). If the glass envelope is missing, the heat loss from the absorber is lost directly to the environment. The model assumes all temperatures, heat fluxes, and thermodynamic properties are uniform around the circumference of the HCE. In addition, all flux directions shown in Figure (III.2) are positive.

With the help of Figures (III.2) and (III.3), the energy balance equations are determined by conserving energy at each surface of the HCE cross-section, both with and without the glass envelope intact. [105]

- **with the glass envelope**

$$\dot{q}'_{12conv} = \dot{q}'_{23cond} \quad \textbf{(III.1.a)}$$

$$\dot{q}'_{3solabs} = \dot{q}'_{34conv} + \dot{q}'_{34rad} + \dot{q}'_{23cond} \quad \textbf{(III.1.b)}$$

$$\dot{q}'_{34conv} + \dot{q}'_{34rad} = \dot{q}'_{45cond} \quad \textbf{(III.1.c)}$$

$$\dot{q}'_{45cond} + \dot{q}'_{5solabs} = \dot{q}'_{56conv} + \dot{q}'_{57rad} \quad \textbf{(III.1.d)}$$

$$\dot{q}'_{heatloss} = \dot{q}'_{56conv} + \dot{q}'_{57rad} \quad \textbf{(III.1.e)}$$

- **without the glass envelope:**

$$\dot{q}'_{12conv} = \dot{q}'_{23cond} \quad \textbf{(III.2.a)}$$

$$\dot{q}'_{3solabs} = \dot{q}'_{36conv} + \dot{q}'_{37rad} + \dot{q}'_{23cond} \quad \textbf{(III.2.b)}$$

$$\dot{q}'_{heatloss} = \dot{q}'_{36conv} + \dot{q}'_{37rad} \quad \textbf{(III.2.c)}$$

In the case without the glass envelope, Equations (III.1.c) and (III.1.d) drop out, and the 4 subscript for the convection and radiation from the absorber change to 6 and 7, respectively, since the heat loss from the absorber outer surface escapes directly to the environment instead of through the glass envelope .Note that the solar absorptance $\dot{q}'_{3solabs}$ and $\dot{q}'_{5solabs}$ are treated as heat flux terms. All the terms in Equations (III.1) and (III.2) are defined in Table (III.1). Dotted variables indicate rates and the prime indicates per unit length of receiver [105].

Table III. 1. *Heat Flux Definitions [105]*

Heat flux (w/m)	Heat transfer mode	Heat transfer path	
		from	**to**
$\dot{q}'_{12conv}$	**convection**	Inner absorber pipe surface	Heat transfer fluid
$\dot{q}'_{23cond}$	**conduction**	Outer absorber pipe surface	inner absorber pipe surface
$\dot{q}'_{3solabs}$	**Solar irradiation absorption**	Incident solar irradiation	Outer absorber pipe surface
$\dot{q}'_{34conv}$	**Convection**	Outer absorber pipe surface	Inner glass envelope surface
$\dot{q}'_{34rad}$	**radiation**	Outer absorber pipe surface	Inner glass envelope surface
$\dot{q}'_{45cond}$	***Conduction***	Inner glass envelope surface	Outer glass envelope surface
$\dot{q}'_{5solabs}$	**Solar irradiation absorption**	Incident solar irradiation	Outer glass envelope
$\dot{q}'_{56conv}$	**convection**	Outer glass envelope surface	Ambient
$\dot{q}'_{57rad}$	**Radiation**	Outer absorber pipe surface	sky
$\dot{q}'_{36conv}$	**convection**	Outer absorber pipe surface	Ambient
$\dot{q}'_{37rad}$	**radiation**	Outer absorber pipe surface	sky
$\dot{q}'_{heatloss}$	**Convection and radiation**	Heat absorber pipe surface	Ambient and sky

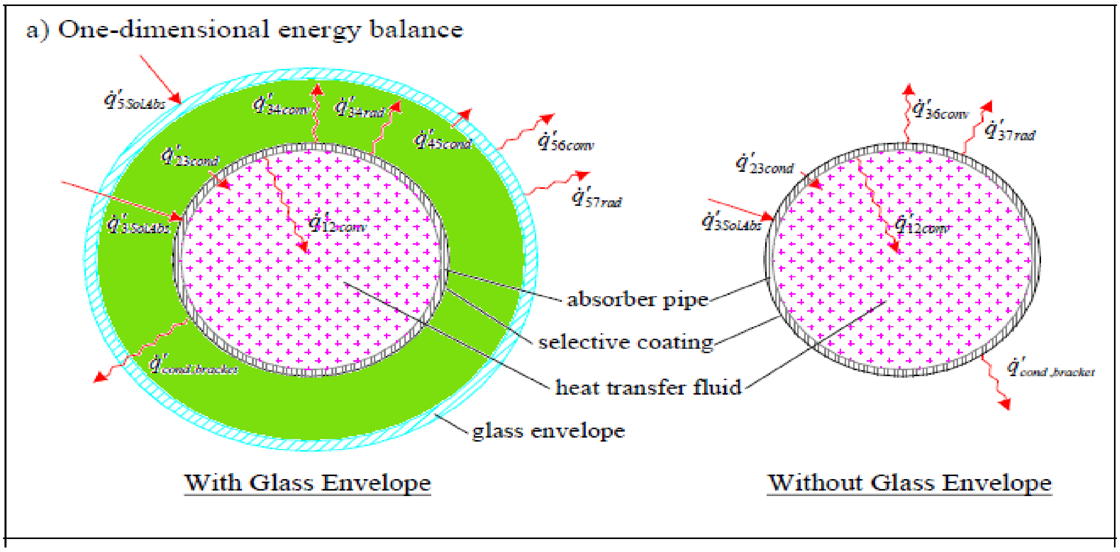

Figure III. 2. *Heat transfer model in a cross sectional area of the HCE (absorber) [105]*

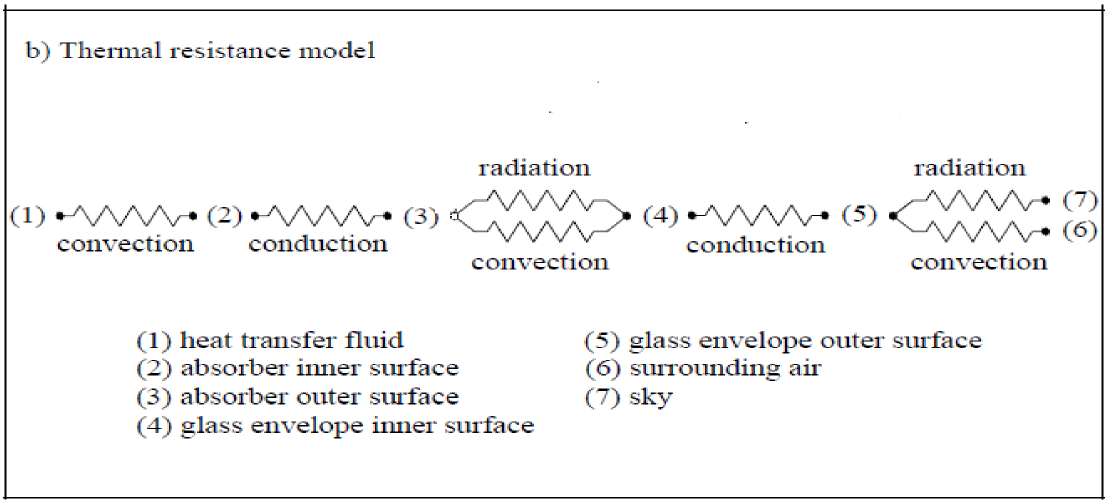

Figure III. 3.*Thermal resistance model [105]*

The solar absorption at the glass envelope and the absorber tube are treated as heat flux, which can facilitate the solar absorption terms and make the heat transfer through the glass envelope and the absorber tube linear .The receiver is divided into N number of segments, which have equal length, as it can be seen in Figure (III.4),to analyze each segment, the radial heat fluxes are presumed to be normal on the surface of the segment and uniform, and it can be calculated at the average temperature of the left and right sides of the segment. Thus, the radial heat transfer can be demonstrated applying one-dimensional heat energy balance as Forristall carried out [105]. According to the first law of thermodynamics for open systems [109] for segment i:

$$\frac{dE}{dt} = \dot{Q} - \dot{W} + \sum_{inlet} \dot{m}(h + KE + PE) - \sum_{outlet} \dot{m}(h + KE + PE) \quad \textbf{(III.3)}$$

There are many assumptions for this equation:

- Steady state process
- No work
- Kinetic energy (KE) equal to zero
- Potential energy (PE) equal to zero

After applying these assumptions for the heat balance equation, the new equation became:

$$0 = \dot{q}'' A_i + \dot{m}(h_{i,inlet} - h_{i,outlet}) \quad \textbf{(III.4)}$$

By assuming that the heat transfer fluid (HTF) is dependent on the temperature, the HTF enthalpy is approximated to be:

$$h_{inlet,i} \approx cp_{inlet,i}\, T_{inlet,i} \qquad \textbf{(III.5)}$$

The solar irradiation stated in equation (III.5**)** $\dot{q}"$, includes the solar irradiation absorbed by the absorber and the glass envelope $\dot{q}'_{5solabs}, \dot{q}'_{3solabs}$,and the heat loss.

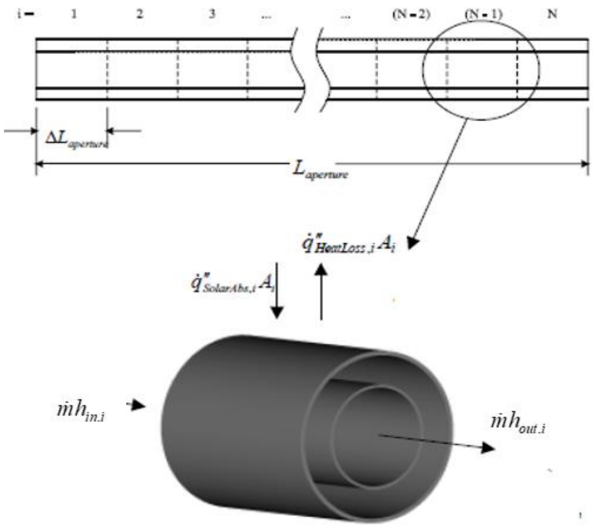

Figure III. 4. *2D heat transfer model [105]*

The net heat flux ($\dot{q}_i^{"}$) in Equations (III.4) includes solar absorption and heat loss.

$$\dot{q}" A_i = \dot{q}"_{solar\ abs,i}\, A_i - \dot{q}"_{heatloss,i}\, A_i \qquad \textbf{(III.6)}$$

The solar absorption term includes both the absorber（$\dot{q}'_{3solabs,i}$） and the glass envelope $\left(\dot{q}'_{5solabs,i}\right)$

$$\dot{q}^{"}_{solar\,abs,i} A_i = \dot{q}^{'}_{3sol\,abs,i} \Delta L_{aperture} + \dot{q}'_{5solabs,i}\, \Delta L_{aperture} \qquad \textbf{(III.7)}$$

The heat loss in Equation (III.6) includes the radiation and convection heat losses from the glass envelope and the conductive losses [105].

$$\dot{q}^{"}_{heatloss,i} A_i = \dot{q}^{'}_{57rad,i} \Delta L_{aperture} + \dot{q}'_{56conv,i}\, \Delta L_{aperture} \qquad \textbf{(III.8)}$$

Substituting equations (III.9) (III.8) and (III.6) in equation (III.5) and solving for outlet Temperature:

$$T_{out,i} = T_{in,i} + \frac{1}{\dot{m} C_1} \left(\dot{q}'_{3solabs,i} + \dot{q}'_{5solabs,i} - \dot{q}'_{56conv,i} - \dot{q}'_{57rad,i} \right) \Delta L_{aperture} \qquad \textbf{(III.9)}$$

The heat gain by HTF for the segment i is defined as it follows

$$\dot{q}'_{gain.i} = \dot{q}'_{12conv,i} \tag{III.10}$$

After estimating the heat loss, energy delivered to HTF, and outlet temperature for each segment of the receiver, the total heat loss of the system will be as it follows

$$Q_{heat\,loss} = \sum_{i=1}^{N} \left(\dot{q}'_{56conv,i} + \dot{q}'_{57rad,i} \right) \Delta L_{aperture} \tag{III.11}$$

The total heat gained by HTF per unit length of the receiver is given by:

$$Q_{gain} = \sum_{i=1}^{N} \dot{q}'_{12conv,i} \, \Delta L_{aperture} \tag{III.12}$$

III.4.1. Temperature distribution in parabolic trough collector

Before going into the model details, the distribution of the temperature should be comprehended. There are two directions of temperature distributions, x and y, as shown in the left of Figure III.5. For x direction, at any fixed y, temperature distribution is seen in the middle of Figure III.5.The temperature distribution order from the highest to the lowest is presented in the following:

- Outer absorber surface temperature
- Inner absorber surface temperature
- Heat transfer fluid (HTF) temperature
- Inner glass envelope temperature
- Outer glass envelope temperature
- Ambient temperature
- Sky temperature

For y direction, at a fixed x, temperature distribution is seen in the right in Figure (III.3). The heat transfer fluid temperature (HTF) increases gradually as it passes through the absorber [110].

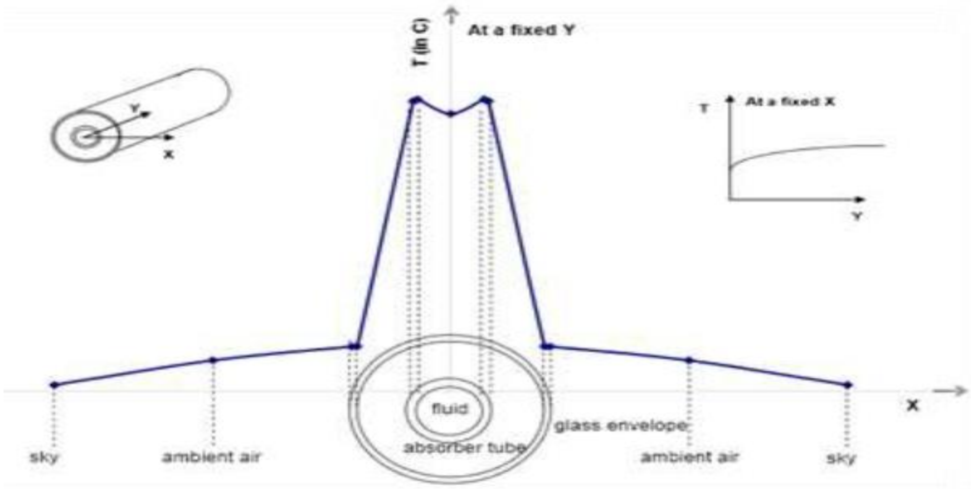

Figure III. 5.*Temperature distribution of PTSC [111]*

III.4.2. Convection Heat Transfer between the HTF and the Absorber

From Newton's law of cooling, the convection heat transfer from the inside surface of the absorber pipe to the HTF is [112]:

$$\dot{q}'_{12conv} = h_1 D_2 \pi \left(T_2 - T_1\right) \quad \textbf{(III.13)}$$

With:

$$h_1 = Nu_{D2}\frac{k_1}{D_2} \quad \textbf{(III.14)}$$

Where h_1 = HTF convection heat transfer coefficient at T_1 (W/m^2-K)

D_2 = inside diameter of the absorber pipe (m)

T_1 = mean (bulk) temperature of the HTF (^{o}C)

T_2 = inside surface temperature of absorber pipe (^{o}C)

Nu_{D2} = Nusselt number based on D_2

k_1 = thermal conductance of the HTF at T_1 (W/m-K)

The Nusselt number depends on the type of flow through the HCE. At typical operating conditions, the flow in an HCE is well within the turbulent flow region. However, during off-solar hours or when evaluating the HCE heat losses on a test platform, the flow in the HCE may become transitional or laminar because of the viscosity of the HTF at lower temperatures.

III.4.2.1. Turbulent and Transitional Flow Cases

To model the convective heat transfer from the absorber to the HTF for turbulent and transitional cases (Reynolds number > 2300) the following Nusselt number correlation developed by Gnielinski [113] is used.

$$Nu_{D2} = \frac{f_2/8\left(\mathrm{Re}_{D2}-1000\right)\mathrm{Pr}_1}{1+12.7\sqrt{f_2/8}\left(\mathrm{Pr}_1^{2/3}-1\right)}\left(\frac{\mathrm{Pr}_1}{\mathrm{Pr}_2}\right)^{0.11} \quad \textbf{(III.15)}$$

With:

$$\mathrm{Re}_{D2} = \frac{\rho_{HTF} V_{HTF} D_2}{\upsilon_{HTF}} \quad \textbf{(III.16)}$$

$$f_2 = \left(1.82\log_{10}(\mathrm{Re}_{D2})-1.64\right)^{-2} \quad \textbf{(III.17)}$$

Where:

f_2 = friction factor for the inner surface of the absorber pipe
Pr_1 = Prandtl number evaluated at the HTF temperature, T_1
Pr_2 = Prandtl number evaluated at the absorber inner surface temperature, T_2

Along with being valid for turbulent pipe flow, this Nusselt number correlation accounts for transitional flow states for Reynolds numbers between 2300 and 4000. Furthermore, the correlation adjusts for fluid property variations between the absorber wall temperature and bulk fluid temperature. The correlation is valid for $0.5 < Pr_1 < 2000$ and $2300 < Re_{D2} < 10^6$.

III.4.2.2. Laminar Flow Case

An option to model the flow as laminar is included in all the one-dimensional versions of the HCE heat transfer codes. When the laminar option is chosen and the Reynolds number is lower than 2300, the Nusselt number will be constant. For pipe flow, the value will be 4.36[112].

III.4.3. Conduction Heat Transfer through the Absorber Wall

Fourier's law of conduction through a hollow cylinder describes the conduction heat transfer through the absorber wall [114]:

$$\dot{q}'_{23cond} = 2\pi k_{23}\left(T_2 - T_3\right)/\ln\left(D_3/D_2\right) \quad \textbf{(III.18)}$$

k_{23} = absorber thermal conductance at the average absorber temperature $(T_2+T_3)/2$ (W/m-K)

T_2 = absorber Inside surface temperature (K)

T_3 = absorber outside surface temperature (K)

D_2 = absorber inside diameter (m)

D_3 = absorber outside diameter (m)

In this equation, the conduction heat transfer coefficient is constant, and is evaluated at the average temperature between the inner and outer surfaces. The conduction coefficient depends on the absorber material type. The HCE performance model includes three stainless steels: 304L, 316L, and 321H, and one copper: B42. If 304L or 316L is chosen, the conduction coefficient is calculated with equations indicated in Table (III.2).

Table III. 2.*Thermal properties of different types of stainless steel [115]*

Material	**Thermal conductivity K_{23}W/m K**	**Density kg/m3**	**Specific heat kJ/kg K**
304L	$0.0130T_{23}+14.9732$	8027.1	0.5024
316L	$0.0130\ T_{23}+14.9732$	8027.1	0.5024
321H	$0.0151\ T_{23}+14.5837$	8027.1	0.5024

III.4.4. Heat transfer from the absorber to the glass envelope

In the annulus, there are two heat transfer mechanisms: convection and radiation heat transfer. The convection heat transfer relies on the annulus pressure. If the pressure <0.013, molecular conduction takes place. At high pressures >0.013Pa, the mechanism of heat transfer is free convection [116]. As a result of temperature differences between the absorber and the glass envelope, thermal radiation is occurring, assuming that the surfaces are gray $\alpha = \rho$. In addition, the glass envelope is assumed to be opaque to infrared radiation

III.4.4.1. Convection heat transfer (Vacuum in annulus)

As mentioned, heat loss of the receiver is reduced by evacuation the annulus between the absorber and glass tube, pressure <0.013 Pa, due to the lack of moving liquid. As a result of that, the convection heat transfer takes place by free-molecular convection. The correlation used to calculate convection heat transfer in the annulus under low pressure is developed by Ratazel [116,117].

$$\dot{q}'_{34conv} = \pi D_3 h_{34}\left(T_3 - T_4\right) \tag{III.19}$$

With:

$$h_{34} = \frac{k_{std}}{\left(D_3/2\ln\left(D_4/D_3\right) + b\lambda\left(D_3/D_4 + 1\right)\right)} \tag{III.20}$$

$$b = \frac{\left(2-a\right)\left(9\psi - 5\right)}{2a\left(\psi + 1\right)} \tag{III.21}$$

$$\lambda = \frac{2.331E\left(-20\right)\left(T_{34} + 273.15\right)}{P_a \delta^2} \tag{III.22}$$

Where:

D_3 = outer absorber surface diameter (m)
D_4 = inner glass envelope surface diameter (m)
h_{34} = convection heat transfer coefficient for the annulus gas at T_{34} (W/m^2-K)
T_3 = outer absorber surface temperature (^{o}C)
T_4 = inner glass envelope surface temperature (^{o}C)
k_{std} = thermal conductance of the annulus gas at standard temperature and pressure (W/m-K)
b = interaction coefficient

λ = mean-free-path between collisions of a molecule (cm) a = accommodation coefficient

ψ = ratio of specific heats for the annulus gas
T_{34} = average temperature (T3 + T4)/2 (^{o}C)
Pa = annulus gas pressure (mmHg)

δ = molecular diameter of annulus gas (cm)

P_a is the annulus gas pressure in (mmHg), δ represents the molecular diameter of annulus gas (cm), and $(T_3 + T_4)/2$ is the average temperature of the annulus
According to Forristall [105], the molecular diameter of air is 3.53E-5 cm. the mean

path between collisions of a molecule is 88.76 cm. Also, the thermal conductivity of the air at standard conditions is 0.02551 W/m.k , and the interaction coefficient is 1.571. The ratio of specific heats for the air is 1.39. These values are for an average temperature of 300C and insolation of 940 W/m^2.

III.4.4.2. Convection heat transfer (pressure in annulus)

Natural convection heat transfer occurs in the space between the absorber and the glass envelope when the pressure in the annulus is higher than 0.013 Pa due to leakage. Therefore, Raithby and Hollands [118] developed a correlation for natural convection between two concentric cylinders:

$$q'_{34conv} = \frac{2.42 k_{34}\left(T_3 - T_4\right)\left(\Pr Ra_{D3} / \left(0.861 + \Pr_{34}\right)\right)^{1/4}}{\left(1 + \left(D_3 / D_4\right)^{3/5}\right)^{5/4}} \qquad \textbf{(III.23)}$$

$$Ra_{D3} = \frac{g\beta\left(T_3 - T_4\right) D_3^3}{\alpha} \qquad \textbf{(III.24)}$$

For an ideal gas:

$$\beta = \frac{1}{T_{avg}} \qquad \textbf{(III.25)}$$

k_{34} = thermal conductance of annulus gas at T34 (W/m-K)
T_3 = outer absorber surface temperature (^oC)
T_4 = inner glass envelope surface temperature (^oC)
D_3 = outer absorber diameter (m)
D_4 = inner glass envelope diameter (m)
Pr_{34} = Prandtl number
Ra_{D3} = Rayleigh number evaluated at D_3
β = volumetric thermal expansion coefficient (1/K)
T_{34} = average temperature, $(T_3 + T_4)/2$ (^oC)

This correlation assumes long, horizontal, concentric cylinders at uniform temperatures, and is valid for $Ra_{D4} > (D_4 / (D_4 - D_3))^4$. All physical properties are evaluated at the average temperature $(T_3 + T_4)/2$.

III.4.5. Radiation Heat Transfer

The radiation heat transfer between the absorber and glass envelope ($\dot{q}'_{34rad}$) is estimated with the following equation [114].

$$\dot{q}'_{23rad} = \frac{\sigma \pi D_3 \left(T_3^4 - T_4^4\right)}{\left(1/\varepsilon_3 + \left(1-\varepsilon_4\right) D_3 / \left(\varepsilon_4 D_4\right)\right)} \tag{III.26}$$

Where:

σ = Stefan-Boltzmann constant 5.672E-8 (W/m^2-K^4)

D_3 = outer absorber diameter (m)

D_4 = inner glass envelope diameter (m)

T_3 = outer absorber surface temperature (K)

T_4 = inner glass envelope surface temperature (K)

ε_3 = Absorber selective coating emissivity

ε_4 = glass envelope emissivity

In order to drive this correlation, many assumptions were made:

- Gray surfaces
- The glass envelope is opaque to infrared radiation
- Long concentric isothermal cylinders
- Nonparticipating gas in the annulus
- Diffuse reflection and irradiations

The assumptions stated above are not completely true. As an example, both the glass envelope and absorber coating are not gray. Also, the glass envelope is not totally opaque to infrared radiation. Nevertheless, if there were some errors with these assumptions, it would be relatively small

III.4.6. Conduction heat transfer through the glass envelope

The correlation used for conduction heat transfer through the glass envelope is the same correlation described in section (III.3.3) The temperature distribution is presumed tube linear. Additionally, the thermal conductivity of the glass envelope, which is Pyrex glass is constant (1.04 W/m -K) [105]

$$\dot{q}'_{45cond} = \frac{2\pi k_{45}\left(T_4 - T_5\right)}{Ln\left(\frac{D_5}{D_4}\right)} \qquad \textbf{(III.27)}$$

III.4.7. Heat transfer from the glass envelope to the ambient

Heat transfer between the glass envelope and ambient occurs in two mechanisms: convection and radiation. Convection heat transfer occurs in two ways; natural convection in case of no wind, and forced convection in the presence of wind. Radiation heat transfer happens as a result of the difference in temperature between the outer glass temperature and the sky temperature. All these heat transfer mechanisms are described in the following.

III.4.7.1. Convection heat transfer

According to Newton's law of cooling, the convection heat transfer formula from the glass tube to the ambient is given by [114]:

$$\dot{q}'_{56conv} = h_{56}\pi D_5\left(T_5 - T_6\right) \qquad \textbf{(III.28)}$$

$$h_{56} = \frac{k_{56}}{D_5} Nu_{D5} \qquad \textbf{(III.29)}$$

Where:

T_5 = glass envelope outer surface temperature (^oC)

T_6 = ambient temperature (^oC)

h_{56}= convection heat transfer coefficient for air at $(T_5 – T_6)/2$ (W/m^2-K)

k56 = thermal conductance of air at $(T_5 – T_6)/2$ (W/m-K)

D_5 = glass envelope outer diameter (m)

Nu_{D5}= average Nusselt number based on the glass envelope outer diameter

The Nusselt number depends on whether the convection heat transfer is natural (no wind) or forced (with wind).

III.4.7.1.1. No wind condition

In case of no wind, the convection heat transfer between the glass envelope and the surrounding occurs by natural convection. Churchill and Chu [114] developed a correlation used to calculate the Nusselt number for natural convection over a horizontal cylinder:

$$\bar{N}u_{D5} = \left\{ 0.60 + \frac{0.387 Ra_{D5}^{\ 1/6}}{\left[1 + \left(0.559/\Pr_{56}\right)^{9/16}\right]^{8/27}} \right\}^2 \tag{III.30}$$

$$Ra_{D5} = \frac{g\beta\left(T_5 - T_6\right) D_5^3}{\alpha_{56}\nu_{56}} \tag{III.31}$$

$$\beta = \frac{1}{T_{56}} \tag{III.32}$$

$$\Pr_{56} = \frac{\nu_{56}}{\alpha_{56}} \tag{III.33}$$

Where:

Ra_{D5} = Rayleigh number for air based on the glass envelope outer diameter, D5
g = gravitational constant (9.81) (m/s^2)

α_{56} = thermal diffusivity for air at T_{56} (m^2/s)
β = volumetric thermal expansion coefficient (ideal gas) (1/K)
Pr_{56} = Prandtl number for air at T_{56}
ν_{56} = kinematic viscosity for air at T_{56} (m2/s)
T_{56} = film temperature $(T_5 + T_6)/2$ (K)

This correlation is valid for $10^5 < Ra_{Do} < 10^{12,}$ and assumes a long isothermal horizontal cylinder. Also, all the fluid properties are determined at the film temperature, $(T_5 + T_6)/2$.

III.4.7.1.2. Wind Case

If there is wind, the convection heat transfer from the glass envelope to the environment will be forced convection. The Nusselt number in this case is estimated with Zhukauskas' correlation for external forced convection flow normal to an isothermal cylinder [112].

$$\bar{N}u_{D5} = C \,\mathrm{Re}_{D5}^{\ m} \Pr_6^n \left(\frac{\Pr_6}{\Pr_5}\right)^{1/4} \tag{III.34}$$

Table III. 3. *Values of C and m as a function of Reynolds number*

Re_{D5}	C	m
1-40	*0.75*	0.4
40-1000	0.51	0.5
1000-200000	0.26	0.6
200000-1000000	0.076	0.7

$$n = 0.37 \ for \ \Pr \leq 10 \quad \textbf{(III.35)}$$

$$n = 0.36 \ for \ \Pr \succ 10 \quad \textbf{(III.36)}$$

This correlation is valid for $0.7 < Pr_6 < 500$, and $1 < Re_{D5} < 10^6$. All fluid properties are evaluated at the atmospheric temperature, T_6, except Pr_5, which is evaluated at the glass envelope outer surface temperature.

III.4.7.2. Radiation Heat Transfer

The useful incoming solar irradiation is included in the solar absorption terms. Therefore, the radiation transfer between the glass envelope and sky, discussed here, is caused by the temperature difference between the glass envelope and sky. To approximate this, the envelope is assumed to be a small convex gray object in a large blackbody cavity (sky). The net radiation transfer between the glass envelope and sky becomes [112].

$$\dot{q}'_{57rad} = \sigma D_5 \pi \left(T_5^4 - T_7^4 \right) \quad \textbf{(III.37)}$$

Where

σ = Stefan-Boltzmann constant 5.670E-8 (W/m^2-K^4)

D_5 = glass envelope outer diameter (m)

ε_5 = emissivity of the glass envelope outer surface

The sky temperature is lower than the ambient temperature, and it is affected by the atmospheric conditions; clouds and wind. Many studies have been carried out to relate the sky temperature to other measurable parameters. These studies relate the sky temperature to the local ambient temperature, water vapor temperature, and dew point temperature. For simplicity, Previous heat loss models have assumed the sky temperature to be 8°C less than the ambient temperature [105] [116], and these thermal models showed a good match with the test data. So, for this model, the sky temperature is assumed to be T_7 = Ta-8°C. Fortunately, the effective sky temperature does not highly affect the collector performance [119].

III.4.8 Solar Irradiation Absorption in the Glass Envelope

The solar absorption into the glass envelope is treated as a heat flux to simplify the model. Physically this is not true. The solar absorption in the glass envelope is a heat generation phenomenon and is a function of the glass thickness. However, this assumption introduces minimal error since the solar absorptance coefficient is small for glass, 0.02, and the glass envelope is relatively thin, 6 mm. Also, an optical efficiency is estimated to calculate the solar absorption. With this stated, the equation for the solar absorption in the glass envelope becomes

$$q'_{5solabs} = q'_{si}\rho_{trough}\gamma\alpha_{env}K\left(\theta\right)X_{end} \qquad \textbf{(III.38)}$$

q'_{si} = solar irradiation per receiver length (W/m)

α_{env} = absorptance of the glass envelope (glass)

$K(\theta)$ = incident angle modifier (as defined in chapter)

The solar irradiation term (q'_{si}) in Equation is determined by multiplying the direct normal solar irradiation by the projected normal reflective surface area of the collector (aperture area) and dividing by the receiver length.

III.4.9 Solar Irradiation Absorption in the Absorber

The solar energy absorbed by the absorber occurs very close to the surface; therefore, it is treated as a heat flux, the equation for the solar absorption in the absorber becomes

$$q'_{3solabs} = q'_{si}\eta_0 \qquad \textbf{(III.39)}$$

Where is the optical efficiency from equation (II.14)

III.4.10. Performance of PTC

Thermal efficiency: The thermal efficiency is defined as the ratio of the instantaneous useful heat gained by the HTF and the instantaneous direct solar radiation (I_d) incident on the given aperture area (A_a) of the collector [120].

$$\eta = \frac{Q_u}{Q_a} \tag{III.40}$$

Useful heat gain: The amount of heat gained by the HTF flowing through the receiver tube.

$$Q_u = \dot{m}.Cp.\left(T_{out} - T_{in}\right) \tag{III.41}$$

Direct solar radiation (Id) incident on the given aperture area (Aa) of the collector:

$$Q_a = A_a.I_d \tag{III.42}$$

Where, m is the mass flow rate (kg/s), Cp is the specific heat capacity (J/kgK), Id is the direct solar radiation (W/m^2), Tout is the outlet temperature of the HTF, Tin is the inlet temperature of the HTF.

III.4.11. Governing Equations

Fluid flow and heat transfer in both domains solid and fluid are described by a system of four equations to be simultaneously solved. This system is presented hereafter [26]:

- **Continuity:**

$$\frac{\partial \rho}{\partial t} + \nabla\left(\rho U\right) = 0 \tag{III.43}$$

- **Momentum**

$$\frac{\partial\left(\rho U\right)}{\partial t} + \nabla.\left(\rho U \otimes U\right) = -\nabla p + \mu \nabla.\nabla U \tag{III.44}$$

- **Thermal energy**

$$\frac{\partial\left(\rho h\right)}{\partial t} + \nabla\left(\rho U h\right) = \nabla.\left(k \nabla T\right) \tag{III.45}$$

Where, U is the velocity vector, p is the fluid pressure, T is the temperature and h is the enthalpy.

III.5 Chapter summary

This chapter is devoted to the theories and definitions relating to the different modes of heat transfer in the PTC system. All heat transfer modes are present: radiation, conduction, and convection.

Heat transfer by radiation is determined by the optical analysis. The resulting heat flux as well as its distribution around the absorber tube is determined by SolTrace code.

Convection between the outer surface of the tube and the atmosphere is not taken into account. This can be justified by two reasons: either the air velocity is zero, or the tube is covered with a transparent glass envelope.

Conduction through the thickness of the (solid) tube, convection between the inner surface of the tube and the heat transfer fluid, and conduction in the heat transfer fluid as well as the flow of the fluid inside the tube are governed by the system of equations (III.43) to (III.45). As can be seen, the physical properties of the tube material and the heat transfer fluid play an important role in these equations.

The resolution of governing equations provides, inter alia, the temperature of the heat transfer fluid at the outlet of the tube at each instant. The value of this temperature determines the performance of the system described by equations III.40 and III.41.

Chapter IV

Modeling and Numerical Resolution

Modeling and Numerical Resolution

IV.1. Introduction

The complexity of the physical or technological systems to be designed or studied has led to the use of numerical methods based on the principle of approaching a nominal solution as close as possible, but these require large calculations using efficient calculators. In this chapter, we present the Methods used for our simulation with a representation of the calculation codes (Soltrace, Ansys CFX).

IV.2. SOLTRACE code presentation

Optical modeling of our solar concentrator was performed using the SolTrace software which allows to quantify the intensity of the concentrated solar flux received at the absorber. The "SolTrace" code is developed by the American laboratory NREL (the National Renewable Energy Laboratory). The code was first written in early 2003, but has seen some changes but has seen some changes and changes since its inception including the conversion of a development platform, a software based on Pascal , C + +. The code uses the ray-tracing method.

IV.2.1. Monte-Carlo ray tracing method (MCRT)

The method of (MCRT) is a mathematical method based on probabilities, this method is very used in many domains (image processing, renewable energies and especially in radiative phenomena) It is a technique that consists in launching a number of rays or photons from a luminous source for example the sun, Each particle transports a certain Amount of energy, We follow the trajectory of each of the particles. This method is well adapted to very complex geometries, and to the reflection phenomena, refraction and transmission, only it is necessary to launch a very important number of rays to approach the phenomena correctly. Today there are many codes based on this method, as the SOLTRACE code, these are used for the optical simulation of different systems. For example: the concentration of solar radiation using a parabolic trough concentrator. See further details in [107].

IV.3.6. Ray Tracing optical properties

The distribution of heat flux over the absorber tube is vital for heat transfer analysis. Some studies have presented that heat flux distribution over the absorber significantly affects the thermal performance of the PTC receiver [107]. In the present work, SolTrace software, which uses Monte Carlo Ray Tracing method, is used to calculate the solar flux distribution over the absorber tube.

Ray tracing simulation conditions are as follows: Sun has been modeled as a Gaussian distribution with a cone angle of 2.73 mrad. Aluminum is selected as the material of the reflector plate with a reflectivity of 1, a shape error of 3 mrad, and a specular reflection error of 0.5mrad. For the secondary reflector, the reflectivity of metal collector tube is of 0.05, the shape error is of 0.0001mrad, and the specular reflection error is of 0.0001mrad. A sample ray tracing in SolTrace is shown in Figure (IV.1)

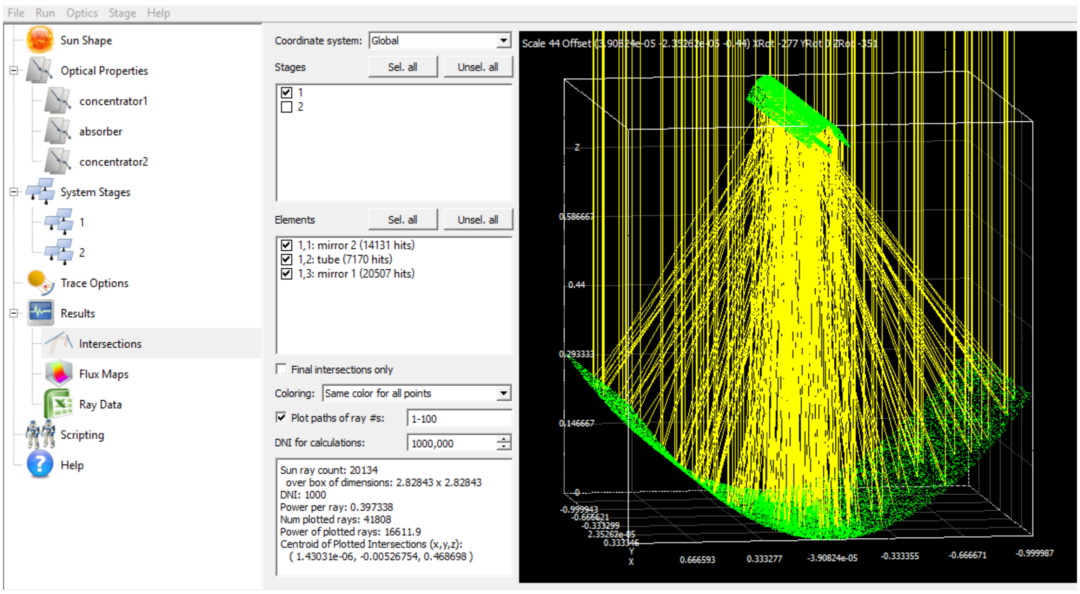

Figure IV. 1. *Ray tracing of PTC with secondary*

The following figure shows the distribution of the solar flux on the external surface of absorber tube on 3D:

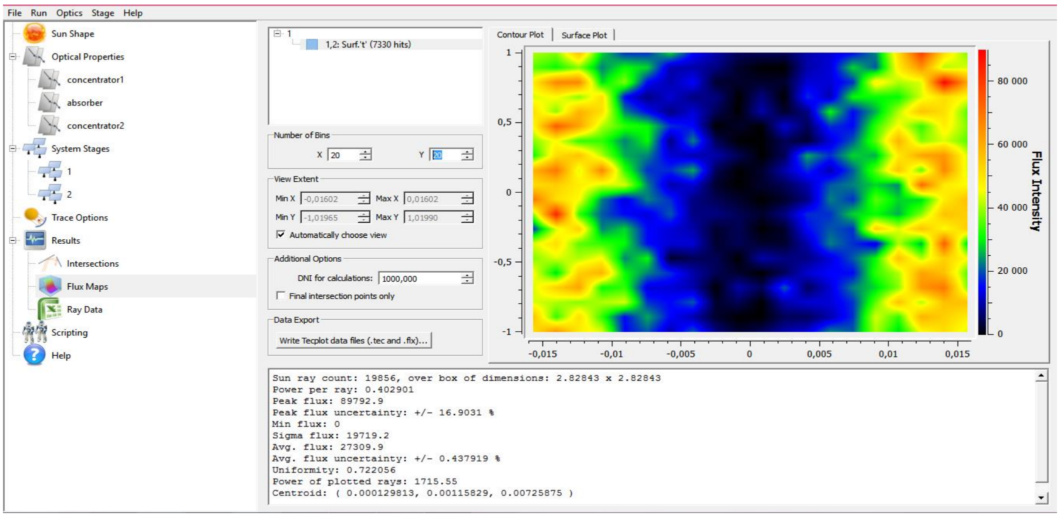

Figure IV. 2 . *Plot of heat flux for a parabolic trough collector with SR*

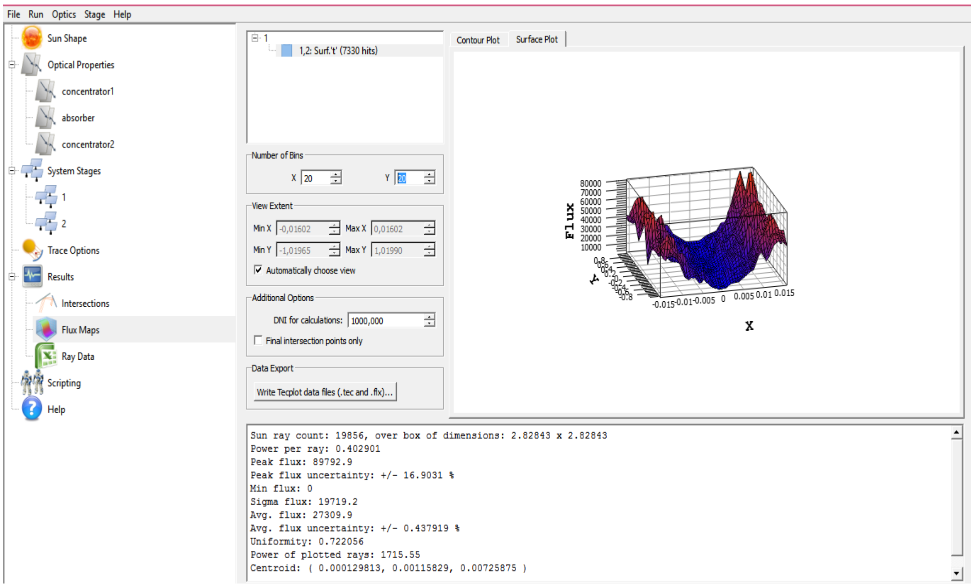

Figure IV. 3. *Solar radiation flux distribution on the outer wall of PTC with secondary reflector*

IV.3. Computational fluid dynamics (CFD) presentation

A CFD model consists of numerically solving the equations governing the motion of a fluid. The equations to be solved can be Euler equations, Navier-Stokes equations coupled with other equations (or a combination of these equations with equation of energy for example). In our case, the numerical model, represented by the system of equations **(III.43)**, **(III.44)**, and **(III.45)** without source terms. These partial differential equations, in their integral form, are approximated by finite volume expressions and subsequently transformed into algebraic equations to allow numerical computation in a specified domain. This task, carried out by means of the following steps [122] are required to set up the computer:

- position of the problem
- numerical solution
- exploitation of the results

These steps involve the development of a calculation code generally using one of the following known machine languages: FORTRAN, C, C++, etc...The development of calculation software is a difficult and tedious task. In addition, there are currently many CFD software packages in use around the world. (ANSYS-CFX, ANSYS-FLUENT, ABAQUS, COMSOL, FLOW3D, etc.).

Using these programs allows the researcher to concentrate on the essential part of his work and to free himself from the difficulties related to the complete implementation of a calculation code. We chose the ANSYS-CFX software. This chapter is devoted to the presentation of the numerical model of absorber of parabolic trough collector with secondary reflector developed in the background of this thesis. We will review:

- the description of parabolic trough collector problem;
- the geometry of the absorber and meshing of the computational domain;
- Initial and boundary conditions.
- The discretization and resolution of the governing equations.

IV.3.1. CFD program structure

As mentioned in the previous section the commercial code ANSYS-CFX was used in this thesis. Usually, a commercial code is structured around a set of robust numerical algorithms that can solve fluid flow problems. In an optimized manner In order to facilitate their use almost all CFD software packages CFD commercials include applications and user-friendly graphic environments for entering the problem parameters and processing the results. Thus, these software’s are generally structured as shown in the following figure:

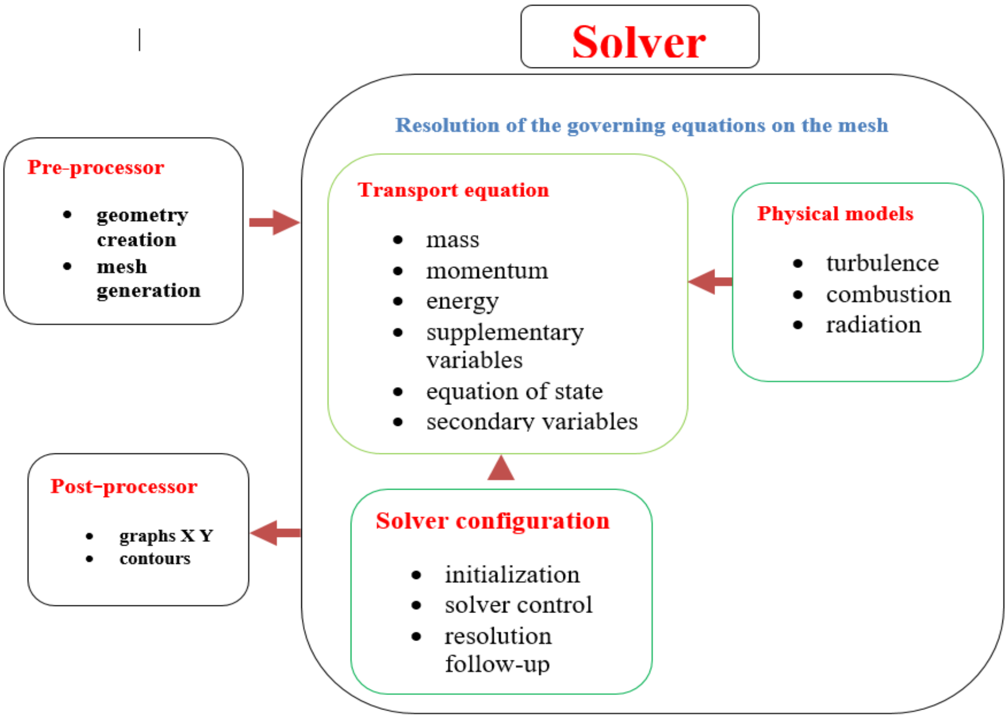

Figure IV. 4 . *General structure of a CFD*

IV.4. Parabolic trough collector with secondary reflector

A PTC is a line-focusing system that uses a parabolic reflector to concentrate solar radiation onto a linear receiver. Reflector is one of the vital part of the PTC as it decides the fraction of solar irradiance to be collected by the absorber tube. The PTC has a length of 2 m and an area of 2×2 m^2.We have introduced a secondary reflector, which has a cylindrical parabolic shape, made following the same steps as the main reflector with difference in height see figure (IV.5).The PTC has a single axis tracking system, from East-West and it is positioned in a South–North direction. Therminol Vp-1 and water are chosen as a heat transfer fluid. Table (IV.1) summarizes the geometric characteristics of the PTC.

The proposed thermal model for the solar parabolic cylindrical concentrator is shown in Figure (IV.5). The geometrical parameters of the parabolic cylindrical collector and the absorber tube for this study are shown in Table (IV.1). In order to carry out our study, we consider the following hypotheses:

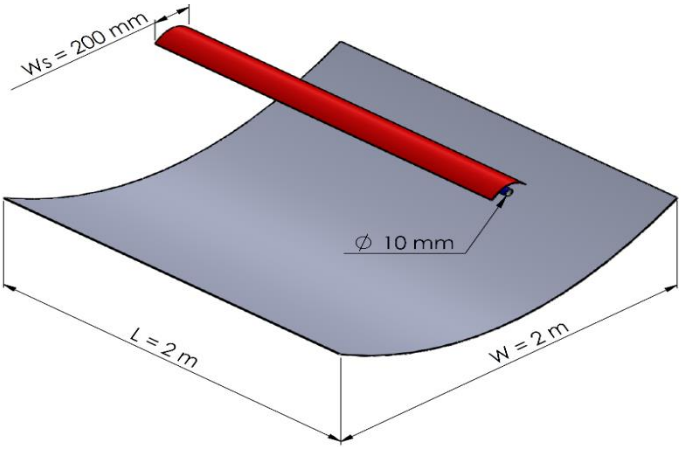

Figure IV. 5. *PTC module with secondary reflector*

Table IV. 1.*Geometrical parameters of the PTC*

parabolic trough collector and absorber tube	**Values**
Focal length of the primary concentrator	0.83m
Focal length of the secondary reflector	0.05m
Distance between primary and secondary reflectors	0.88m
Absorber tube inner radius	0.008m
Absorber tube outer radius	0.01m
Aperture width of the primary concentrator	2m
Aperture width of the secondary concentrator	0.2m

IV.4.1 Schematic representation

Figure (IV.1) Shows the schematic diagram of an absorber tube after simplification.

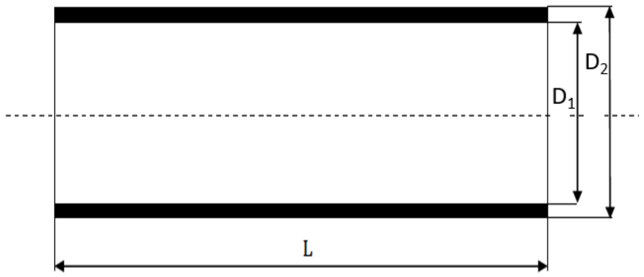

Figure IV. 6*.Creation of the geometry of the absorber tube*

ANSYS provides its users with several complete tools for the design of geometries and their meshes. In particular, the ICEM CFD software is dedicated to CFD issues .This software allows, with the help of a graphical user interface and a command interface, to trace the shapes, coupled by the fluids, ranging from simple geometries to more or less complex assemblies. Note, however, that ICEM CFD is a mesher and is not normally intended to create geometries too elaborate. In our case, the geometries considered are relatively simple and the software is more than sufficient to process them.

The design of a geometry begins with the creation of the points delimiting the domain. The sides connecting the vertices are then drawn to form the domain. ICEM CFD can also be used to create multiple types of surfaces from points or lines. Volumes can also be defined from points or areas. Figure (IV.7) represents the geometry of the absorber tube

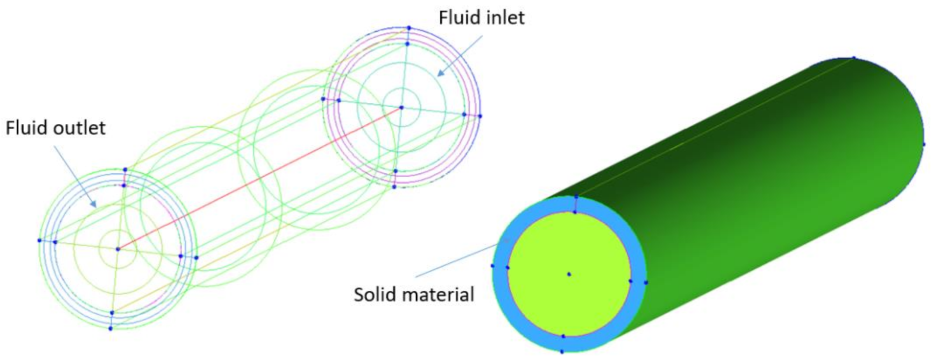

Figure IV. 7 *The absorber tube realized by ICEMCFD.*

IV.3.2. Mesh generation

Meshing consists in discretizing the geometry into a finite number of elements, cells or well-defined meshes. Each element is composed of a set edges limited by points called nodes. The objective is to approximate the equations of the movement at these points. The solutions obtained are then extrapolated for the entire continuous medium using functions called "shape functions".

The ICEM CFD mesher allows the creation of structured, unstructured, multiblock meshes. As well as hybrid arrays with different cell geometries. The created meshes can then be exported to different CFD solvers such as ANSYS-CFX and ANSYS-FLUENT. Among the techniques used for meshing, ICEM CFD offers a multi-block method called "Blokingstrategy". This technique consists of dividing the domain geometrically in several zones (blocks) on which the properties of the mesh are defined. The main advantage of this method is that each block can be processed independently of the others (number of nodes, dimensions of the elements, etc.).This makes it possible to create fine meshes in specific areas of interest (interfaces, close to walls, etc...) And coarse meshes in less important areas

The physical domain is composed of two sub-domains solid and fluid. To analyze this assembly numerically, we use the blocking method in the ANSYS-ICEMCFD mesh generator. This technique makes it possible to define each domain (fluid and solid) in the solver. In addition, it offers the advantage of minimizing the number of nodes in the mesh. As a result, simulation calculations are also minimized, as shown in Figure **(**IV.8), two blocks are merged. The structured block represents the solid domain (tube) and the O-grid block represents the fluid domain. After a mesh independence study, we chose the following distribution of the nodes: 101 nodes / meter in *z* direction; 21 nodes in *x* and *y* directions; and 3 nodes along the thickness of the tube.

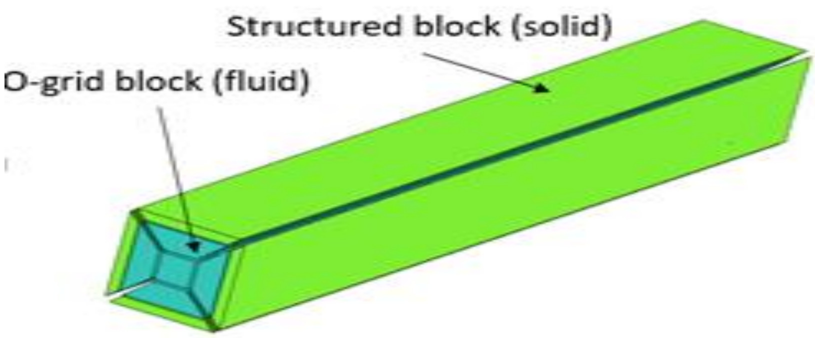

Figure IV. 8. *Shows the Domain blocking (in green)*

IV.3.3. Mesh Convergence

The choice of the dimensions (fineness) and the typology of a mesh essential question in CFD simulations more the mesh is finer more the results will be precise. However, on the other hand, the calculation time will be long. It is therefore necessary to find a good compromise between precision and calculation cost. In other words, we need to find the limit at which the solution is independent of mesh fineness for a given calculation precision. This process is called: convergence study in mesh.

Ideally, at least three different and significant mesh resolutions will be employed [122] the independence of the mesh could be examined by comparing the numerical solutions of the fine grids with the solutions corresponding to the reference mesh size using Richardson extrapolation. If this is not possible (Richardson's extrapolation is applicable to uniform grid spacing), selective local refinement of the reference mesh in regions of specific interest can be applied. Another alternative is to compare different spatial discretization orders on the same mesh.

In the present work, we have followed, for the choice of typology and finesse of a mesh, the recommendations presented in Tu et al [122]. (We recommend that readers consult this book for more details and bibliographical references)Thus, our approach to the study of mesh independence is summarized in the following steps:

- First of all, an acceptable accuracy must be predefined (10^{-4} in terms of RMSE).Then, a first coarse mesh (reference mesh) is generated. The next step is to make sure that the initial and boundary conditions as well as that the time step chosen (see section next) are well compatible with the physical problem. If the residuals converge to the required precision, proceed to the next step. Otherwise, refine the mesh and repeat. A verification of the form report “aspect ratio” of the elements allows for to choose the appropriate refinement report .It should be noted that the ANSYS-CFX solve allows you to follow in real time the values of the residuals of all variables. This option allows you to stop the simulation at any time if the required precision is not reached.
- Once the convergence criteria are filled, make a refinement (We will use a refinement report, global or selective, from 1.5).Run the simulation and ensure that the residuals fall below the desired precision. If the results obtained in this step are the same as those obtained (at the same points) with the mesh size of

Reference, we will use the reference mesh as a model. If not go to the next step. Note that the solutions to be compared (target solutions) can be the variables in the equations to be solved or the solutions derived from them. [122]

- As long as the solution evolves with the fineness of the mesh, the mesh-independent solution has not yet been reached. We need to further refine obtained for consecutive meshes. We'll always remember the mesh the coarsest which guarantees the solution independence of the mesh dimensions so, the calculation time is reduced to the minimum acceptable value.

IV.4.3.1. Example of illustration (our case)

The mesh size is selected in order to minimize the CPU time and to achieve the desired accuracy. In other words, we must find the limit from which the solution is independent of the mesh refinement for a given accuracy of calculation. In the present work, we have followed the recommendations presented by Tu et al. [122]. First, acceptable precision must be predefined (10^{-4} in terms of RMSE) for all variables. Then a series of five meshes are generated (see Table IV.1). The solution to be compared (target solution) is the fluid outlet temperature. As it can be seen in Figure (IV.9), starting from mesh 3 the solution becomes independent from the mesh refinement. Table (IV. 2) illustrates the meshes characteristics.

Table IV. 2*.Characteristics of meshes used for the mesh independency study*

Mesh	Refinement ratio	Element number	Calculation time
M1		22000	1min
M2	1.5	60000	3min
M3	1.5	144000	6min
M4	1.5	264000	10min
M5	1.5	416000	17min

The simulation results obtained for each mesh are then plotted on a graph for the purpose of comparison.

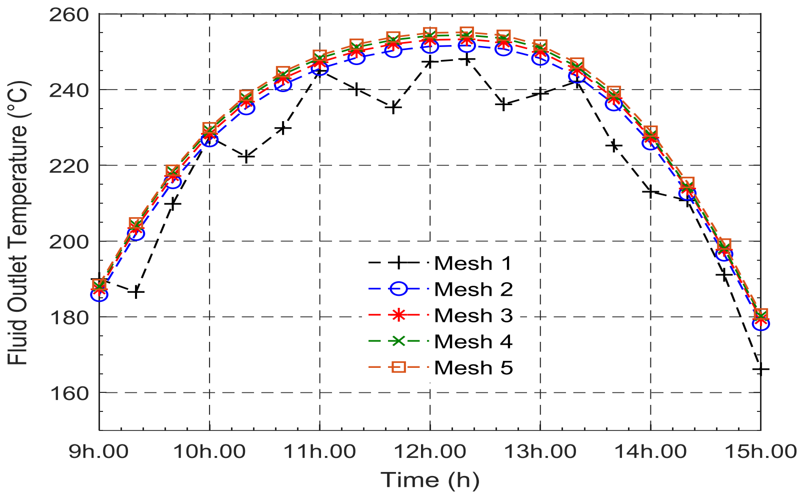

Figure IV. 9*. Illustration of mesh independence study*

IV.3.4. Initial and boundary conditions

Before solving the governing equations, domain initialization and boundary conditions must be specified. The domain is initialized as follows: At time t=0s, we consider that the fluid and the solid are at the same temperature T_0; the fluid velocity and pressure are set to zero. The boundary conditions are illustrated in Figure (IV.10).The values of the pressures at the tube inlet and outlet must be greater than the saturation pressure corresponding to the maximum temperature obtained (275°C in the present study (Oil Therminol VP-1)). The pressure drop across the tube is determined based on the mass flow through the tube (0.005 kg/s). Accordingly, we have chosen the following pressure values: 138 kPa at the inlet, 137.98 kPa at the outlet, which corresponds to a pressure drop of 0.05 kPa.

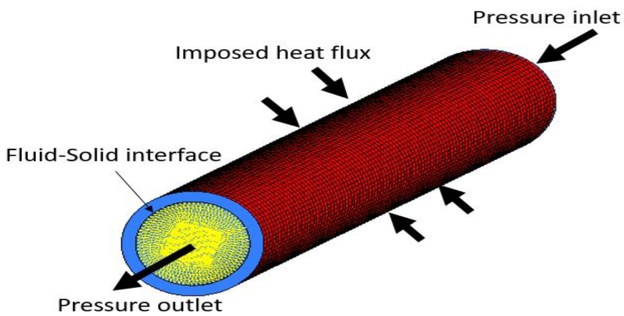

Figure IV. 10 *. Illustration of the boundary conditions applied on the absorber tube*

For water as working fluid and to solve a transient problem we must introduce the solution at the initial time (t = 0) to be able to start the process of resolution in time. In our case, the solid-fluid domain is initialized as follows: At time t=0s, we consider that the fluid and the solid are at the same temperature T_0; the fluid velocity and pressure are set to zero. To solve the problem in space, the boundary conditions must be specified at the tube inlet, mass flow rate is imposed.

- At the tube outlet, the same mass flow rate is imposed.

The mass flow rate is selected in order to ensure a laminar flow within the tube. A laminar flow is determined by the condition (R_e< 2000), where R_e is the Reynolds number

- On the lateral surface of the tube, a transient heat flux is continuously imposed. Since this quantity varies over time, we used temporal interpolation functions (Gaussian functions). These functions are implemented in the solver as expressions by using the CEL language.
- A domain interface is to be specified at the interface solid-fluid.

Figure (IV.11).illustrates the boundary conditions applied to the absorber tube.

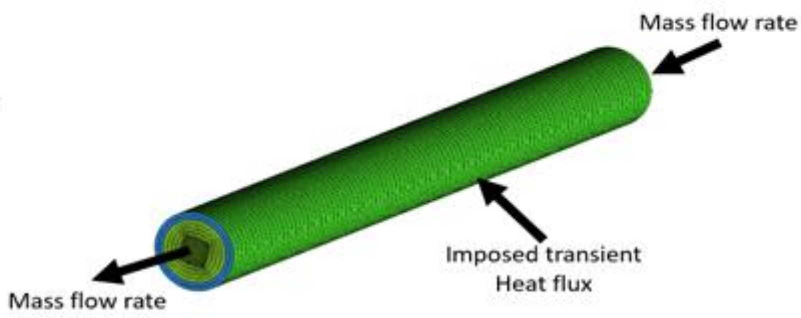

Figure IV. 11. *Boundary conditions applied to the absorber tube (for water as working fluid)*

In addition to the initial conditions and the boundary conditions, some configurations of the solver are required. Laminar model is selected to solve fluid flow and thermal energy model is selected to solve conjugate heat transfer. The time step chosen is 5min, while the total simulation time is 8hours. The calculation accuracy is set to 10^{-4} in terms of Root Mean Square Error (RMSE) for all variables. The advection scheme is set to High resolution and Second order backward Euler method is selected for the transient scheme.

Under these conditions, the solver CFX solves the system of equations (**(III.43)**, (**III.45)**). The target result is obviously the water temperature, at the outlet of the receiver tube, as a function of time. The heat flux boundary conditions is implemented in CFX solver by using CFX Expression Language (CEL).

IV.4.5. Discretization of governing equations

Numerical modelling is based on the reformulation of the equations of conservation on each element of the mesh. In this paragraph, we present, in broad outline, the principles of discretization of the equations of movement by a hybrid method based on a coupling element-based finite volume

Figure (IV.12) shows a two-dimensional mesh composed of a series of elements (meshes) of different shapes. The solutions and fluid properties are stored at the nodes. A control volume (area surrounded by the broken line) is built around each node of the mesh by joining, by straight segments, the centers of the edges and elements surrounding the node.

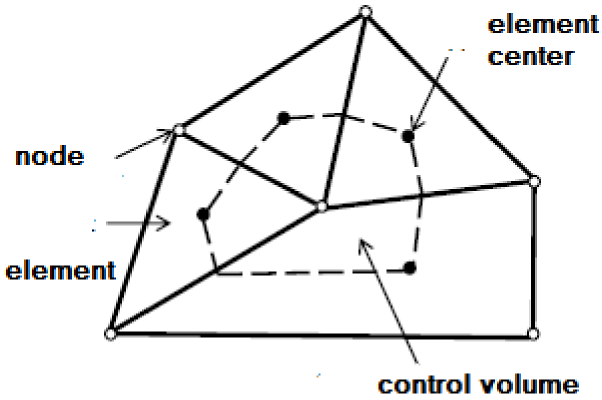

Figure IV. 12 *.Definition of control volume*

To illustrate the finite volume discretization method, consider the equations of continuity and momentum as follows

$$\frac{\partial \rho}{\partial t}+\frac{\partial}{\partial x_j}\left(\rho U_j\right)=0 \qquad \textbf{(IV .1)}$$

$$\frac{\partial}{\partial t}(\rho U_i)+\frac{\partial}{\partial x_j}(\rho U_i U_j)=-\frac{\partial p}{\partial x_i}+\frac{\partial}{\partial x_j}\left[\mu\left(\frac{\partial U_i}{\partial x_j}+\frac{\partial U_j}{\partial x_i}\right)\right] \quad \textbf{(IV .2)}$$

By integrating these equations on each control volume and applying the divergence theorem we obtain:

$$\frac{\partial}{\partial t}\int_V \rho dV+\int_S \rho U_j dn_j=0 \quad \textbf{(IV .3)}$$

$$\frac{\partial}{\partial t}\int_V \rho U_i dV+\int_S \rho U_i U_j dn_j=-\int_S p dn_j+\int_S \mu\left(\frac{\partial U_i}{\partial x_j}+\frac{\partial U_j}{\partial x_i}\right)dn_j+\int_V S_{U_i} dV \quad \textbf{(IV .4)}$$

Where: V and S, represent respectively the volume and the area of integration. nj, represents the normal (output) vector on the surface S. Volume integrals represent source or accumulation terms or accumulation and surface integrals represent the summation of the fluxes.

The next step is to discretize the integrals of volumes and surfaces. To illustrate this technique, considering a single element as shown in Figure (IV.13).

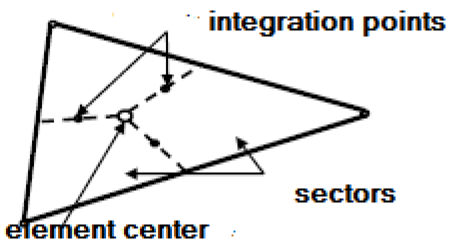

Figure IV. 13 *.Simple triangular element with three nodes*

The volume integrals are discretized in each sector of the element and are then, accumulated to the control volume to which the sector relates. The integrals of surface are, in turn, discretized at integration points (ipn), located in the center of each surface segment in the element, and then distributed to adjacent control volumes. The integral equations, after discretization, become:

$$V\left(\rho-\rho^0\right)+\sum_{ip}\dot{m}_{ip}=0 \quad \textbf{(IV.5)}$$

$$V\left(\frac{\rho U_i-\rho^0 U_i}{\Delta t}\right)+\sum_{ip}\dot{m}_{ip}\left(U_i\right)_{ip}=\sum_{ip}\left(p\Delta n_i\right)_{ip}+\sum_{ip}\left[\mu\left(\frac{\partial U_i}{\partial x_j}+\frac{\partial U_j}{\partial x_i}\right)\Delta n_j\right]+\bar{S}_{U_i}V \quad \textbf{(IV .6)}$$

With: $\dot{m}_{ip}=\left(\rho U_j \Delta n_j\right)_{ip}$ **(IV .7)**

Where: Δt, represents the time step; Δn_j, the discrete (output) normal vector; the index (ip), relates to the evaluation at an integration point; the index (°), refers to the old level of time

Note that the first-order delayed Euler scheme was used in these equations , although a second-order scheme is generally preferable for a transient approximation [122].

IV.4.5.1. Form functions

Form functions, initially used in the finite element approach, describe variations in a variable, Φ, inside an element. They have the following general form:

$$\Phi = \sum_{1}^{n} N_i \Phi_i \qquad \textbf{(IV .8)}$$

Where: N_i, represents the form function for node (i); Φ_i, the value Φ of at node (i) and n, the number of nodes of the element.

These functions have the following properties:

$$\sum_{1}^{n} N_i = 1 \qquad \textbf{(IV. 9)}$$

At the node $j : N_i = \begin{cases} 1 & si\ i = j \\ 1 & si\ i \neq j \end{cases}$

(IV .10)

ANSYS-CFX uses linear form functions in terms of parametric coordinates. As an example, for a tetrahedral element see Figure (IV.14), these functions are defined as follows:

$$N_1 = 1 - \zeta_1 - \zeta_2 - \zeta_3$$

$$N_2 = \zeta_1$$

$$N_3 = \zeta_2$$

$$N_4 = \zeta_3$$

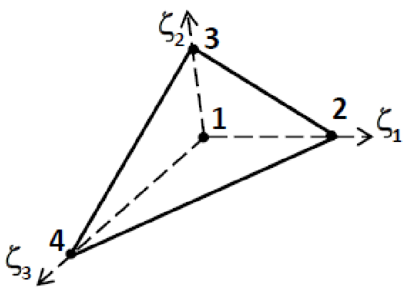

Figure IV. 14 . Definition of a tetrahedral element

IV.4.5.2. Compressibility

Mass flow terms in the continuity equation involve a produces density and advection velocity. For compressible flow, the discretization of this product is carried out according to the linearization of Newton-Raphson:

$$\left(\rho U\right)^{n} A \approx \rho^{n} U^{\circ} A + \rho^{\circ} U^{n} A - \rho^{\circ} U^{\circ} A \qquad \textbf{(IV .11)}$$

The exponents (n) and (°) indicate respectively iterations, current and previous. The value of, n, is linearized in terms of pressure as follows:

$$\rho^{n} = \rho^{\circ} + \left.\frac{\partial \rho}{\partial P}\right|_{r} \left(p^{n} - p^{\circ}\right) \qquad \textbf{(IV.12)}$$

Where: T, representing temperature.

IV.4.5.3. Transitory Term

For a non-deformable control volume, the approximation of the transient term to the n^th^ step is given by:

$$\frac{\partial}{\partial t}\int_{V} \rho \Phi dV \approx V\,\frac{\left(\rho\Phi\right)^{n+1/2} - \left(\rho\Phi\right)^{n+1/2}}{\Delta t} \qquad \textbf{(IV.13)}$$

Where: the values at the beginning and end of the time step are designated by the exponents (n-1/2) and (n+1/2) respectively.

With the implicit Euler scheme of order 1, the resulting discretization is:

$$\frac{\partial}{\partial t}\int_{V} \rho \Phi dV = V\left(\frac{\rho\Phi - \rho^{\circ}\Phi^{\circ}}{\Delta t}\right) \qquad \textbf{(IV .14)}$$

With the implicit Euler scheme of order two, we'll have:

$$\left(\rho\Phi\right)^{n-1/2} = \left(\rho\Phi\right)^{\circ} + \frac{1}{2}\left[\left(\rho\Phi\right)^{\circ} - \left(\rho\Phi\right)^{\circ\circ}\right] \qquad \textbf{(IV .15)}$$

$$\left(\rho\Phi\right)^{n+1/2} = \left(\rho\Phi\right) + \frac{1}{2}\left[\left(\rho\Phi\right) - \left(\rho\Phi\right)^{\circ}\right] \qquad \textbf{(IV .16)}$$

Substituting equations ***(IV .15)*** and ***(IV .16)*** into equation ***(IV .13)*** will result:

$$\frac{\partial}{\partial t}\int_{V} \rho \Phi dV \approx V\,\frac{1}{\Delta t}\left[\frac{3}{2}\left(\rho\Phi\right) - 2\left(\rho\Phi\right)^{\circ} + \frac{1}{2}\left(\rho\Phi\right)^{\circ\circ}\right] \qquad \textbf{(IV. 17)}$$

IV.4.5.4. Solving discrete equations

By applying the finite volume discretization method for all elements of the domain, we get a linear system of equations in the form

$$\sum_{nb_i} a_i^{nb} \Phi_i^{nb} = b_i \qquad \textbf{(IV .18)}$$

Where: Φ , represents the solution; b is the second member and a represents the coefficients equations. The index (i): designates the number of the control volume or

node in question and (nb) means Neighbor but also includes the central coefficient multiplying the solution to the i^th location.
A node can have any number of its neighbors so that the method applies indifferently to structured and non-structured meshes. For a field scalar (e.g. turbulent kinetic energy), the terms a_i^{nb} , Φ_i^{nb} , et b_i are each unique numbers. For coupled fields, mass-momentum three-dimensional, these terms are matrices (4×4) for a_i^{nb} and vectors (4×1) Φ_i^{nb} ,b_i for nb and b given as follows:

$$a_i^{nb} = \begin{bmatrix} a & a & a & a \\ a_{uu} & a_{uv} & a_{uw} & a_{up} \\ a_{vu} & a_{vv} & a_{vw} & a_{vp} \\ a_{pu} & a_{pv} & a_{pw} & a_{pp} \end{bmatrix}_i , \Phi_i^{nb} = \begin{bmatrix} u \\ v \\ w \\ p \end{bmatrix}_i , b_i = \begin{bmatrix} b_u \\ b_v \\ b_w \\ b_p \end{bmatrix}_i \quad \textbf{(IV .19)}$$

ANSYS-CFX uses a coupled solver. In other words terms, the transport equations hydrodynamics (u, v, w, p) are solved simultaneously as a single system. Some solvers [122] use a separation strategy based on the resolution of conservation equations of the momentum in the first place, using an estimated pressure value. The result is a pressure correction equation. The resolution is thus obtained according to the principle "estimator-corrector". The main disadvantage of this technique is that it requires a large number of iterations in addition to the need for a judicious selection of relaxation parameters
Figure (IV.12) shows the Organizational of the different resolution steps followed by the CFX solver.

IV.4.5.4.1 Linear system resolution

The linear system of equations, described above, can be written in the following matrix form:

$$[A][\Phi]=[b] \quad \textbf{(IV .20)}$$

Where: [A], represents the coefficient matrix; [Φ], the solution vector and [b], the second member vector.

Equation *(IV .22)* can be solved iteratively by starting from an approximation of the solution Φ^n which has to be improved by a correction $\Phi^{'}$ to obtain the best solution Φ^{n+1}. And so:

$$\Phi^{n+1} = \Phi^n + \Phi' \qquad \textbf{(IV .21)}$$

Where: Φ' is a solution of the next equation:

$$A\Phi' = r^n \qquad \textbf{(IV .22)}$$

r^n, means the residual obtained from the expression:

$$r^n = b - A\Phi^n \qquad \textbf{(IV .23)}$$

Repeated application of this algorithm will result in a solution corresponding to the desired precision.

Figure (IV.15) shows the progress (in real time) of the CFX solver. During the resolution of an example it is possible to visualize the residuals obtained for each flow variable

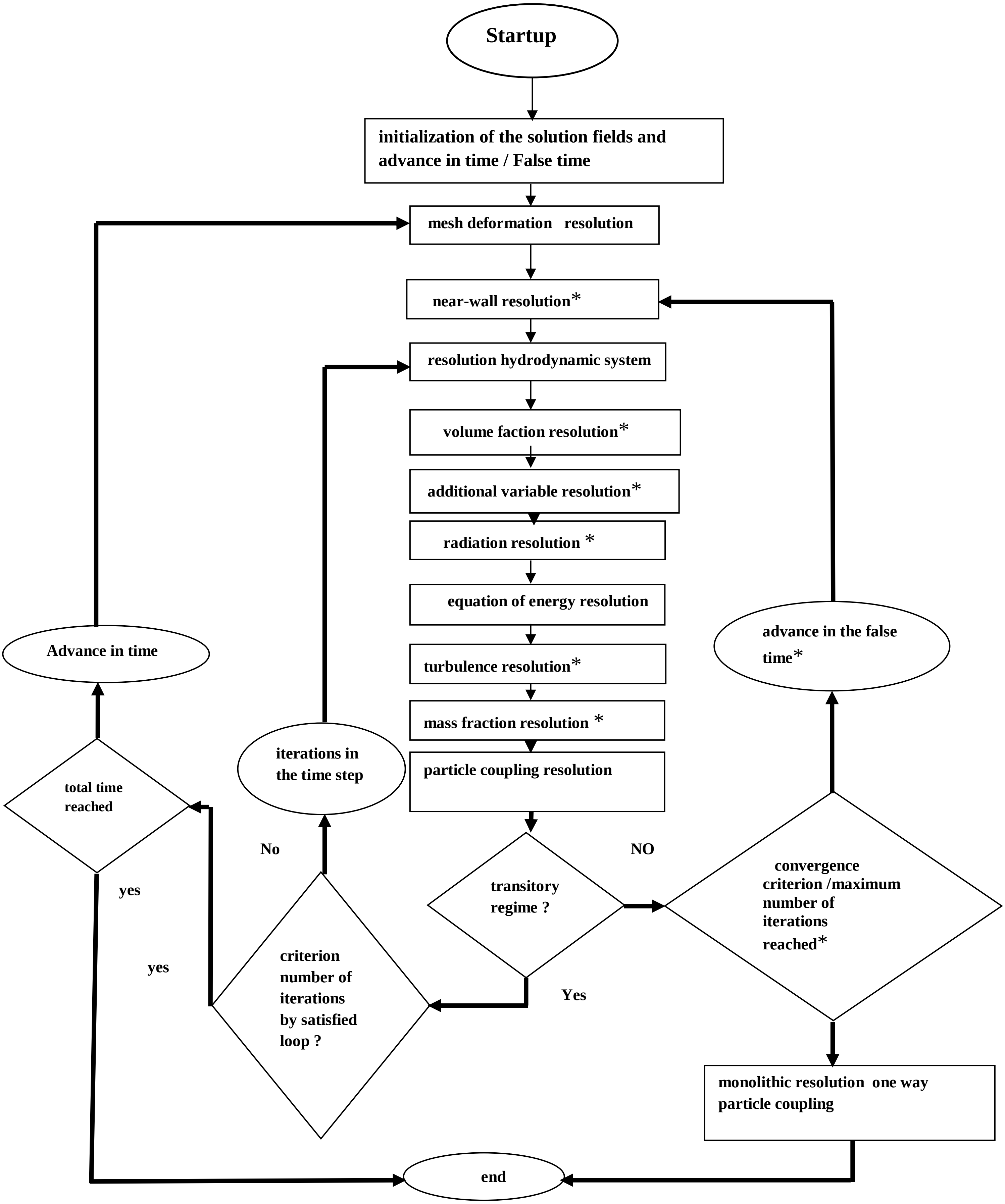

Figure IV. 15. *General plan for the resolution of a fluid dynamics problem by ANSYS-CFX.*

The sign (*) means that the present study is not concerned by the step in question.

IV.5. Presentation of the CFX software

CFX is a general software for numerical simulation of flows in fluid mechanics and heat transfer. This software permits to implement a complete numerical simulation of the modeling, of the geometric creation, and the visualization of the results, through mesh creation and calculation. The CFX software is divided into 3 modules: CFX-Pre, CFX-Solve and CFX-Post. Each module has a specific use Figure (IV.16).

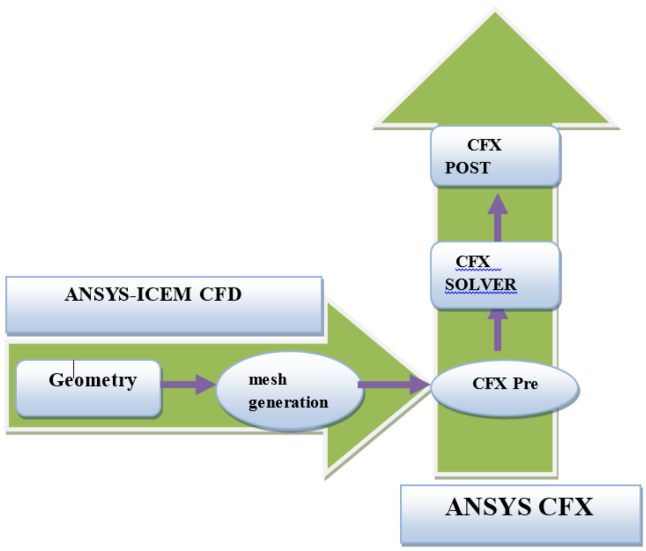

Figure IV. 16. *The principle modules of the CFX- CFD*

IV.5.1. CFX-Pre

The CFX-Pre Figure (IV.17) module is used to define the boundary and initial conditions of the system. As well as the equations to be solved, the type of resolution (steady-state or transitory) the parameters of the solver, including: the time step, the number of iterations, the convergence criterion as well as the nature of the fluids (liquid or solids) in presence. There are 5 types of boundary conditions: inlet, outlet, opening, wall and symetry

- Inlet type conditions are used in the case of an incoming flow inside the domain.
- Outlet-type conditions are used in the case of an outflow outside the domain.

The opening condition is used in the case of the condition for wall-type limits is attributed to the with flow impermeable walls.

- The opening condition is used in the case of a determination of nature of the inlet or outlet flow
- Finally, if the flow has a plane of symmetry it is possible to attribute the symmetry condition to this plane.

Once all the parameters have been defined, CFX-Pre generates a ".def" file containing all the information about the mesh. Boundary and initial conditions, as well as all other parameters entered in CFX-Pre. It's this file that's going to be the base of the solver's work.

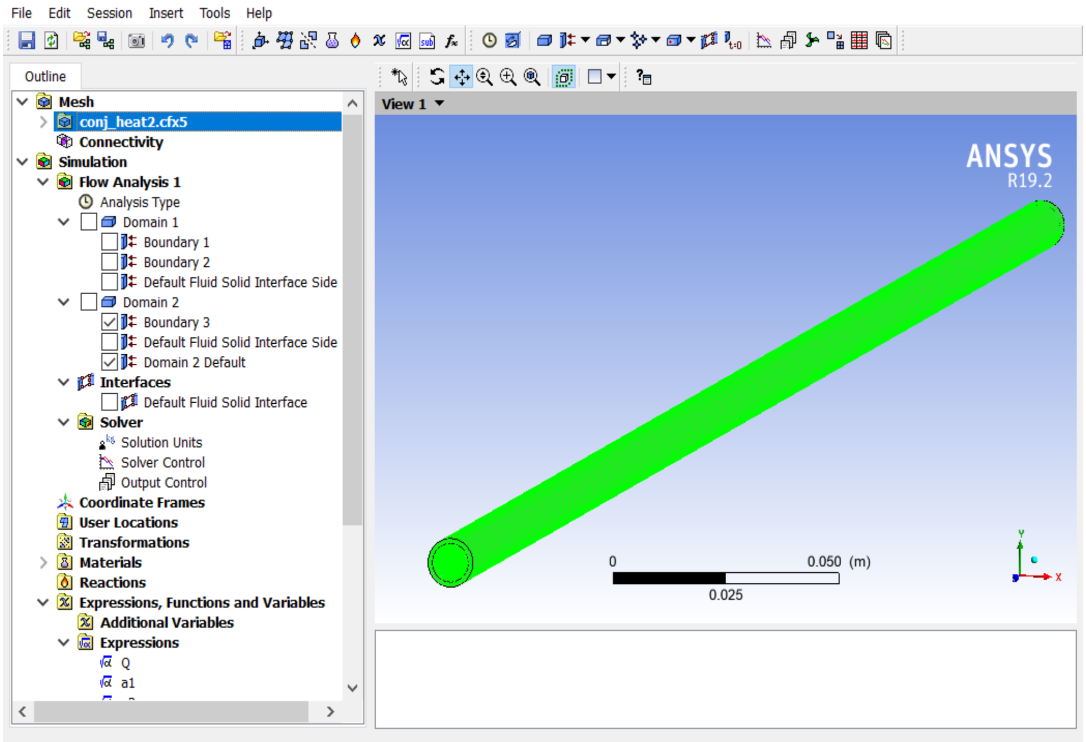

***Figure IV. 17 .** Graphical user interface of the CFX-Pre.*

IV.5.2. CFX- Solver

The CFX-solve module Figure (IV.18) is the module that performs the calculations. It is based on the integration of Navier Stockes equations in each mesh and has additional models to take into consideration laminar and thermal radiation.

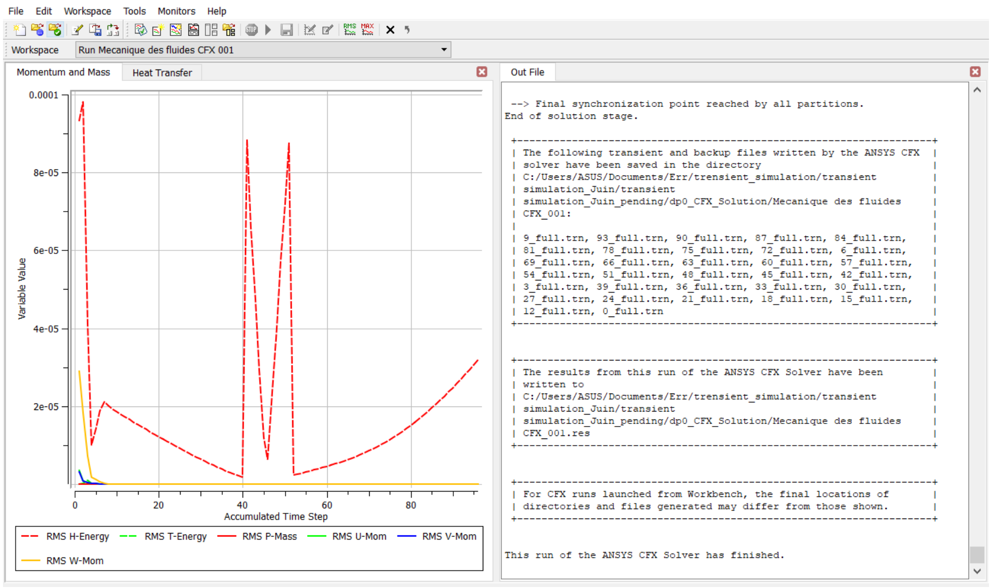

Figure IV. 18. *Graphical interface of the CFX-Solver module*

In the case of a steady state resolution, the calculation is continued until either the maximum number of iterations demanded by the user is reached, either the solution satisfies the convergence criterion. In the case of a transitory resolution, the calculation ends when the resolution time of the studied phenomenon is reached, at the end of the calculation, CFX-solve generates two types of:

- an "out" file readable by a text editor. This file resumes the progress of the calculation. It contains, among other things, the .def information, as well as the mass balance of the system.
- a ".res" file containing all the results. This file is directly exploitable by CFX-post.

IV.5.3. CFX-Post

The CFX-post module Figure (IV.19) is a graphical tool for processing and visualizing results. It allows you to apply textures to the geometry, to visualize contours, iso-surfaces, currents lines, velocity fields.

It also allows results to be exported in numerical form, such as, for example, the value of the different variables on each node, in photographic and even animated.

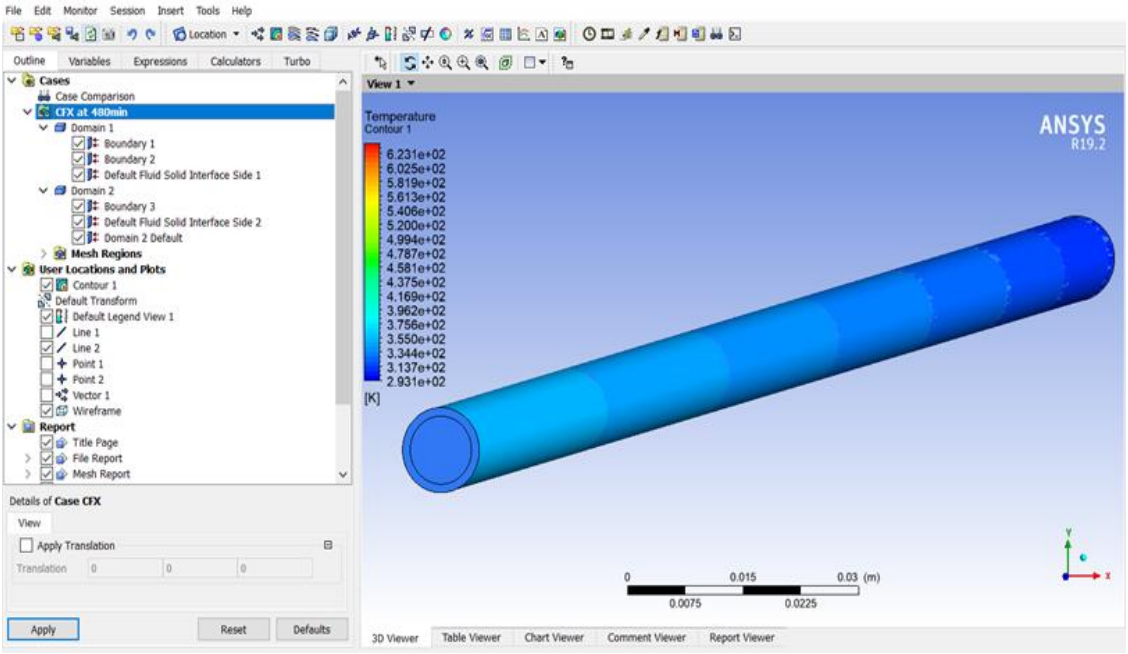

Figure IV. 19. *Graphical user interface of the CFX Post module.*

IV.5.4. Organizational chart

The solar intensity at the start of each hour (provided by PVSYST software) is introduced in Soltrace code and the outputs (data table) are interpolated by an appropriate Gaussian temporal function. Next, this function is implemented in CFX by using CEL language specific to the solver. Thereafter, it is specified as a boundary condition on the lateral surface of the tube receiver. The following figure (IV.20) shows the principal procedures for our simulation.

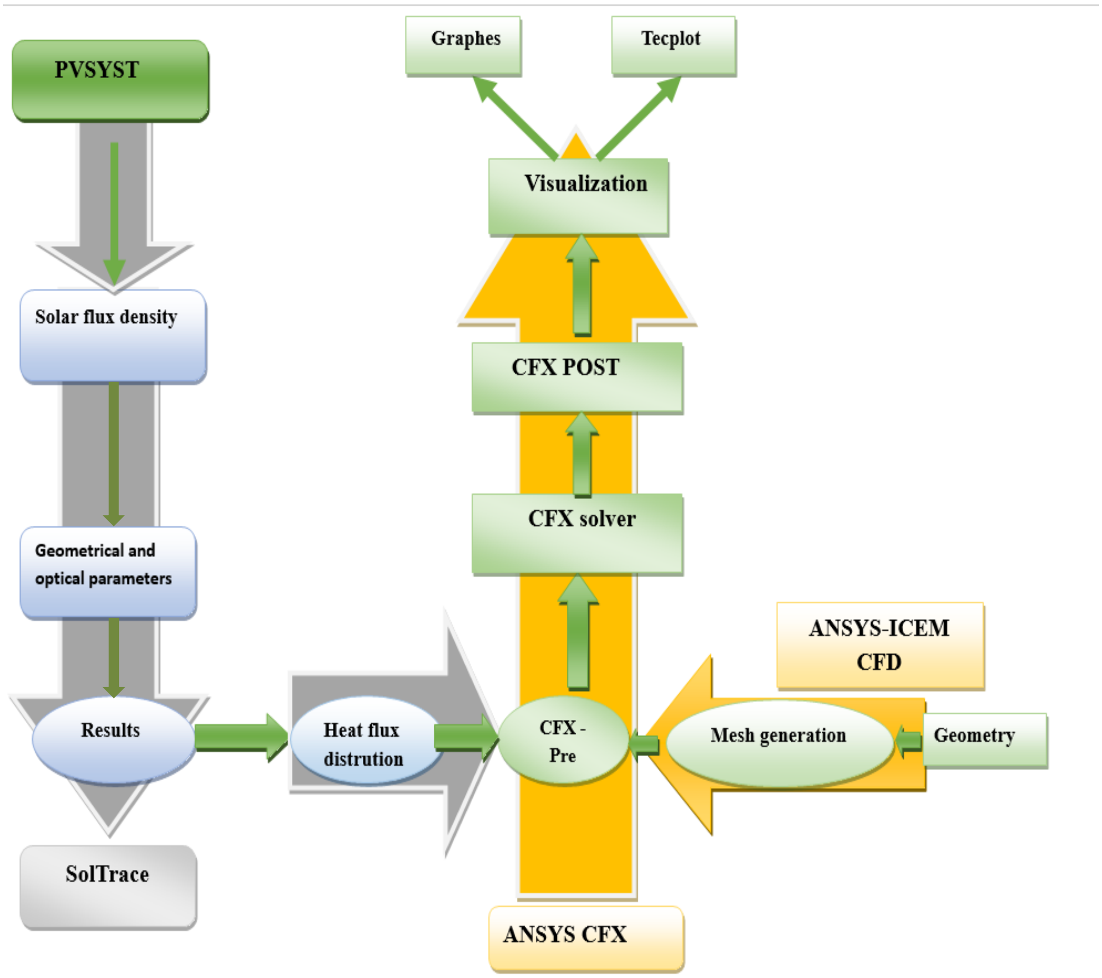

Figure IV. 20. *Organizational chart of the principal steps of the simulation*

IV.6 Chapter summary

At the end of this chapter, we think it is useful to remember the main steps in the development of the numerical modeling of the PTC. It is carried out in two main steps:

- The heat flux distribution around the tube absorber is calculated by the ray tracing method. This is established by Monte-Carlo ray tracing method (MCRT), which is a mathematical method based on probabilities and that allows to quantify the concentrated solar flux received at the absorber. This method is implemented in SolTrace code. The obtained numerical temporal values of the heat flux resulting from radiation serve as boundary conditions for the CFD solver. In order to introduce this values in the CFD solver, they were interpolated by Gaussian functions. This is allows to implement the transient heat flux boundary condition in the CFD solver by using the CEL language specific to ANSYS-CFX.

- The numerical modeling of the conjugated heat transfer and the fluid flow inside the absorber tube is discretized by the so called "based-element finite-volume". The procedure is performed in the following steps:

  - The geometrical domain is divided in two subdomains: solid and fluid. Each subdomain is discretized into a set of elements whose vertices are called nodes.
  - The system of equations III.43 to III.45 is then discretized at each node.
  - The result of this discretization is a set of algebraic equation, which is resolved by iterations.
  - The main variable to solve is the temperature distribution on the tube absorber and in the fluid heat transfer at each instant.

Chapter V

Results and interpretations

Results and interpretations

V.1. Introduction

In a first step, the geometry and performance of the solar collector were determined using an optical model developed with the SolTrace software, which made it possible to quantify the solar flux distribution on the absorber tube. Then, the results of the optical simulation, which determines the distribution of the solar energy on the absorber tube. are taken as boundary conditions. Solar flux density values for four days in different seasons have been taken. SolTrace code is used to determine the heat flux distribution on the absorber tube. The conjugate heat transfer and fluid flow equations in the tube absorber are solved by using ANSYS-CFX CFD software.

And in the end, A comparison between two cases of geometry concerning the secondary reflector (PTC with parabolic secondary reflector and flat secondary reflector) in order to get the best and high distribution of the heat flux with high temperature of HTF in the outlet of the absorber the next step is to compare the results of PTC accompanied by secondary reflector with classic PTC , for the same working fluids (Therminol VP-1 and water) than to draw a conclusion .

V.2. Model validation

To be able to analyze the performance of a PTC using the proposed model, it is important to validate it. For this purpose, the model is applied to the system described in reference [56]. It is a small-sized PTC equipped with two types of second reflector, the triangular reflector and the parabolic reflector. Here we are only interested by the parabolic reflector. The simulation results are compared with experimental results reported in this reference. The results to be compared are the fluid (water) temperature at the absorber tube outlet.

The absorber tube has the following dimensions: inner diameter 10.7 mm, outer diameter 12.7 mm, and length 2.5 m. The data and tests results are summarized in Table 3. Note that, these tests have been performed on 03/05/ 2018.

The obtained results for the fluid outlet temperature are presented in Figure (V.1) . As it can be seen, the maximum temperature value obtained by simulation is slightly deviated to the left compared to the experimental value. This is due to the calculation errors, the conditions of the experiment, as well as to the energy storage. However, Error range recorded is about 2.73 °C (maximum deviation), the mean absolute error is about 1.43 °C, the standard deviation is 0.74, and the root mean square error is 1.56. According to these values, we can conclude that the present model is in good agreement with the experimental data. Therefore, the model can be used to analyze the optical and thermal performance of PTC.

Table V. 1. *Experimental data for PTC with parabolic secondary reflector [56].*

.

Time (h)	I_b(W/m^2)	T_{in} (°C)	T_{out} (°C)
09.00	399.1	29.5	33.5
09.30	489.2	29.6	35.1
10.00	598.7	29.6	37.8
10.30	687.4	29.8	39.9
11.00	688.3	30.1	41.8
11.30	737.4	30.2	43.1
12.00	859.8	30.9	45.7
12.30	862.6	31.5	46.6
13.00	826.0	31.8	48.4
13.30	746.2	31.9	49.2
14.00	653.5	31.6	45.6
14.30	547.3	33.3	44.5
15.00	447.4	33.4	42.1
15.30	330.1	33.0	39.8
16.00	227.0	33.2	37.5

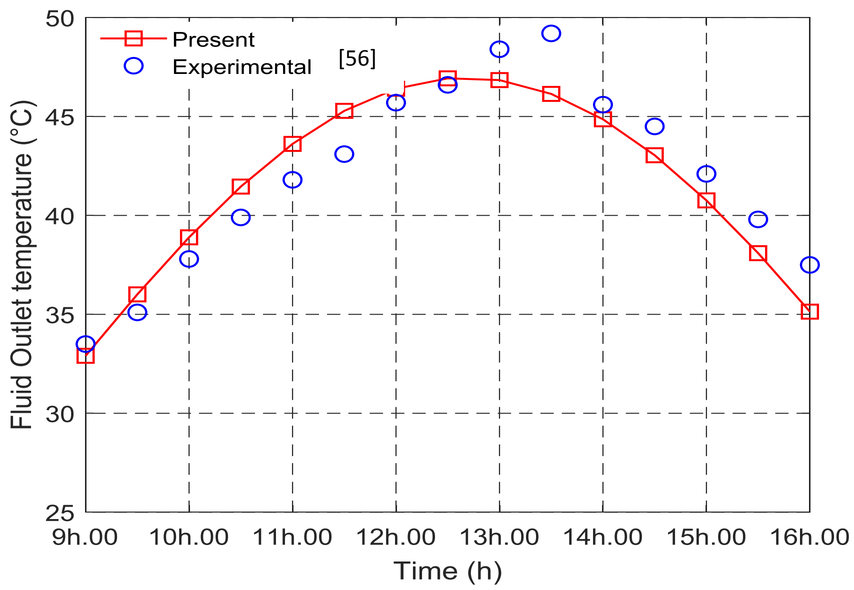

Figure V. 1. *Fluid outlet temperature versus time. Comparison between experimental data and simulation results*

V.3. Materials Properties

Many industry research and development projects, and the centers of research is actually working to find heat transfer fluids (HTF) for solar thermal power plants. From the various HTF available, the Therminol VP-1Has been selected for solar applications dedicated to energy production. This fluid appear to be Promising options for plant improvements

Therminol VP-1 heat transfer fluid is an ultra-high temperature synthetic heat transfer fluid designed to meet the demanding requirements of vapor phase systems or liquid phase system

- **Performance Benefits**

• Superb Heat Transfer Properties - Therminol VP-1 is a synthetic heat transfer fluid which combines exceptional thermal stability and low viscosity for efficient, dependable, uniform performance in a wide optimum use range of 12° to 400°C; Therminol VP-1 has the highest thermal stability of all organic heat transfer fluids.

• Low Viscosity - Therminol VP-1 has a low viscosity to 12°C; Because of its crystallization point of 12°C (54°F), this fluid may require tracing in colder climates to avoid operational problems.

• Vapor Phase Heat Transfer Fluid - Therminol VP-1 is a eutectic mixture of diphenyl oxide (DPO) and biphenyl. It can be used as a liquid heat transfer fluid or as a boiling-condensing heat transfer medium up to its maximum use temperature. It is miscible and interchangeable (for top-up or design purposes) with other similarly constituted diphenyl-oxide (DPO)/biphenyl fluids.

• Precise Temperature Control - Due to its ability to operate as a vapor-phase heat transfer fluid, Therminol VP-1 is excellent for use in heat transfer fluid systems requiring very precise temperature control.

In this work, the materials in question are copper for the tube Therminol VP-1 , water for the working fluid. Copper and water physical properties are predefined in CFX solver. Therminol VP-1 properties (Density, Thermal Conductivity, Heat Capacity and Viscosity) are tabulated in Ref. [123] according to the temperature. In order to implement fluid properties in the solver we use interpolation functions. Accordingly, these properties are described by the following equations:

$$\rho\,(kg/m^3) = -1.587T*^4 - 4.715T*^3 - 8.35T*^2 - 113.6T* + 895.1 \quad \textbf{(V.1)}$$

$$k\,(W/m.K) = -0.002794T*^2 - 0.02037T* + 0.1107 \quad \textbf{(V.2)}$$

$$Cp\,(J/kg.K) = 8.152T*^5 + 11.92T*^4 - 8.463T*^3 - 17.87T*^2 + 383.4T* + 2103 \quad \textbf{(V.3)}$$

$$\mu\,(Pa.s) = 1.995\times10^{-6}\exp(-4.583T*) + 3.678\times10^{-4}\exp(-0.8132T*) \quad \textbf{(V.4)}$$

$$\text{Where: } T* = \left(T(K) - 493.0802\right)/125.2891 \quad \textbf{(V.5)}$$

Note that these expressions are valid only for the temperature range [12-425] °C. The previous properties equations are implemented in the solver as expressions by using CFX Expression Language (CEL) specific to CFX software.

V.4. Solar radiation

Figure (V.1 represents the solar radiation as a function of time for 4 days from four months (March 21, June 21, September 21 and December 21). The numerical temporal intensity of solar radiation are obtained by using PVSYST software for a location (2°56 Longitude and 33°46 Latitude)

Note that for the day of June 21, the solar radiation is maximal at the real solar noon, which can reach 1037 W/m².The minimal solar radiation, about 600 W/m^2, is recorded during the month of December.

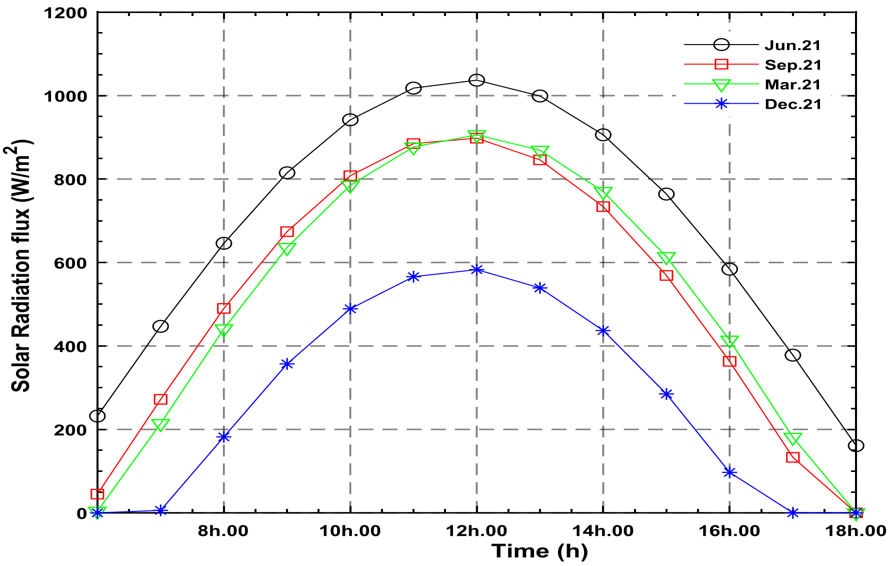

Figure V. 2. *Variation of modeled solar radiation with time for 4months in region of Laghouat*

V.5. Optical modeling of different geometry of secondary reflector

The main objective of the optical modeling is to determine the concentration of power in the absorber tube, and the evolution of the heat flux at the absorber according to a variation of the incidence angle of solar rays.

Figure (V.3*)* shows the path of the rays reflected by the concentrator on the absorber tube. It can be seen from this figure that the absorber tube of the classic PTC (Figure V.3 **a**) is subjected to a concentrated solar flux on the bottom part while the upper one is subjected to a non-concentrated solar flux; and adding a secondary reflector with different geometries ; the solar rays can reach the upper part after reflected by the additional parabolic and flat reflectors as shown in Figure (V.3 **b**), (V.3 **c**)

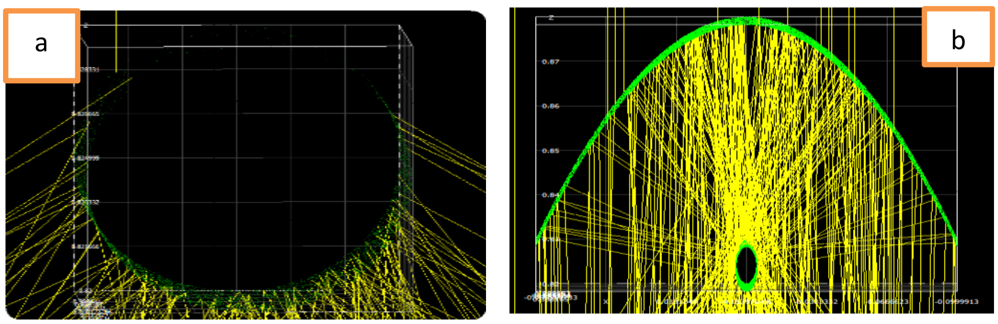

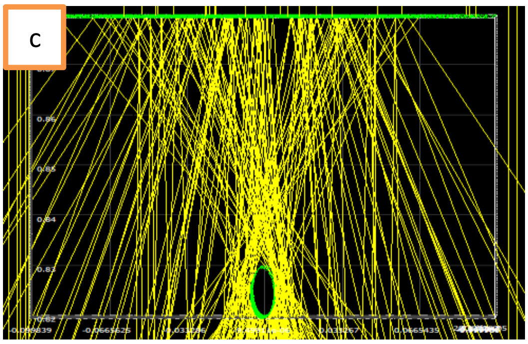

Figure V. 3. *Rays incident on the absorber for (a) without secondary reflector (b) with parabolic secondary reflector (c) with flat secondary reflector*

.

V.5.1. Case a: PTC without secondary reflector

Figure V.4 show ray tracing of PTC without secondary reflector and The heat flux distribution on the absorber tube as estimated by SolTrace is shown in Figure(V.5) It is to be noted that the heat flux distribution on the absorber surfaces were estimated for an incident beam flux of 1000 W/m^2 . The two dimensional plan view of the PTC tube outer surface heat flux is shown in Figure. (V.5)(Case a_1) for the tube diameter D_2=10 mm. The abscissa represents the circumferential perimeter length of the absorber tube and the ordinate represents the tube axial length. The three dimensional heat flux distribution on the PTC is shown in Figure. (V.5) (case a_2). The value of heat flux for the case (a) . Since most of the reflected sun rays are focusing to the bottom of the absorber, higher heat flux is high on the lower portion of the absorber tube due to concentrated solar flux from the primary reflector, decreases towards the tube top. At the absorber top, the heat flux is mostly from the direct beam radiation. The average heat flux density of absorber is 10000 W/m^2

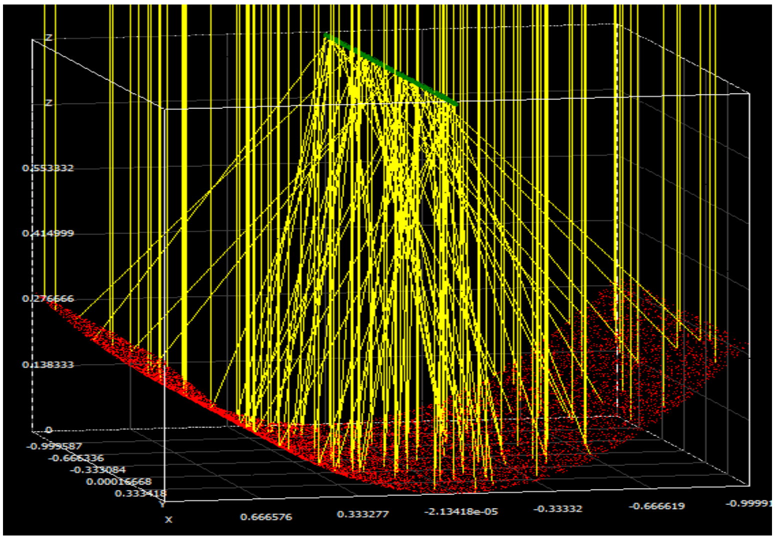

Figure V. 4. *Ray tracing of classic PTC in SOLTRACE*

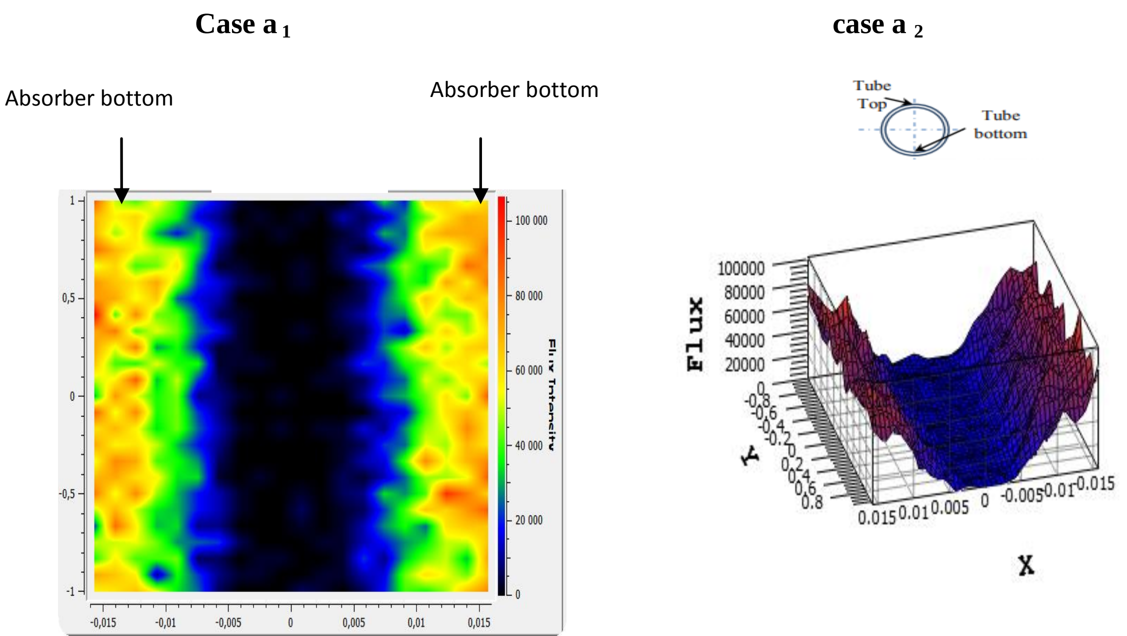

Figure V. 5. *Heat flux distribution on the absorber of classic PTC case a_1 and the three dimensional heat flux case a_2 from SolTrace*

V.5.1. Case b: PTC with secondary reflector

Figure (V.6) show ray tracing of PTC with parabolic secondary reflector and Case (b_1) and (b_2) show the corresponding plan view and the three dimensional map of the heat flux distributions on the absorber top surface used parabolic secondary reflector It can be seen that flux on the top took the shape of the parabolic secondary reflector and missed radiation can be redirected to the absorber ,An additional advantage of the inclusion is increase of uniformity of the flux around the absorber

Figure (V.7) show the heat flux distribution on the circumference of absorber tube obtained by ray tracing. The value of heat flux for the case (b) is high on around all the absorber tube due to concentrated of the primary reflector and parabolic secondary one. A non-linear heat flux distribution is observed over the absorber, which leads to a high temperature gradient. The contour and the surface plot of the average heat flux intensity in the top of the absorber, the average heat flux density of absorber is 90000 W/m^2, which is numerically simulated using SolTrace software

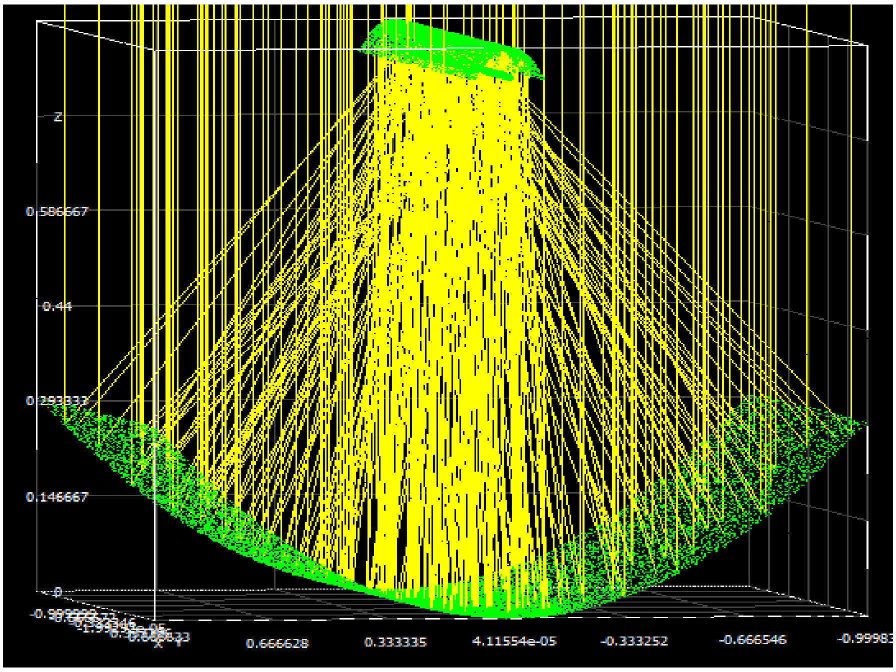

Figure V. 6. *Ray tracing of PTC with secondary reflector in soltrace*

Case b_1 **Case b_2**

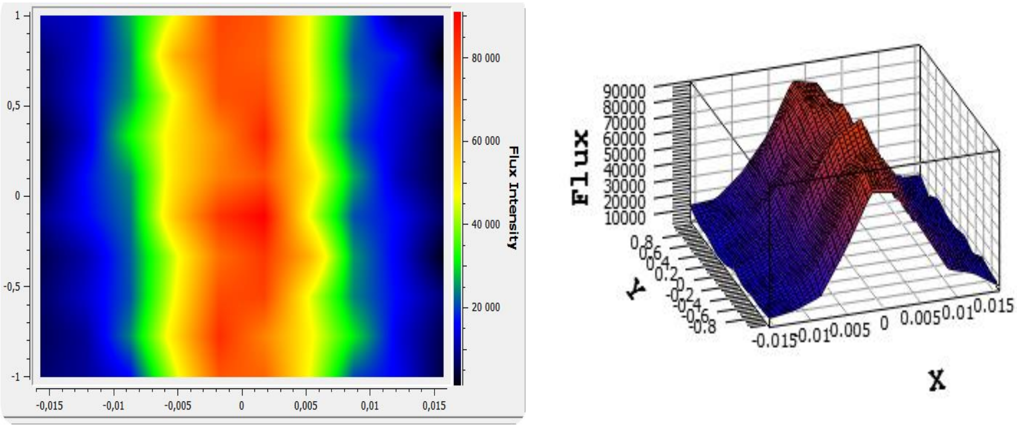

Figure V. 7. *Heat flux distribution on the top of absorber case b1 and the three dimensional map of the heat flux distributions case b_2 in PTC with flat secondary reflector from SolTrace*

V.5.2. Case c: PTC with flat secondary reflector

Figure V.8 show the Ray tracing of PTC with flat secondary reflector, And Figure (V.9) (c_1) ,(c_2) show consecutively the contour and the surface plot of the average heat flux intensity on the top of the absorber It can be seen from this figure the flux is large on the top so it took the shape of flat secondary reflector . The average heat flux density of receiver is 90000 W/m^2, which is numerically simulated using SolTrace software.

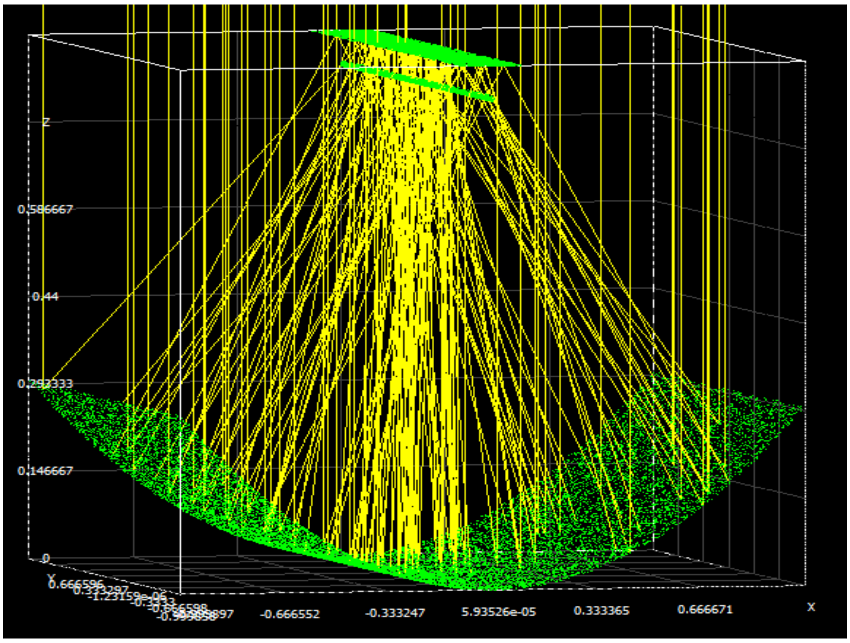

Figure V. 8. *Ray tracing of PTC with flat secondary reflector in SolTrace*

Case c1

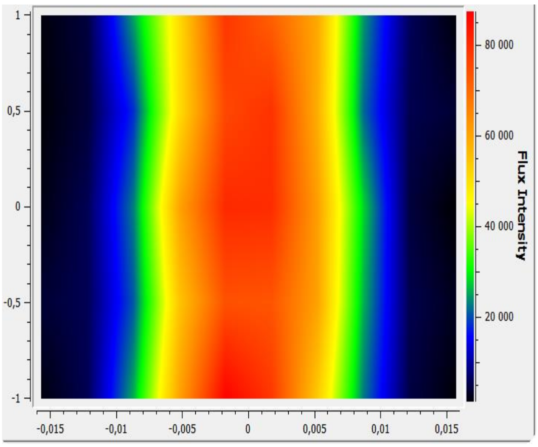

Case c2

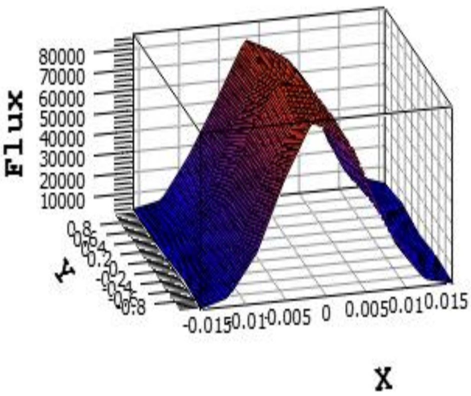

Figure V. 9. *Heat flux distribution on the top of absorber in PTC with flat secondary reflector from SolTrace case c_1 and the three dimensional map of the heat flux distributions case c_2 in PTC with flat secondary reflector from SolTrace*

Table V. 2. *Heat flux distribution on the absorber of 3cases a, b, c on the month of March*

March

Time (h)	Solar radiation W/m²	Heat flux without secondary reflector w/m²	Heat flux with parabolic secondary reflector w/m²	Heat flux with flat secondary reflector w /m²
4	0	0	0	0
5	0	0	0	0
6	4	450,042	370,346	308,644
7	214	24077,2	19813,5	16512,5
8	441	49617,1	40830,6	34028
9	636	71556,6	58885	49074,4
10	785	88320,7	72680,4	60571,4
11	877	98671,6	81198,3	67670,2
12	906	101934	83883,3	69907,9
13	869	97771,5	80457,5	67052,9
14	770	86633	71291,6	59414
15	614	69081,4	56848,1	47376,9
16	414	46579,3	38330,8	31944,7
17	181	20364,4	16758,1	13966,1
18	0	0	0	0
19	0	0	0	0

Table V. 3 . *Heat flux distribution on the absorber of 3cases a b c on the month of juin*

Juin

Time (h)	Solar radiation W/m^2	Heat flux without secondary reflector w/m^2	Heat flux with parabolic secondary reflector w/m^2	Heat flux with flat secondary reflector w/m^2
4	0	0	0	0
5	29	3262,8	2685,01	2237,67
6	232	26102,4	21480,1	17901,4
7	447	50292,1	41386,1	34491
8	646	72681,7	59810,8	49846
9	815	91696	75457,9	62886,2
10	942	105985	87216,4	72685,7
11	1018	114536	94253	78549,9
12	1037	116673	96012,1	80016
13	999	112398	92493,9	77083,9
14	906	101934	83883,3	69907,9
15	764	85957,9	70736	58951
16	584	65706,1	54070,5	45062
17	378	42528,9	34997,7	29166,9
18	161	18114,2	14906,4	12422,9
19	0	0	0	0

Table V. 4. *Heat flux distribution on the absorber of 3cases a b c on the month of September*

September

Time (h)	Solar radiation W/m^2	Heat flux without secondary reflector w/m^2	Heat flux with parabolic secondary reflector w/m^2	Heat flux with flat secondary reflector w/m^2
4	0	0	0	0
5	0	0	0	0
6	45	5062,97	4166	3472,25
7	272	30602,8	25183,5	20987,8
8	490	55130,1	45367,4	37808,9
9	674	75832	62403,3	52006,5
10	808	90908,4	74809,8	62346,1
11	885	99571,7	81939	68287,5
12	898	101034	83142,6	69290,6
13	846	95183,8	78328,1	65278,2
14	734	82582,2	67958,4	56636,2
15	569	64018,4	52681,7	43904,6
16	363	40841,3	33608,9	28009,5
17	133	14963,9	12314	10262,2
18	0	0	0	0
19	0	0	0	0

Table V. 5. *Heat flux distribution on the absorber of 3cases a b c on the month of December.*

December

Time (h)	Solar radiation W/m^2	Heat flux without secondary reflector w/m^2	Heat flux with parabolic secondary reflector w/m^2	Heat flux with flat secondary reflector w /m^2
4	0	0	0	0
5	0	0	0	0
6	0	0	0	0
7	6	675,062	555,519	462,966
8	182	20476,9	16850,7	14043,3
9	357	40166,2	33053,4	27546,5
10	489	55017,6	45274,8	37731,7
11	566	63680,9	52403,9	43673,1
12	583	65593,6	53977,9	44984,9
13	539	60643,1	49904,1	41589,8
14	437	49167	40460,3	33719,4
15	285	32065,5	26387,1	21990,9
16	97	10913,5	8980,88	7484,62
17	0	0	0	0
18	0	0	0	0
19	0	0	0	0

The missed radiation on the absorber can be redirected to the receivers by the addition of a second-stage optics, according to the results of heat flux distribution on the absorber tube with the secondary parabolic and flat reflector presented in the tables (V. 3),(V. 4), (V.6), and (V.7). We notice that the parabolic geometry show the increasing of uniformity of the heat flux around the absorber so the parabolic geometry chosen in our study is the one that allows the highest outlet temperature, in order to make a comparison between two cases (traditional PTC and PTC with parabolic secondary reflector).

V.6. Output of the Optical Modeling

The purpose of the optical modeling is to determine the concentration of heat flux on the portion of the receiver tube surface exposed to the reflected rays from the primary reflector. In Soltrace program, we introduce the optical characteristics of the system, the geographic data, and the solar flux density concerning the city of Laghouat for two cases: PTC without secondary reflector and PTC with secondary reflector. The obtained results are reported in Figure (V.10) .As we can see, the variation of the concentration of the heat flux around the tube follows the same profile as that of the incident radiation. In case (a), the heat flow is concentrated only on the lower side of the tube, so there will be a high temperature gradient between the two sides of the tube. On the other hand, in case (b) the heat flow is distributed over the entire lateral surface of the tube. Therefore, the heat flux boundary condition in case (a) is applied to the lower half of the tube lateral surface, and in case (b) it applies to the entire surface of the tube. Note that the data in Figure 4 are interpolated by Gaussian functions and implemented in CFX solver as transient heat flux boundary conditions.

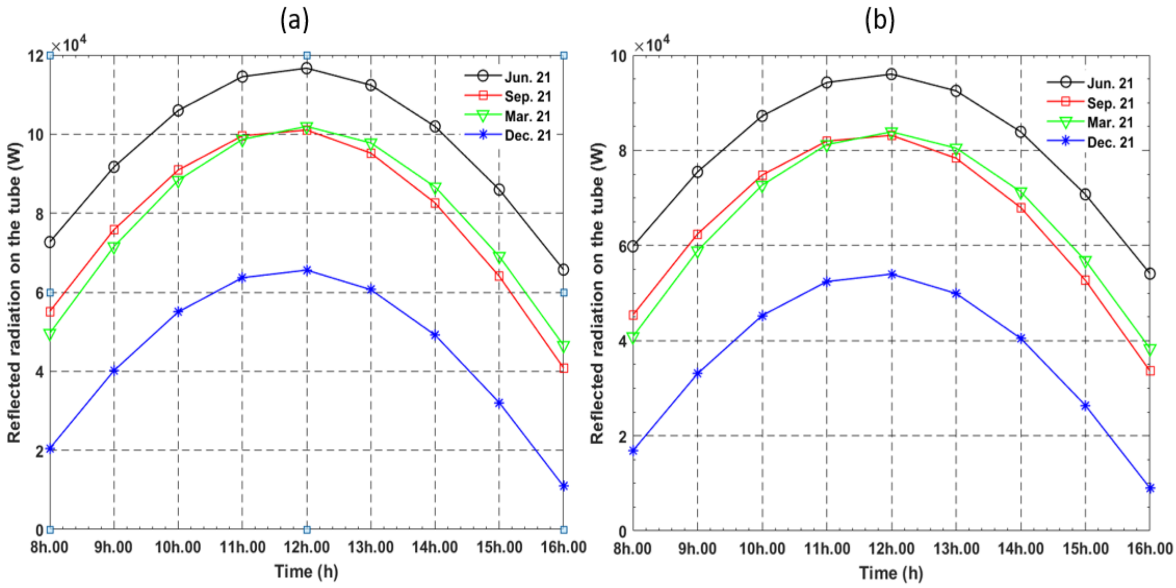

Figure V. 10. Transient heat flux applied on the receiver tube (a) without secondary reflector, (b) with secondary reflector**.**

Figure (V.11) shows the heat flux distribution on the circumference of absorber tube obtained by ray tracing. The value of heat flux for the case (b) is high on around all the absorber tube due to concentrated of the primary reflector and secondary one. The maximum radiation obtained is about 80000W/m^2. A non-linear heat flux distribution is observed over the absorber, which leads to a high temperature gradient. The value of heat flux for the case (a) is high on the lower portion of the absorber tube due to concentrated solar flux so and low on the upper portion due to direct sunlight for the absorber.

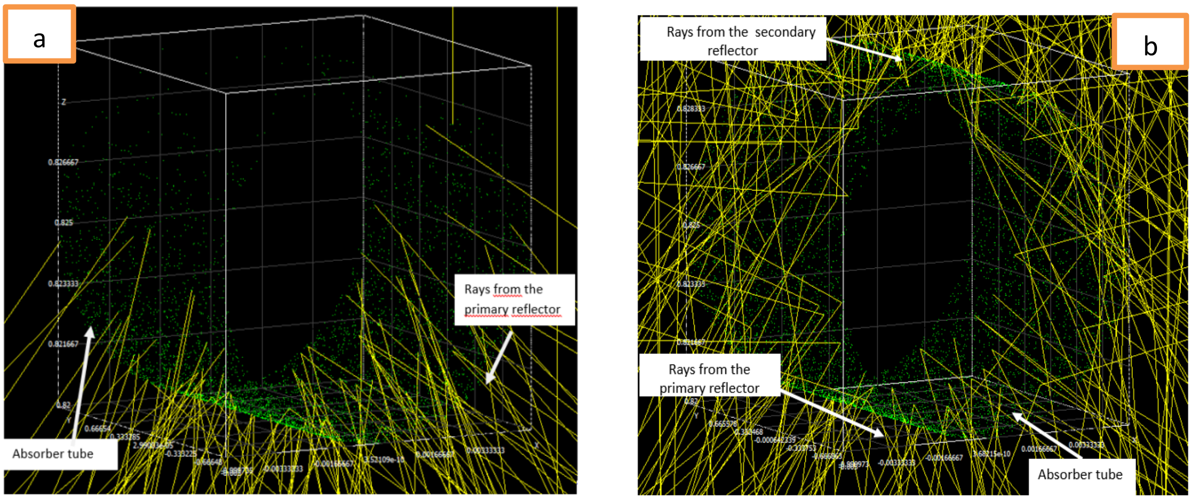

Figure V. 11. *Rays incident on the absorber for (a) without SR (b) with SR*

V.7 Results of using Therminol VP-1 for the working fluid.

V.7.1 Fluid outlet temperature

The variations of the temperature, at the tube outlet, during different days are represented in Figure (V.12) for both cases: with and without secondary reflector. As it can be seen, the fluid temperature at the outlet of the absorber tube is proportional to the direct sunlight. As the density of the solar flux increases, the temperature of the fluid increases until it reaches the maximum. Then, it decreases with the solar flux until the end of the day. It mainly depends on the heat quantity absorbed by the tube, which is based on optical and geometric parameters of concentrator. We note that for every day and in both cases, the temperature pick is reached around 12.00 h. We also notice a difference in maximum temperatures (June) of about 90 °C and in minimum temperatures (December) about 50°C between the two cases.

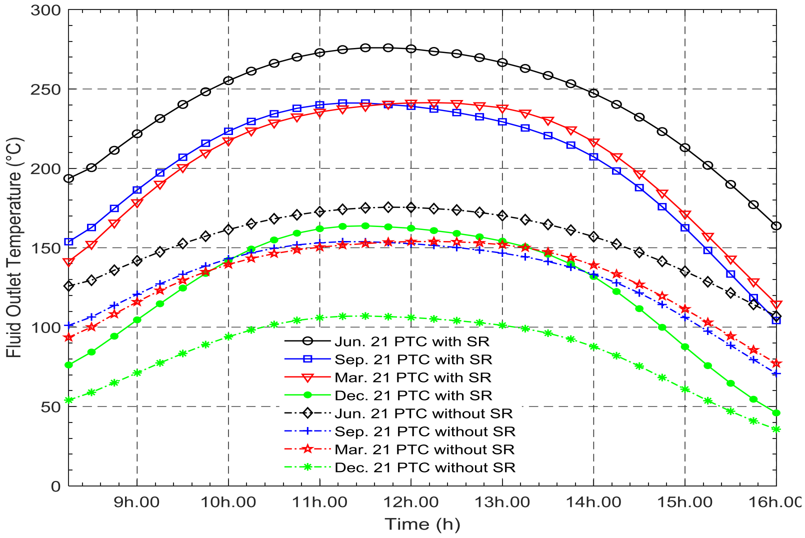

Figure V. 12. *Variation of fluid temperature at the tube outlet versus time*

V.7.2. Useful thermal energy

The Therminol VP-1 oil is used as heat carrier fluid. During the simulation, the physical properties of the heat carrier fluid are varied depending on the temperature of the fluid according to equations (V.1) to (V.5).Variations of the heat transported by the carrier fluid are shown in Figure (V.13). We notice that the variation profiles are similar to those of the temperature at the tube outlet. We also note that the difference in useful heat between the two cases (a) and (b) is about 540 W during the month of June and 140 W during the month of December.

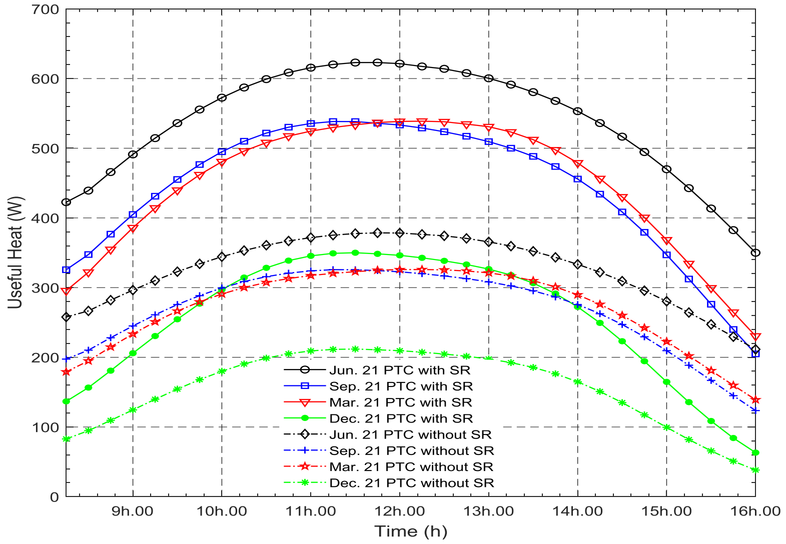

Figure V. 13. *Variation of useful thermal energy with respect to time.*

V.7.3. Thermal efficiency

The PTC thermal efficiency values obtained by numerical simulation are reported in Figure V.14 (a) and (b) (For clarity, we have represented each case on a separate graph). As it can be seen, the efficiency is approximately constant equal to 30 % in case (a) for all seasons. For case (b), the efficiency is around 18% for the four seasons. We record then a ratio of 1.65 between the two cases as shown in Table (V.6) .

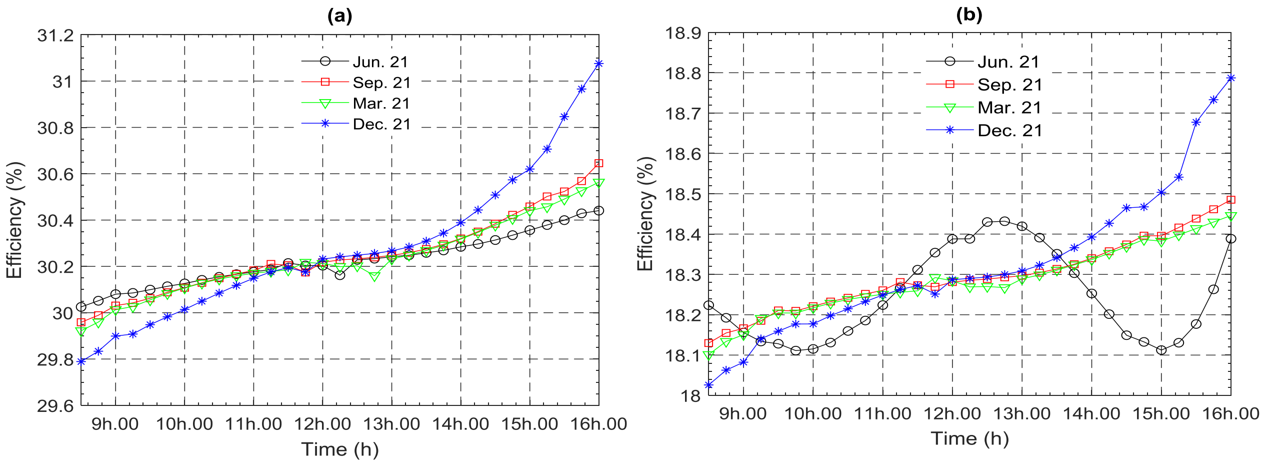

Figure V. 14. *Variation of instantaneous thermal efficiency versus time,(a)PTC with SR,* *(b)PTC without SR.*

Table V. 6 *.Performance comparison between PTCs with and without secondary reflector*

	Mean Efficiency (%)		
	PTC with second reflector	PTC without second reflector	Ratio
June 21	30.2	18.3	1.65
September 21	30.2	18.3	1.65
December 21	30.2	18.3	1.65
March 21	30.2	18.3	1.65

V.8. Results of using water for the working fluid

V.8.1. Fluid Outlet Temperature

Figure V.15. Shows the temperature contour in the entire domain (June 21at 12.00h) for a PTC system with secondary reflector. As can be seen, the temperature increases gradually along the tube until reaching the maximum at the outlet (about 700 K).However, it gradually decreases in the radial direction to reach the minimum in the center of the tube (about 380 K). In this study, we consider the outlet water temperature at the center of the tube. Figure **(**V.16). Represents the evolution of the temperature of the water leaving the absorber tube for four days, June 21, September 21, March 21 and December 21 of the year 2019. The temperature temporal profile is similar to that of the heat flux concentrated on the tube surface and the maximum is reached at noon. We also notice that the obtained temperatures in case (a) (PTC with second reflector) are much higher than the obtained temperatures in case (b) (PTC without second reflector).This is because the heat flow in case (a) is more intense and uniform than in case (b). This is obviously due to the presence of the second reflector.

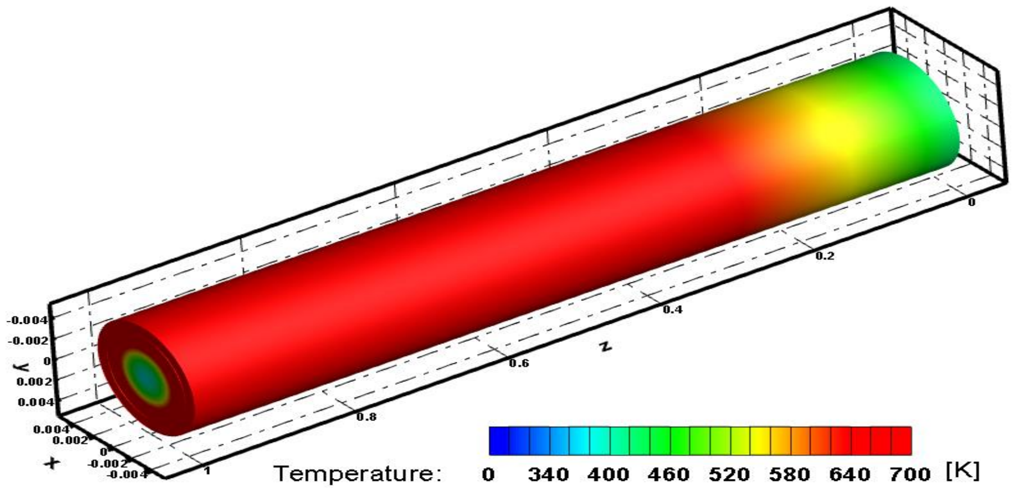

Figure V. 15. *Temperature contour on the absorber tube for a PTC with second reflector (June 21 at 12.00*

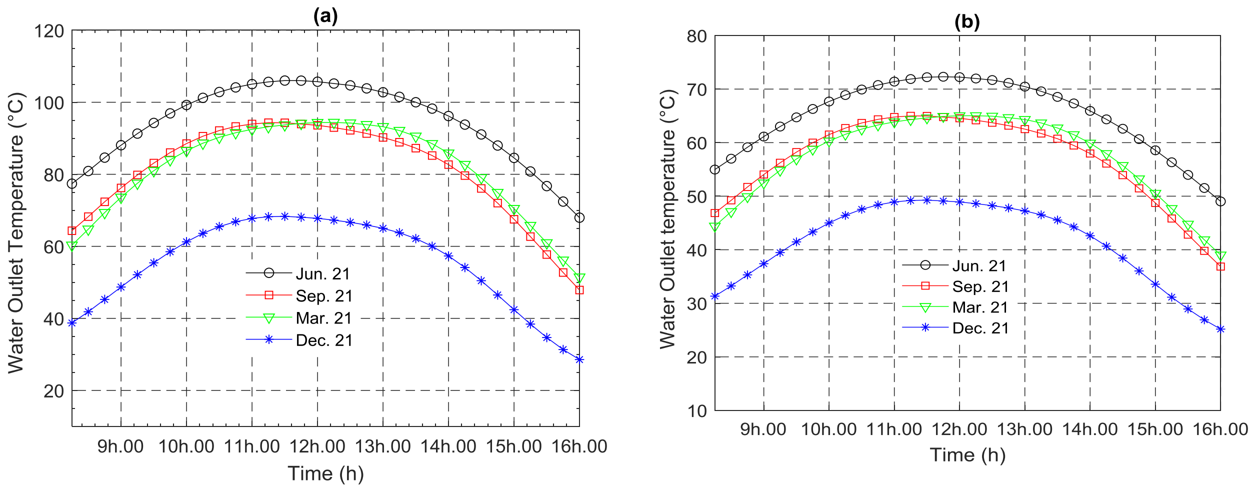

Figure V. 16. *Evolution of water temperature at the tube outlet, (a)PTC with secondary reflector, (b) PTC without secondary reflector*

V.8.2. Useful Thermal Energy

Once the temperatures at the outlet of the tube are determined, the heat flux absorbed by the tube is calculated according to Equation ((**III.34)**). Water mass flow across the tube is about 0.0025 kg/s. The corresponding mean Reynolds number is about 400, which corresponds to a fully laminar flow. Figure (V.17) (a) and (b) represents the variations of the useful heat as a function of time in both cases (PTC with and without second reflector). The maximum gained energy is recorded in the month of June (900 W in case (a) and 550 W in case (b)), while the minimum absorbed energy is recorded in the month of December (500 W in case (a) and 300 W in case (b)).For the months of March and September, the maximum energy absorbed at noon is the same (about 800 W in case (a) and 470 W in case (b)).

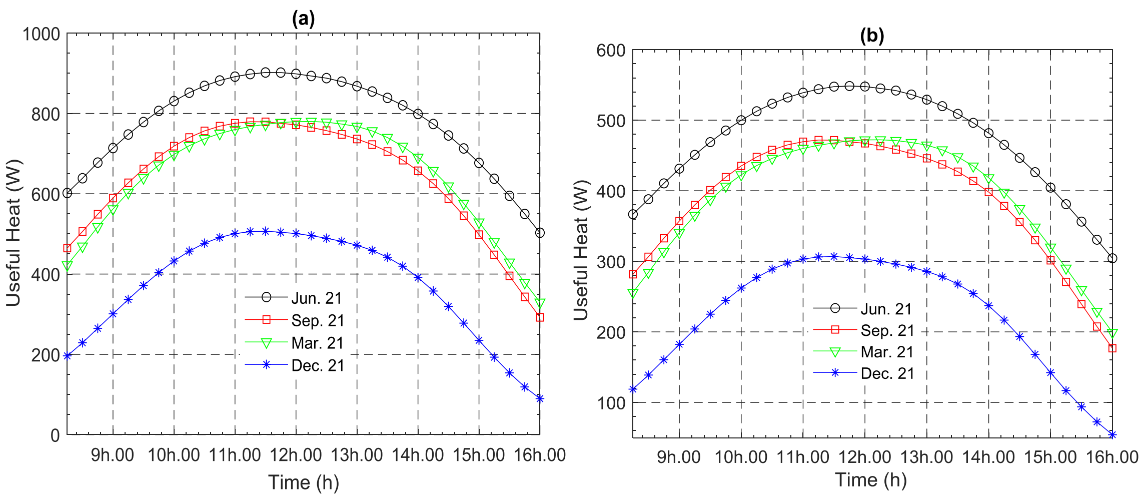

Figure V. 17. *Variation of collected energy with respect to time, (a) PTC with secondary reflector, (b) PTC without secondary reflector.*

V.8.3. Thermal efficiency

The thermal efficiency of the system is determined from equation (2). The values calculated for the two cases are represented in figure (V.18). The maximum efficiency obtained is recorded during the month of June (approximately 44% for case (a) and 27% for case (b) during the whole day), while the minimum value is obtained during the month of December (around 27% in case (a) and 15% in case (b) at noon). Concerning the months of March and September, the maximum efficiency is the same (38% in the case (a) and 23% in the case (b)) but reached in different times (11.00h for the month of September and 13.00h for the month of March). Therefore, we note that the use of a second reflector can increase the system performance by a ratio in the range of 1.62 to 1.67.

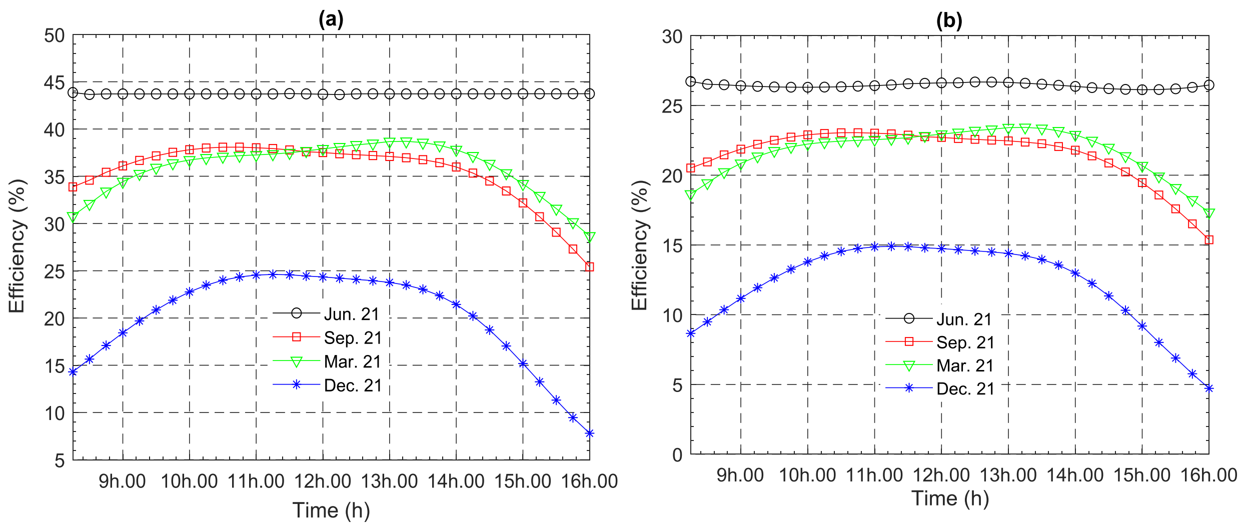

Figure V. 18. *Variation of instantaneous thermal efficiency versus time, (a) PTC with secondary reflector, (b) PTC without secondary reflector.*

V.9. Chapter Summary

In this chapter, several test cases were conducted on a small-size PTC. Two cases were considered: PTC with and without secondary reflector. Two heat transfer fluids were considered: Therminol VP-1 and water. The physical properties of Therminol VP-1 vary with temperature. The data concerning these properties were interpolated by polynomial functions and implemented CFX Solver using the CEL language specific to the solver.

Firstly, after performing a mesh independence study, the analysis model is validated by experimental data obtained from the literature. A good agreement was observed between the results obtained by numerical simulation and the experimental data.

The next step is to calculate the performance of a PTC system during four days in different seasons. The results obtained allow us to draw the following conclusions:

- Cases where Therminol VP-1 is used as a heat transfer fluid:

- The PTC efficiency is constant for the four seasons in both studied cases (with and without secondary reflector).
- The performance of the system with a second reflector is better than that without a second reflector with a ratio of about 1.65.

- Cases where water is used as a heat transfer fluid:

- The maximum thermal performance of the PTC system (with and without secondary reflector) is obtained during the month of June, while during the month of December the performance is minimum. For the months of March and September, the performance is approximately the same.
- The distribution of the heat flux through the tube surface is more intense and uniform when a secondary reflector is introduced.
- Using a second reflector can increase system performance by a ratio of about 1.62 to 1.67.

General Conclusion

General Conclusion

Parabolic Trough Collector (PTC) Concentrators are the linear concentrators most widely used for the thermodynamic conversion of solar energy especially in industrial and domestic domains that demand an operating temperature between 80°C and 160°C. The production of electricity requires high temperatures from 400°C to 1200°C. We can produce overheated steam in power plants with parabolic trough concentrators, where the temperature up to 1500°C and higher. Parabolic trough concentrators are the most promising technologies to take the place of non-renewable energies (fossil energy and nuclear energies), especially in the industrial domains (power plants, hybrid systems, desalination, air conditioning, refrigeration, irrigation, etc.).

In this research work, an analysis and simulation of thermal performance of a small sized PTC is performed. Two cases are the subject of the simulation: PTC with and without secondary reflector. The simulation is conducted on four different days in the four seasons. Monte Carlo Ray tracing method is used to calculate the solar flux distribution over the absorber tube. Conjugate heat transfer and fluid flow equations within the tube are solved by using ANSYS-CFX solver. Oil Therminol VP-1 and water are used as carrier fluids. The oil physical properties according to temperature are implemented in the solver and Physical properties of copper and water are predefined in CFX solver. The obtained results showed the followings:

In case of using Oil Therminol VP-1 as working fluid:

- The missed radiation can be redirected to the receivers by the addition of a second-stage optics
- The PTC efficiency is constant for the four seasons in both studied cases.
- The advantage of using a secondary reflector is that the heat flux around the receiver tube is distributed more uniformly.
- The performance of the system with a second reflector is better than that without a second reflector with a ratio of about 1.65

In case of using water as working fluid:

- The maximum thermal performance of the PTC system (with and without secondary reflector) is obtained during the month of June, while during the month of December the performance is minimum. For the months of March and September, the performance is approximately the same.

- The distribution of the heat flux through the tube surface is more intense and uniform when a secondary reflector is introduced.
- Using a second reflector can increase system performance by a ratio of about 1.62 to 1.67.

The combination of ray tracing and CFD simulations and the implementation of a secondary parabolic reflector in a real receiver suggests that in a real application it would be possible to increase the thermal performance of parabolic troughs with secondary parabolic reflectors, and especially in high-temperature applications they will contribute to enhancing the performance of parabolic troughs.

This study puts into perspective several factors to consider such as the dimensions of the system, the heat transfer fluid, the ambient conditions, the materials, and the energy storage.

Future plans also include numerical investigations to study performance of a small-scale parabolic trough solar concentrator integrated with thermal energy storage system. The novel design using a concentric tube with a PCM the use of a PTC with PCM in the receiver periphery can improve the thermal performance of the presented system in the absence of intense radiation

References

References

[1] Word Energy Outlook. Paris: International Energy Agency, 2012.

[2] International Energy Outlook. Washington: U.S. Energy Information Administration, 2010.

[3] Boukelia T E, Simulation et optimisation d'un modèle de capteur cylindro-parabolique mechanical engineering PhD thesis University of Constantine 2016.

[4] Boutghan C, amelioration des performances d'un collecteur solaire , Physics Magister thesis University of Constantine 2012

[5] http://fr.solarpedia.net/wiki/index.php?title=Solaire_thermique_%C3%A0_concentration

[6] Gama A , M. Haddadi M , Malek A Etude et réalisation d'un concentrateur cylindro parabolique avec poursuite solaire aveugle , Revue des Energies Renouvelables . 11 3 :437 – 451 2008

[7] Bouguetaia N, Contribution à l'Etude et a la Simulation d'un Concentrateur Cylindro-Parabolique. magister thesis University of Constantine 2013[7bis] Regue, H. Etude expérimental d'un capteur cylindro parabolique à double réflexion. Magister thesis University of Laghouat 2013

[8] Behar O, Khellaf A, Mohammedi K. A review of studies on central receiver solar thermal power plants. Renew Sustain Energy Rev 2013;23:12–39. doi:10.1016/j.rser.2013.02.017

[9] Py X, Azoumah Y, Olives R. Concentrated solar power: Current technologies, major innovative issues and applicability to West African countries. Renew Sustain Energy Rev 2013;18:306–15. doi:10.1016/j.rser.2012.10.030

[10] Zhang HL, Baeyens J, Degrève J, Cacères G. Concentrated solar power plants: Review and design methodology. Renew Sustain Energy Rev 2013;22:466–81. doi:10.1016/j.rser.2013.01.032.

[11] Xu X, Vignarooban K, Xu B, Hsu K, Kannan AM. Prospects and problems of concentrating solar power technologies for power generation in the desert regions. Renew Sustain Energy Rev 2016;53:1106–31. doi:10.1016/j.rser.2015.09.015.

[12] EERE O of EE& RE. Linear Concentrator System Basics for Concentrating Solar Power. Energy.gov 2013. https://energy.gov/eere/energybasics/articles/linear-concentrator-system-basics-concentrating-solar-power (accessed July 11, 2017).

[13] (DLR) I for SR of the GAC. DLR - Institute of Solar Research - Line Focus Systems - Proven technology with development potential n.d. http ://www.dlr.de / sf/ en/ desktopde fault.aspx / tabid-7088/18782_read-43608/ (accessed July 11, 2017).

[14] (DLR) I for SR of the GAC. DLR - Institute of Solar Research - Point Focus Systems n.d. http://www.dlr.de/sf/en/desktopdefault.aspx/tabid-7089/17123_read-43304/ (accessed July 11, 2017

[15] Kodama T. High-temperature solar chemistry for converting solar heat to chemical fuels. Progress in Energy and Combustion Science 2003;29.

[16] Pitz-Paal. R., Solar Energy-Concentrating Solar Power-Chapter 19, in Future energy, Elsevier. 405-431. 2014

[17] Barlev D, Vidu R.,P. Stroeve, "Innovation in concentrated solar power," Solar Energy Materials & Solar Cells, vol. 95, 2703-2725, 2011.

[18] K. Lovegrove, W. Stein Csiro, in Concentrating Solar Power Technology, 2012

[19] Zhifeng Wang, in Design of Solar Thermal Power Plants, 2019

[20] Reddy V. S., Kaushik S., Ranjan K , Tyagi S , State of the art of solar thermal power plants - A review, Renewable and Sustainable Energy Reviews, vol. 27. 258-273, 2013.

[21] Schiel W , Keck T . Parabolic dish concentrating solar power (CSP) systems concentrating solar power technology principle , developments and applications woodhead publishing serie in energy , 284- 322 , 2012 https://doi.org/10.1533/9780857096173.2.284

[22] Aurousseau A. Modélisation dynamique et régulation des centrales solaires thermodynamiques linéaires à génération directe de vapeur Génie des procédés. Ecole des Mines d’Albi-Carmaux, 2016

[23] Breeze P, in Power Generation Technologies (Third Edition), 2019

[24] Breeze P, in Solar Power Generation, 2016

[25] Pitz-paal R,Dersch J, Milow B,ECOSTAR Roapmap Document, Technical Report (DLR), 2004.

[26] Garcia P.Outils d’évaluation technico-économique et d’aide à la conception des centrales solaires thermodynamiques du futur.Thèse de doctorat, Université de Perpignan, 2007.

[27] Fernandez-Garcia, A. Zarza E, Valenzuela L Pérez M. "Parabolic-trough solar collectors and their applications." Renewable and Sustainable Energy Reviews 14 : 1695–1721. 2010

[28] Günthe, Matthias, Dirk Krüger and Tobisas Hirsch. Parabolic Trough Technology.Cologne: enerMENA, n.d.

[29] Pytlinski, JT.Solar energy installations for pumping irrigation water. Solar energy Solar Energy Volume 21, Issue 4, 255-262 ,1978

[30] Spencer LC. A comprehensive review of small solar-powered heat engines: Part I. A history of solar-powered devices up to 1950. Sol Energy 1989;43 4 :197–214.1978.

[31] Shaner, WW. and WS. Duff. "Solar thermal electric power systems: comparison of line-focus collectors.Solar Energy 13-49. 1979

[32] Price H., Lüpfert E., Kearney,D, Zarza E, Cohen G., Gee R., Mahoney R. Advances in parabolic trough solar power technology. Journal of Solar Energy Engineering 2002; 124:109.https://doi.org/10.1115/1.1467922

[33] Vazquez, J. and N. Castaneda. The collector for Extresol-1. 600 meters loop test in Andasol-1 and test unit description. 14th intsymp on conc sol power and chemenergy technol. SolarPACES 2008,

[34] Valenzuela L, Zarza E , Berenguel M ,Eduardo F. Camacho, Control concepts for direct steam generation in parabolic troughs, Solar Energy 78 301–311 2005

[35] Lourdes GarciaRodriguez L , Carlos GmezCamacho C, Exergy analysis of the SOL 14 plant (Plataforma Solar de Almeria, Spain , Desalination 137 251258. 2001

[36] Alain FERRIERE (PROMES-CNRS, Odeillo) Laboratoire Procédés, Matériaux et Energie SolaireEcole Polytechnique - 30 janvier 2009

[37] Lauterbach C, Schmitt B, Jordan U, Vajen K. The potential of solar heat for industrial processes in Germany. Renew Sustain Energy Rev 2012;16:5121–30.2012 http://dx.doi.org/10.1016/j.rser.2012.04.032

[38] Shahin MS, Orhan MF, Uygul F. Thermodynamic analysis of parabolic trough and heliostat field solar collectors integrated with a Rankine cycle for cogeneration of electricity and heat. Sol Energy 2016;136:183–96.2016 http://dx.doi.org/10.1016/j. solener.2016.06.057

[39] Fernndez-Garc A, Zarza E, Valenzuela L, Prez M. Parabolic-trough solar collectors and their applications. Renew Sustain Energy Rev;14:1695–721. 2010

[40] Lüpfert E, Riffelmann K-J, Price H, Burkholder F, Moss T. Experimental Analysis of Overall Thermal Properties of Parabolic Trough Receivers. J Sol Energy Eng;130:021007. 2008 http://dx.doi.org/10.1115/1.2888756.

[41] Kalogirou, S A. Seawater desalination using renewable energy sources.Progress in Energy and Combustion Science 31: 242–281. 2005

[42] Kalogirou, S A. "Solar thermal collectors and applications." Progress in Energy and Combustion Science 30: 231-295. 2004

[43] Alfellag M A A Modeling and Experimental Investigation of Parabolic Trough Solar Collector. Master thesis Embry-Riddle Aeronautical University - Daytona Beach usa 2014

[44] Water Desalination Using Renewable Energy ENERGY TECHNOLOGY SYSTEM ANALYSIS PROGRAMME IEA-ETSAP and IRENA Technology Policy Brief I12 – January 2013 -

[45] Zachary, J.et al., Power Corp., , Adding Desalination to Solar Hybrid and Fossil Plants, Electric Power Journal. 2010

[46] El Fadar A., Mimet A. , PerezGarcıa M. , Study of an adsorption refrigeration system powered by parabolic trough collector and coupled with a heat pipe , Renewable Energy 34 2271–2279. 2009

[47] Zou B, Dong J, Yao Y, Jiang Y An experimental investigation on a small-sized parabolic trough solar collector for water heating in cold areas Applied Energy 163 : 396–407 2016

[48] Chafie M, Ben Aissa MF, Bouadila S, Balghouthi M, Farhat A, GuizaniA Experimental investigation of parabolic trough collector system under tunisian climate: design, manufacturing and performance assessment *Applied Thermal Engineering* 2016 http://dx.doi.org/doi: 10.1016/j.applthermaleng.2016.02.073

[49] Ma X, Zheng H, Chen Z. An investigation on a compound cylindrical solar concentrator (CCSC). Appl Therm Eng;120:719–27 2017

[50] Wang Y, Liu Q, Sun J, Lei J, Ju Y, Jin H. A new solar receiver/reactor structure for hydrogen production. Energy Convers Manag;133:118–26 2017

[51] Qu W, Wang R, Hong H, Sun J, Jin H. Test of a solar parabolic trough collector with rotatable axis tracking. Appl Energy;207:7–17 2017

[52] R. Bader P. Haueter A. Pedretti A. Steinfeld Optical Design of a Novel Two-Stage Solar Trough Concentrator Based on Pneumatic Polymeric Structures

Journal of Solar Energy Engineering 131(3):031007-1/9 · 2009 DOI: 10.1115/1.3142824

[53] R Good P, Ambrosetti G, Pedretti A, Steinfeld A. A 1.2MWth solar parabolic trough system based on air as heat transfer fluid at 500 °C — engineering design, modelling, construction, and testing. Sol Energy;139:398–411 2016

[54] Bortolato M , Dugaria S, Del Col D, Experimental study of a parabolic trough solar collector with flat bar-and-plate absorber during direct steam generation Energy 116 1039e1050 2016

[55] Halimi M, Outana I, Diouri J, El Amrani A, Messaoudi C. Experimental investigation of absorbed flux circumferential distribution of an absorber with U-pipe tube exchanger for Parabolic Trough Collectors. Appl Therm Eng;129:1230–9. 2018

[56] Bharti A, Mishra B , Bireswar P Thermal performance analysis of small-sized solar parabolic trough collector using secondary reflectors International Journal of Sustainable Energy 2019 , DOI: 10.1080/14786451.2019.1613991

[57] Rodriguez-Sanchez D, Rosengarten G Improving the concentration ratio of parabolic troughs using a second-stage flat mirror Applied Energy Volume 159, 2015, Pages 620-632 http://dx.doi.org/10.1016/j.apenergy.2015.08.106 0306-2619/ 2015

[58] Krissadang S. Design, construct and performance evaluation of a 2-stage parabolic through solar concentrator in Pathum Thani. Advanced Materials Research 931 1291–1297. 2014

[59] Zhu Y, Shi J, Li Y, Wang L, Huang Q, Xu G. Design and experimental investigation of a stretched parabolic linear Fresnel reflector collecting system. Energy Convers Manag;126:89–98 2016

[60] Abdelhamid M, Widyolar BK, Jiang L, Winston R, Yablonovitch E, Scranton G, Cygan D, Abbasi H, Kozlov A. Novel double-stage high-concentrated solar hybrid photovoltaic/thermal (PV/T) collector with nonimaging optics and GaAs solar cells reflector. Appl Energy;182:68–79. 2016

[61] Ullah I, Shin S. Highly concentrated optical fiber-based daylighting systems for multi-floor office buildings. Energy Build;72:246–61 2014

[62] Liang H, Fan M, You S, Zheng W, Zhang H, Ye T, Zheng X. A Monte Carlo method and finite volume method coupled optical simulation method for parabolic trough solar collectors. Appl Energy;201:60–8 2017

[63] Bennett W, Lun J, Jonathan F, Roland W. Experimental performance of a two-stage (50X) parabolic trough collector tested to 650 °C using a suspended particulate (alumina) HTF. Applied Energy 222 228–243. 2018

[64] Bennett W, Lun J, Jonathan F. Theoretical and experimental performance of a two-stage (50X) hybrid spectrum splitting solar collector tested to 600 °C. Applied Energy 239 514–525. 2019

[65] Wirz M, Petit J, Haselbacher A, Steinfeld A. Potential improvements in the optical and thermal efficiencies of parabolic trough concentrators. Sol Energy;107:398–4142014

[66] Eck M., Feldhoff J. F., Uhlig R., Thermal modelling and simulation of parabolic trough receiver tubes. In: Proceedings of the ASME 4th International Conference on Energy Sustainability, 17-22 May 2010, Phoenix, Arizona, USA, pp. 1–8 2010

[67] Cheng, Z.D., He, Y.L., Xiao, J., Tao, Y.B., Xu, R.J., Threedimensional numerical study of heat transfer characteristics in the receiver tube of parabolic trough solar collector. Int. Commun. Heat Mass 37 (7), 782–787. 2010.

[68] Dudley, V., Kolb, G., Sloan, M., Kearney, D., SEGS LS2 solar collector – test results. Report of Sandia National Laboratories, SANDIA94-1884, USA 1994.

[69] Ya-Ling He et al. “A MCRT and FVM coupled simulation method for energy conversion process in parabolic trough solar collector”. Renewable Energy 36 2011

[70] Cheng Z, He Y, Cui F, et al. Numerical simulation of a parabolic trough solar collector with nonuniform solar flux conditions by coupling FVM and MCRT method. Solar Energy. 2012;86:1770-1784.

[71] Jeter S M. Calculation of the concentrated flux density distribution in parabolic trough collectors by a semifinite formulation. Solar Energy.;37:335-345. 1986

[72] Khanna S, Kedare S B, Singh S. Analytical expression for circumferential and axial distribution of absorbed flux on a bent absorber tube of solar parabolic trough concentrator. Solar Energy.;92:26–40 2013

[73] Wang Y, Liu Q, Lei J, et al. Performance analysis of a parabolic trough solar collector with non-uniform solar flux conditions. International Journal of Heat and Mass Transfer.;82:236-249 2015

[74] Qiu Y, Li M-J, He Y-L, et al. Thermal performance analysis of a parabolic trough solar collector using supercritical CO2 as heat transfer fluid under non-uniform solar flux. Applied Thermal Engineering.;115:1255-1265. 2017

[75] Wu Z, Li S, Yuan G, et al. Three-dimensional numerical study of heat transfer characteristics of parabolic trough receiver. Applied energy.; 113:902-911 2014

[76] Ghomrassi A, Mhiri H, Bournot P. Numerical study and optimization of parabolic trough solar collector receiver tube. Journal of Solar Energy Engineering ; 137:051003. 2015

[77] performance of parabolic trough solar collectors with Monte Carlo Ray Tracing method based on theoretical analysis Solar Energy 147 189–201 2017

[78] Zou B, Dong J, Yao Y , Jiang Y detailed study on the optical performance of parabolic trough solar collectors with Monte Carlo Ray Tracing method based on theoretical analysis Solar Energy 147 189–201 2017

[79] Li Z Y, Huang Z, Tao W Q. Three-dimensional numerical study on fully-developed mixed laminar convection in parabolic trough solar receiver tube. Energy.;113:1288-1303. 2016

[80] Okafor I F, Dirker J, Meyer J P. Influence of non-uniform heat flux distributions on the secondary flow, convective heat transfer and friction factors for a parabolic trough solar collector type absorber tube. Renewable Energy. 108:287-302. 2017

[81] Wang Y, Liu Q, Lei J, et al. A three-dimensional simulation of a parabolic trough solar collector system using molten salt as heat transfer fluid. Applied Thermal Engineering.;70:462-476. 2014

[82] Liang H, You S, Zhang H Comparison of three optical models and analysis of geometric parameters for parabolic trough solar collectors energy 96 37-47 2016

[83] wang Z , .Ni J. zhao L. Shuai Deng Dongpeng zhao Simulation and optimization of parabolic trough receiver with nonuniform heat flux distribution: A review 9th International Conference on Applied Energy, ICAE2017, 21-24 2017, Cardiff, UKEnergy Procedia 142 (2017)700-707 10.1016/j.egypro.2017.12.115

[84] Belkacem agaga B . smaili A , flacoz Q;Coupled simulation method by using MCRT and FVM techniques for performance analysis of a parabolic trough solar collector Mechanical Enginnering and 4th International Conference on Power and Energy Systems Engineering, CPESE , 25-29 2017 Berlin Germany Energy procedia141(2017) 34-38

[85] Spirkl W, Ries H, Muschaweck J, A. Timinger, Optimized compact secondary reflectors for parabolic troughs with tubular absorbers, Sol. Energy 61 153–158. 1997

[86] Serrano-Aguilera J.J., Valenzuela L, Fernández-Reche J, Inverse Monte Carlo Ray-Tracing method (IMCRT) applied to line-focus reflectors, Sol. Energy 124 184–19 2016

[87] Liu Y, Chen Q, Hu K, et al. Flow field optimization for the solar parabolic trough receivers in direct steam generation systems by the variational principle. International Journal of Heat & Mass Transfer.;102:1073-1081. 2016

[88] Sundaram, P. and Senthil,R.Thermal Performance Enhancement of Solar Parabolic Trough Collector using Secondary Reflector. International Journal of Engineering and Technology; 8 (6): 2964–2969. 2017

[89] Loni R, Kasaeian AB, AskariAsli-Ardeh E, Ghobadian B, Najafi G. Comparion study of air and thermal oil application in a solar cavity receiver. Journal of Thermal Engineering; 5(6)-10: 221-229. 2019 https://doi.org/10.18186/thermal.654628

[90] Cao F, Wang, L., Zhu, T. Design and optimization of elliptical cavity tube receivers in the parabolic trough solar collector. International Journal of Photoenergy; 1471594, 2017.https://doi.org/10.1155/2017/1471594

[91] Islam M, Miller S, Yarlagadda P, Karim A. Investigation of the effect of physical and optical trough collector. *Energies* 10 (11),1907. 2017, https://doi.org/10.3390/en10111907

[92] Collares-Pereira M, Gordon JM, Rabl A, Winston R. High concentration two-stage optical for parabolic trough solar collectors with tubular absorber and large rim angle. Solar Energy; 47 :457-466. 1991 https://doi.org/10.1016/0038-092X(91)90114-C

[93] Evangelos B, Christos T. Alternative designs of parabolic trough solar collectors. Progress in Energy and Combustion Science; 71:81–117. 2019 https://doi.org/10.1016/j.pecs.2018.11.001

[94] Kuofei C. Software and codes for analysis of concentrating solar power technologies. 2008;

[95] Cheng Z, He Y, Cui F. A new modelling method and unified code with MCRT for concentrating solar collectors and its applications. Applied energy. 2013;101:686-698.

[96] Pei W, Chang X, Jiaru C, et al. Application of field theory on the non-uniform thermal boundary condition analysis on a parabolic trough collectors[C]. Proceedings of the Power and Renewable Energy (ICPRE), IEEE International Conference on Power and, IEEE,: 589-593 2016

[97] benmouiza M. K Quantification of solar radiation in Algeria, application to the sizing of photovoltaic systems Doctoral thesis 2015

[98] Lomansoc J ,Jun Roloma R ,Seer Paller K Design and Simulation of 100 kWp Solar Photovoltaic (PV) Grid Connected Power Plant Using PVsyst International Journal of Science and Research (IJSR) :2319-7064 2016

[99] Kalogirou, Soteris A. Solar energy engineering: Processes and Systems. 1st. USA:Elsevier, 2009

[100] Garg, H P and J Prakash. Solar energy, fundamentals and application. New Delhi:Tata McGraw-Hill, 2006

[101] Hachicha, A.A, et al. "Heat transfer analysis and numerical simulation of a parabolictrough." Applied Energy 111 : 581-592. 2013

[102] Guven, Halil M. and Richard B. Bannerot. Optical and thermal analysis of parabolic trough collectos for technically for developed countries. Technical report. Houston, 1984.

[103] Fischer, Stephan. "Experience from tests on concentrating and tracking collectors." Technical report. 2012.

[104] Khaled, Ahmed. Technical and economic performance of parabolic trough in Jordan. Master. thesis. Amman, 2012

[105] Forristall, R. Heat transfer analysis and modeling of a parabolic trough solar receiver implemented in Engineering Solver Equation. Technical report. Colorado:National Renewable Energy Laboratory, 2003.

[106] Kajavali A, Computational Methodology Chapter 4 Ph. D. thesis Annamalai Nagar university 2015

[107] Wendelin T. SolTRACE: A New Optical Modeling Tool for Concentrating Solar Optics. Proceedings of ISEC-4490, 253-260 2003. https://doi.org/10.1115/ISEC2003-44090

[108] Kreyszig, Erwin.. Advanced Engineering Mathematics. 10th ed. Hoboken, NJ: Wiley Publication. 2015

[109] Baskharone, Erian A. Thermal Science: Essentials of Thermodynamics, Fluid Mechanics, and Heat Transfer. McGraw-Hill, 2012.

[110] Burkholde, Frank, et al. "Parabolic Trough Receiver Thermal Testing." ASME 2007

[111] Energy Sustainability Conference. California: ASME 2007 Energy Sustainability, 2007. 961-970.

[112] Incropera, F, et al. Fundamentals of heat and mass transfer. 6th. New York: John Wiley and Sons, 2007

[113] Gnielinski, V. "New equations for heat and mass transfer in turbulent pipe and."International chemical engineering 16.16 (1976): 359–368.

[114] Rathore, M.M. and Jr. Raul R.A. Kapuno. Engineering Heat Transfer. USA: Jones & Bartlett Learning, LLC, 2011

[115] Dubey, Swapnil and G.N. Tiwari. Fundamentals of photovoltaic modules and thier applications. Cambridge: The royal society of chemistry, 2010

[116] Kalogirou, Soteris A. "A detailed thermal model of a parabolic trough collector receiver." Energy 48 (2012): 298-306

[117] Ratazel, A, C Hickox and D Gartling. "Techniques for reducing thermal conduction and natural convection heat losses in annular receiver geometries." Journal of Heat Transfer 101.1 (1979): 108-113

[118] Rathakrishnan, Ethirajan. Elements of heat transfer. USA: Taylor & Francis Group, 2012.

[119] Duffie, Jouh A. and William A. Beckman. Solar engineering of thermal processes. 3rd. New Jersey: John Wiley & Sons, 2006.

[120] Tzivanidis, Christos, and Evangelos Bellos. 2016. “The Use of Parabolic Trough Collectors for Solar Cooling - A Case Study for Athens Climate.” Case Studies in Thermal Engineering 8 (September): 403–413. doi:10.1016/j.csite.2016. 10.003

[121] ANSYS-CFX Theory Guide. (2019), ANSYS Inc

[122] J. Tu, G.-H. Yeoh and C. Liu, Computational Fluid Dynamics, , A Practical Approach, Second Edition, Butterworth-Heinemann, Elsevier, Amsterdam, Netherlands, 2013

[123] Therminol VP-1. Vapor Phase/ Liquid Phase Heat Transfer Fluid (Liquid Phase), Solutia Inc, 2017. http://twt.mpei.ac.ru/tthb/hedh/htf-vp1.pdf/, accessed on Mar. 12, 2018.